SUBSIDENCE ANALYSIS OF THE HENGELO, USSELER ES, AND GANZEBOS BRINEFIELDS

TOPICAL REPORT RSI-3316

PREPARED FOR
Nobian
Boortorenweg 27
P.O. Box 25
Hengelo 7550 GC
NETHERLANDS

DECEMBER 2022

RESPEC

SUBSIDENCE ANALYSIS OF THE HENGELO, USSELER ES, AND GANZEBOS BRINEFIELDS

TOPICAL REPORT RSI-3316

PREPARED BY

Cody Vining

RESPEC
3824 Jet Drive
Rapid City, South Dakota 57703
UNITED STATES

PREPARED FOR

Nobian
Boortorenweg 27
P.O. Box 25
Hengelo 7550 GC
NETHERLANDS

DECEMBER 2022

Project Number M0178.22002

TABLE OF CONTENTS

LIST OF TABLES

LIST OF FIGURES

LIST OF FIGURES (CONTINUED)

LIST OF FIGURES (CONTINUED)

LIST OF FIGURES (CONTINUED)

1.0 INTRODUCTION

Nobian operates three brinefields near Hengelo (i.e., Hengelo, Usseler Es, and Ganzebos brinefields), as depicted in Figure 1. Production at the Hengelo brinefield (green caverns) began around 1935, while production at the Usseler Es brinefield (red caverns) and Ganzebos brinefield (blue caverns) began around 2008 and 2015, respectively. Each of these brinefields has caverns at different stages in the life cycle. Experience has shown that developing these caverns cause the ground surface to subside because removing the salt disturbs the stress equilibrium, and the salt responds by creeping toward and into the mined openings. As the mined caverns close, rock salt that surrounds the caverns moves toward the caverns; subsequently, the rock, even farther out from the caverns, moves incrementally inward to maintain continuity within the rock mass. As the process extends away from the caverns (albeit with diminishing displacement magnitudes), the resultant deformation eventually propagates to the ground surface, which causes the surface to subside.

RESPEC has previously performed subsidence predictions for these three brinefields [Vining and Gupta, 2021a and 2021b; Van Sambeek, 2008]. These initial studies estimate ground-surface subsidence, assuming the closure of the caverns occurs at a steady rate. This approach was based on the experience gained from the Hengelo brinefield and was necessary because the caverns were relatively early in the brinefield life cycle, and insufficient data existed to define site-specific parameters accurately. Subsequent elevation surveys suggest the measured subsidence rates for the Usseler Es and Ganzebos brinefields are greater than those predicted assuming the Hengelo parameters.

Subsequent scoping studies conducted by RESPEC provided insight into how the cavern closure rates evolve with time and revealed a correlation between the calculated subsidence rate and the cavern age, with greater closure rates for younger caverns. Based on this insight, Nobian requested a surface-subsidence investigation to reevaluate the closure model parameter values for Hengelo, Usseler Es, and Ganzebos brinefields to more accurately represent the short-term subsidence attributed to the closure of the brine caverns and the long-term steady-state closure rate that have been proven over the Hengelo brinefield.

This report documents the subsidence investigation in five chapters, including this introduction. Chapter 2.0 presents a review of the conventional benchmark-elevation survey and calibration process to determine site-specific parameter values, and Chapter 3.0 provides the evaluation results of the updated subsidence study and presents the anticipated subsidence attributed to the continual cavern closure. The study summary, conclusions, and recommendations are discussed in Chapter 4.0 and cited references are provided in Chapter 5.0. The report concludes with appendices that provide additional information and study results.

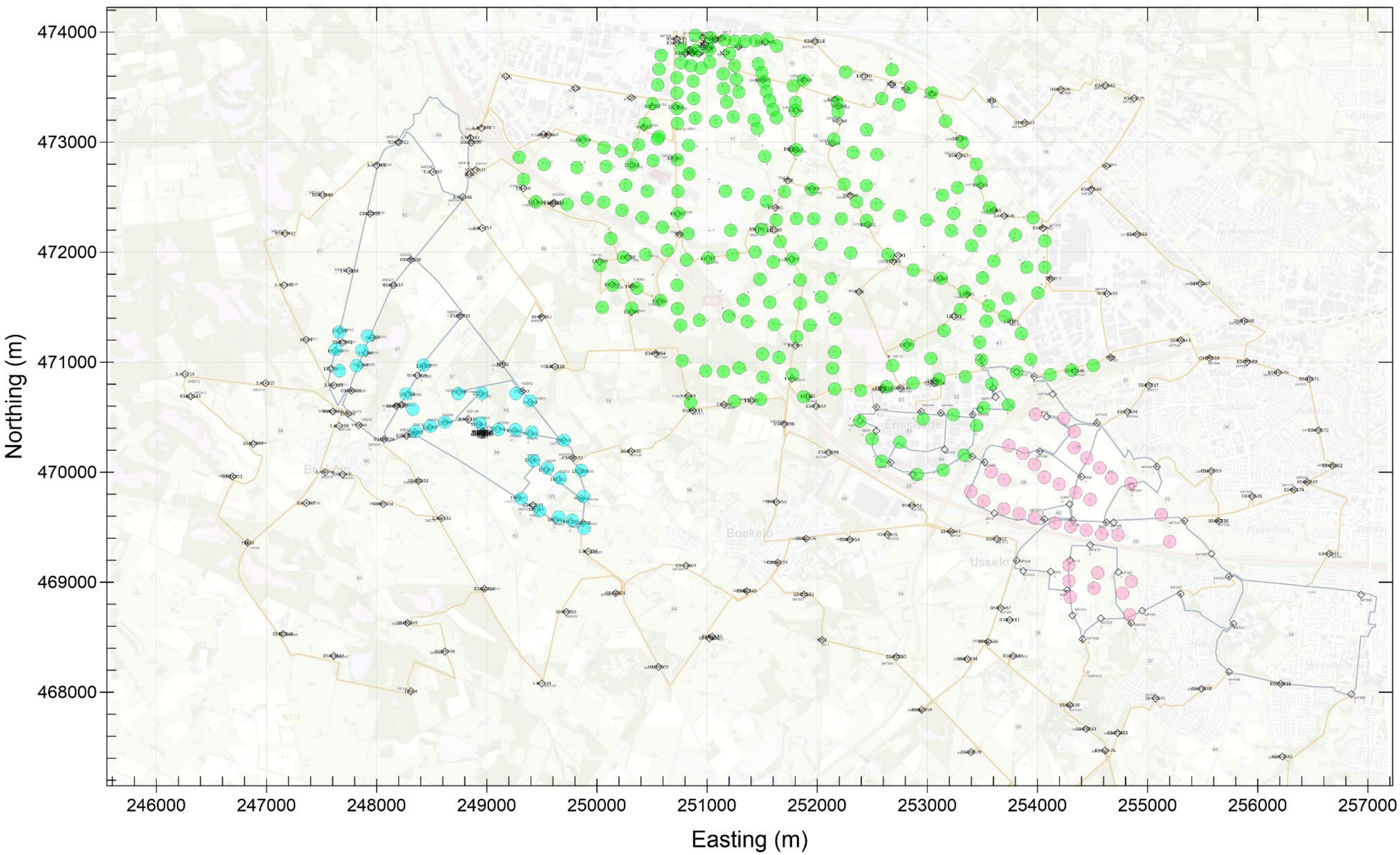

Figure 1-1. Locations of Subsidence Benchmarks That Overlie and Surround the Hengelo, Usseler Es, and Ganzebos Brinefields.

2.0 BENCHMARK DATA REVIEW AND MODEL CALIBRATION

The primary objective of the calibration and validation effort was to develop site-specific subsidence parameter values for the Hengelo, Usseler Es, and Ganzebos brinefields that more accurately predict the short-term subsidence attributed to the convergence of the brine caverns. The parameter values were derived from the results of a fitting process that reduced the error between the predicted displacements made using the Solution Mining Research Institute (SMRI) computer program SALT_SUBSID [Nieland and Van Sambeek, 2010] and those displacements calculated from the available benchmark-elevation surveys.

Nobian has installed a benchmark network to better understand and quantify the ground-surface response to the underground cavern convergence. Figure 1-1 shows the elevation benchmark locations relative to the surface landmarks. The benchmarks (diamonds in Figure 1-1) are located directly above the caverns (blue circles in Figure 1-1) or at varying distances from the caverns. For this study, Nobian provided historical benchmark data overlying the Hengelo brinefield to calibrate and verify the predictive capability of the subsidence model. The data consisted of an initial elevation survey performed in 1935 and 69 subsequent elevation surveys, with the final available survey conducted in 2021. These data were used to assess the ongoing subsidence occurring in the areas overlying and surrounding the Hengelo, Usseler Es, and Ganzebos brinefields.

The subsidence calculations represented the progressive development of the Hengelo, Usseler Es, and Hengelo brinefields by simulating cavern growth and cavern-field expansion, shown in Figure 1-1, based on actual mining dates and cavern volume growth rate through 2021 provided by Nobian. The subsidence model parameter values were derived by reducing the error between the predicted displacements and displacements calculated from the available benchmark-elevation surveys between 1935 and 2019. During the fitting process, the measured subsidence overlying the Hengelo Phase 1 caverns were excluded because these caverns are known to have other processes contributing to the overall subsidence that result in subsidence rates greater than the salt creep closure. For completeness, technical information that supported the study, including historical cavern production records, characteristics of the solution-mining plans, and detailed descriptions of the SALT_SUBSID software, are provided in Appendix A.

Figures A-3 through A-8 in Appendix A are time-series plots comparing the calculated displacements from the measured elevation surveys to the displacements predicted from the subsidence model at select locations overlying the brinefields. The input parameters defining the closure model are provided in Table 2-1 and Figure 2-1 illustrates the evolution of the volumetric convergence rates for each of the closure models. Figure 2-2 compares the measured and predicted displacement rates at selected benchmarks between 1960 and 2018. RESPEC believes that the calibration process resulted in a general agreement between the measured and predicted subsidence rates in areas directly overlying and spatially removed from the Hengelo, Usseler Es, and Ganzebos brinefields. The following notable observations were made from the calibration effort:

- **The subsidence model accurately replicated the spatial distribution of the subsidence bowl.** Comparing the displacement distributions revealed that the subsidence model accurately replicated the greater subsidence rates over areas of more intense mining; as well as the slower subsidence rates anticipated around the mine perimeter where extraction is less.
- **The subsidence model replicated the short-term subsidence rates with reasonable agreement over the Hengelo, Usseler Es, and Ganzebos brinefields.** Comparing the predicted and measured displacements within the first 10 years after initial cavern development revealed that the subsidence model slightly overpredicted the magnitude of the measured subsidence. Further, the closure model represents a transient period represented by the parameter values y_0 and β where the cavern convergence rates are greater than the long-term, steady-state convergence rates (y_{ss}) as illustrated in Figure 2-1.
- **The subsidence model replicated the long-term subsidence rates with reasonable agreement over the Hengelo brinefields, and the approach taken to represent the long-term subsidence rates over the Usseler Es and Ganzebos brinefields is believed to be conservative.** These results indicate that the subsidence parameter value (0.00008) previously determined for the Hengelo brinefield still accurately represents the surface displacements recorded on the surface overlying the Hengelo brinefield. Furthermore, the approach taken to estimate the long-term subsidence over the Usseler Es and Ganzebos caverns account for the change in cavern volumes and depths at the respective brinefield.
- **The subsidence model parameter values likely do not represent the long-term cavern behavior after abandonment.** The parameter values represent a behavior that assumes the caverns would continue to close after mining ceases neglecting any pressure build-up in the cavern after abandonment that would significantly slow and eventually arrest cavern convergence. Thus, the actual subsidence that manifests on the surface after mining has ceased will depend on the chosen abandonment plans which could significantly reduce the predicted magnitudes presented.

Table 2-1. Subsidence-Model Closure Parameters for the Hengelo, Usseler Es, and Ganzebos Brinefields

Mine Block	y_{ss} (1/year)	y_0 (—)	β (1/year)	η (—)
Hengelo Brinefield	0.00008	0.0005	0.4	0.0168
Usseler Es Brinefield	0.00020	0.00055	0.4	0.0168
Ganzebos Brinefield	0.00050	0.001	0.4	0.0168

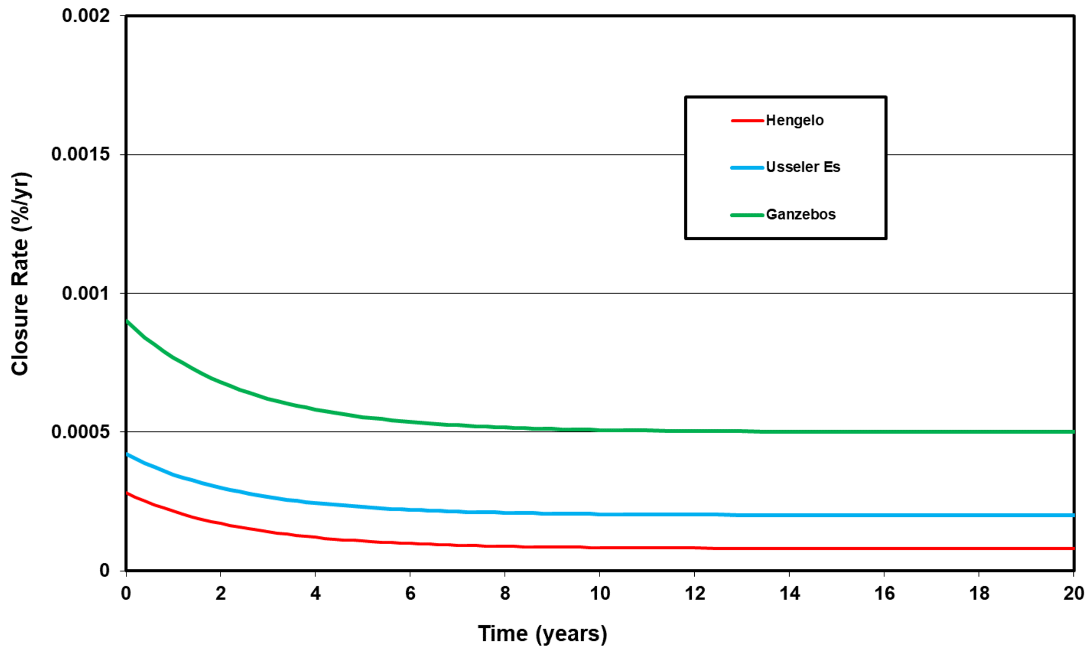

Figure 2-1. Graphical Represenation of the Subsidence Closure Models Illustrating the Volumetric Cavern Convergence Rates Versus Time for the Hengelo, Usseler Es, and Ganzebos Brinefields.

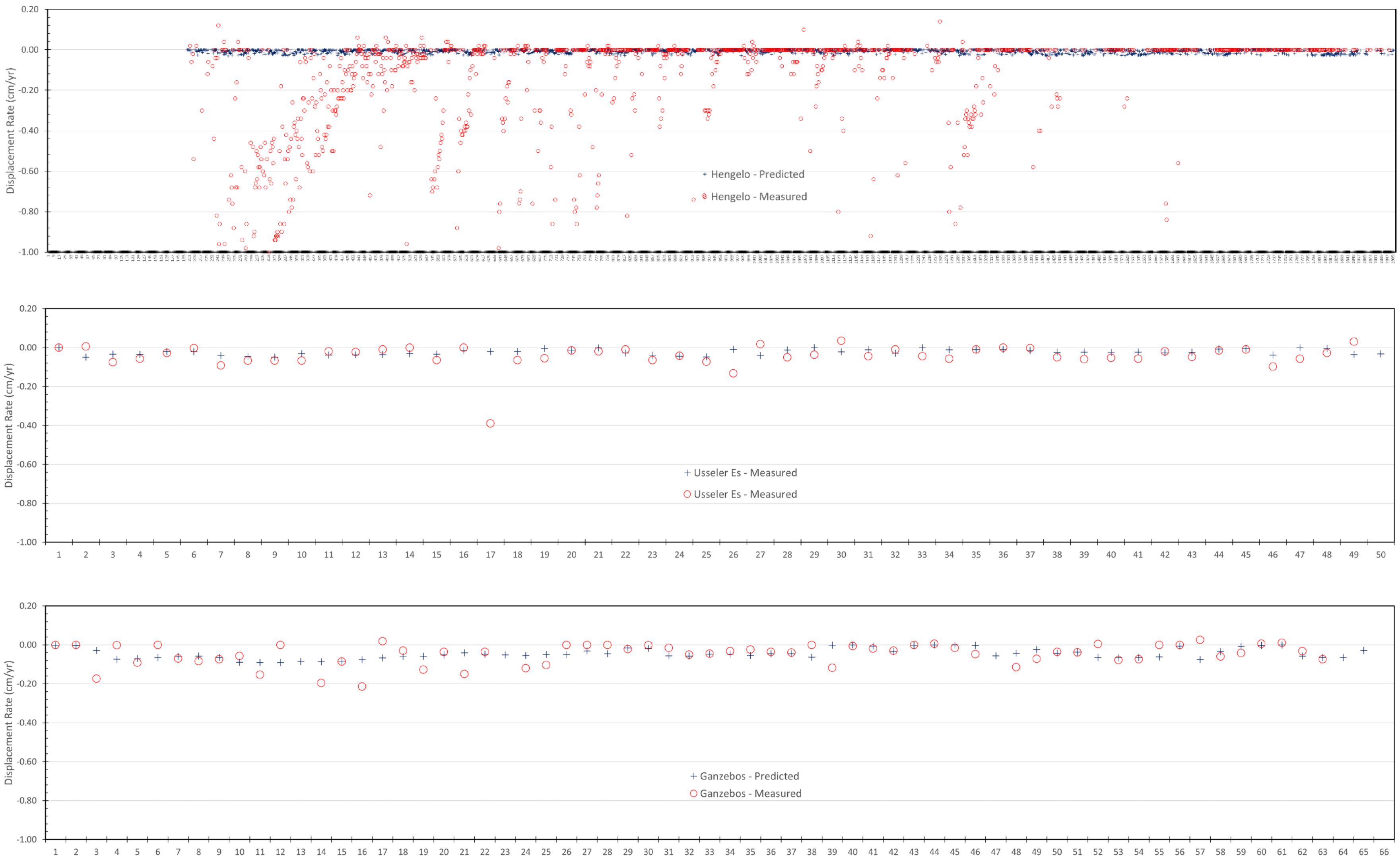

Figure 2-2. Plots Comparing the Measured and Predicted Benchmark Displacement Rates Overlying the Hengelo, Usseler Es, and Ganzebos Brinefields.

3.0 EVALUATION OF THE HENGELO, USSELER ES, AND GANZEBOS BRINEFIELDS

Subsidence calculations were performed to estimate the anticipated ground-surface subsidence attributed to the continual convergence of the Hengelo, Usseler Es, and Ganzebos brinefields. The designed simulation represented the progressive development of the Hengelo, Usseler Es, and Hengelo brinefields annually, based on actual mining dates and cavern volume growth rates. However, the Phase 1 caverns (i.e., 1 through 50) at the Hengelo brinefield were excluded because other processes (i.e., cavern migrations) are having a greater influence on the subsidence that manifests on the surface that typical cavern convergence attributed to salt creep. Removing the Phase 1 caverns from the simulation is believed to have a negligible impact on the predicted subsidence overlying the Phase 3 Hengelo caverns and the Usseler Es and Ganzebos brinefields because the caverns are sufficiently removed so any influence on the subsidence distribution overlying the Phase 3 caverns is negligible.

The method used to evaluate the potential impact that mining-induced subsidence has on the ground-surface response consisted of delineating regions on the surface that would be subject to damage from ground-surface subsidence. The term “surface subsidence” implies the total phenomenon of surface and subsurface movements and includes vertical and horizontal displacements as well as the associated forms of ground movement that result from differential (nonuniform) ground movement. In addition to altering the original ground surface, subsidence components transferred to the surface and subsurface infrastructures within these zones can have an adverse effect on the useful life of the surface and subsurface infrastructures. These additional components include ground-surface tilt and differential vertical movement, curvature (bending), horizontal extension (lengthening), and compression (shortening) of the ground surface. Each of these subsidence components is described in greater detail in Appendix A.

For this study, threshold values developed to indicate the onset of negligible-to-slight damage were used to delineate regions on the surface where mining-induced subsidence may adversely affect surface structures and surface and subsurface. Threshold values that indicate the onset of negligible-to-slight damage used for this study are given in Table 3-1. Additional information on the development of the damage-avoidance criteria values is provided in Appendix A. Vertical displacement that exceeds this limit may impact water drainage for unfavorable surface topographies, and absolute horizontal strain and tilt values that exceed these limits may result in negligible to very slight damage to the surface structures and infrastructures.

Table 3-1. Damage-Avoidance Criteria Values

Component	Unit	Study Threshold Values
Vertical Displacement	mm	150
Absolute Horizontal Strain	(microstrain)	1,000 to 2,000
Ground-Surface Tilt	mm/km	2000

(microstrain) = 1 × 10^{-6} strain
mm = millimeter
mm/km = millimeter per kilometer.

3.1 ASSESSMENT OF THE CURRENT BRINEFIELD SOLUTION-MINING PLAN

The predicted ground displacements in the Years 2025, 2050, 2075, 2100, and 2125 were scrutinized to delineate regions on the surface where subsidence attributed to the continued convergence of the caverns may have an adverse effect on surface structures and infrastructures. Year 2050 was arbitrarily selected to assess the impact of the solution-mining plans on the surface response shortly after mining ceased in the final cavern. Year 2100 was chosen for results to directly compare with the previous study and assess the impact cavern convergence will have on the long-term subsidence distribution.

The following sections discuss the results predicted in Years 2050 and 2100 regarding the (1) vertical subsidence rates, (2) vertical subsidence, (3) horizontal surface strains, and (4) ground-surface tilts. Subsidence distributions predicted in Years 2025, 2075, and 2125 are provided in Appendix B.

3.1.1 VERTICAL SUBSIDENCE AND SUBSIDENCE RATE

Figures 3-1 and 3-2 show contours of the predicted vertical displacement rates (in millimeters per year [mm/yr]) that overlie and surround the brinefields in Years 2050 and 2100, respectively. The smallest contoured vertical displacement rate is 0.05 mm/yr, which is an arbitrary cutoff of the actual subsidence distribution. As expected, the surface regions with the greatest subsidence rate correspond to areas above the cavern field where the greatest salt volume will have been extracted. The maximum subsidence rate predicted in Year 2050 (Figure 3-1) is 1.2 mm/yr, which is identical to the maximum subsidence rate predicted in Year 2100 (1.2 mm/yr).

Figures 3-3 and 3-4 show contours of the predicted vertical displacements in millimeter (mm) that surround the brinefields and illustrate the impact that the current brinefield solution-mining plan will have on the ground surface in Years 2050 and 2100. The smallest contour in each figure is 1 mm, which is an arbitrary cutoff of the actual vertical displacement distribution. The maximum vertical displacement predicted in Year 2050 that is attributed to the current brinefield solution-mining plan (Figure 3-3) is approximately 35 mm. At Year 2100, the maximum vertical displacement increases to approximately 96 mm. These magnitudes of vertical displacement are less than the 150 mm threshold, suggesting that the accumulated subsidence is unlikely to cause surface water to begin collecting in low-lying areas of unfavorable topographies that do not have adequate drainage.

3.1.2 HORIZONTAL EXTENSIONAL AND COMPRESSIONAL STRAINS

Ground lengthening (extension) occurs along the underground mine perimeter, where the surface becomes convex, while ground shortening (compression) occurs near the midspan of the underground mine, where the surface becomes concave. As strains are transferred to the surface, cracks may form in high-extensional strain zones, and bulging may occur in the high-compression areas. Additionally, horizontal strains have the potential to damage linear structures (e.g., elongated buildings, roads, and pipelines) that are unfavorably orientated.

RESPEC

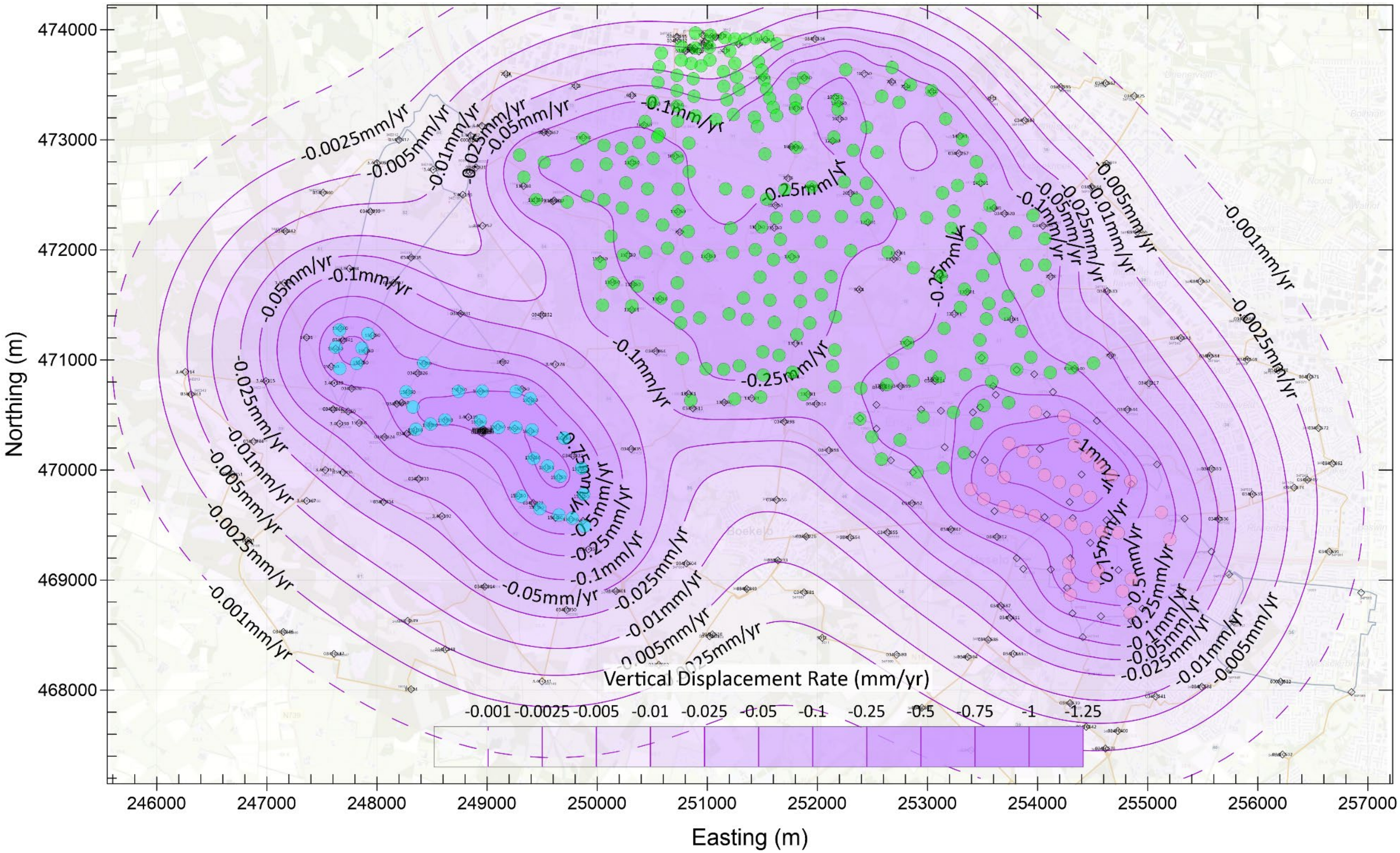

Figure 3-1. Vertical Displacement Rate (Millimeters per Year) Predicted Over the Hengelo, Usseler Es, and Ganzebos Brinefields in Year 2050.

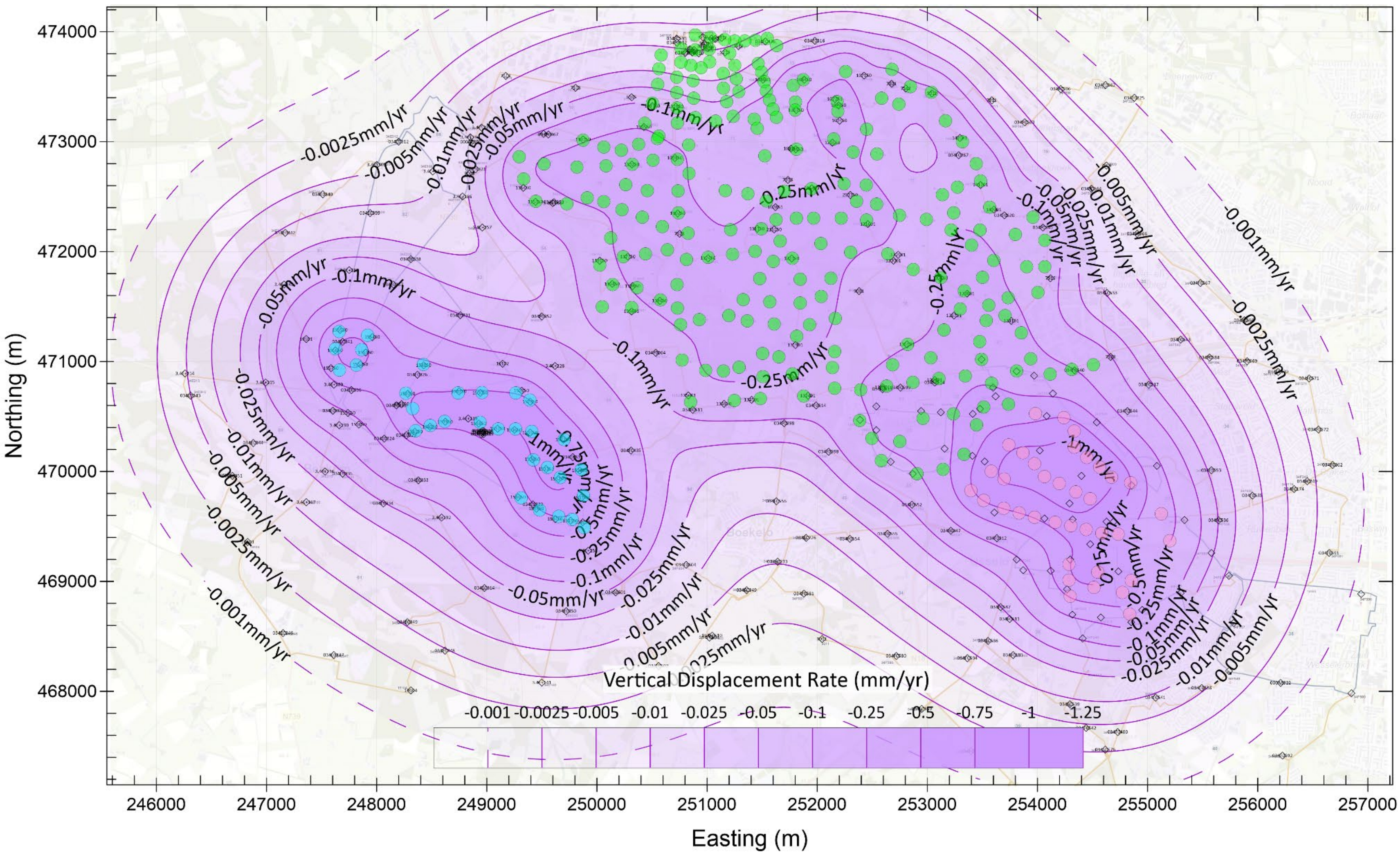

Figure 3-2. Vertical Displacement Rate (Millimeters per Year) Predicted Over the Hengelo, Usseler Es, and Ganzebos Brinefields in Year 2100.

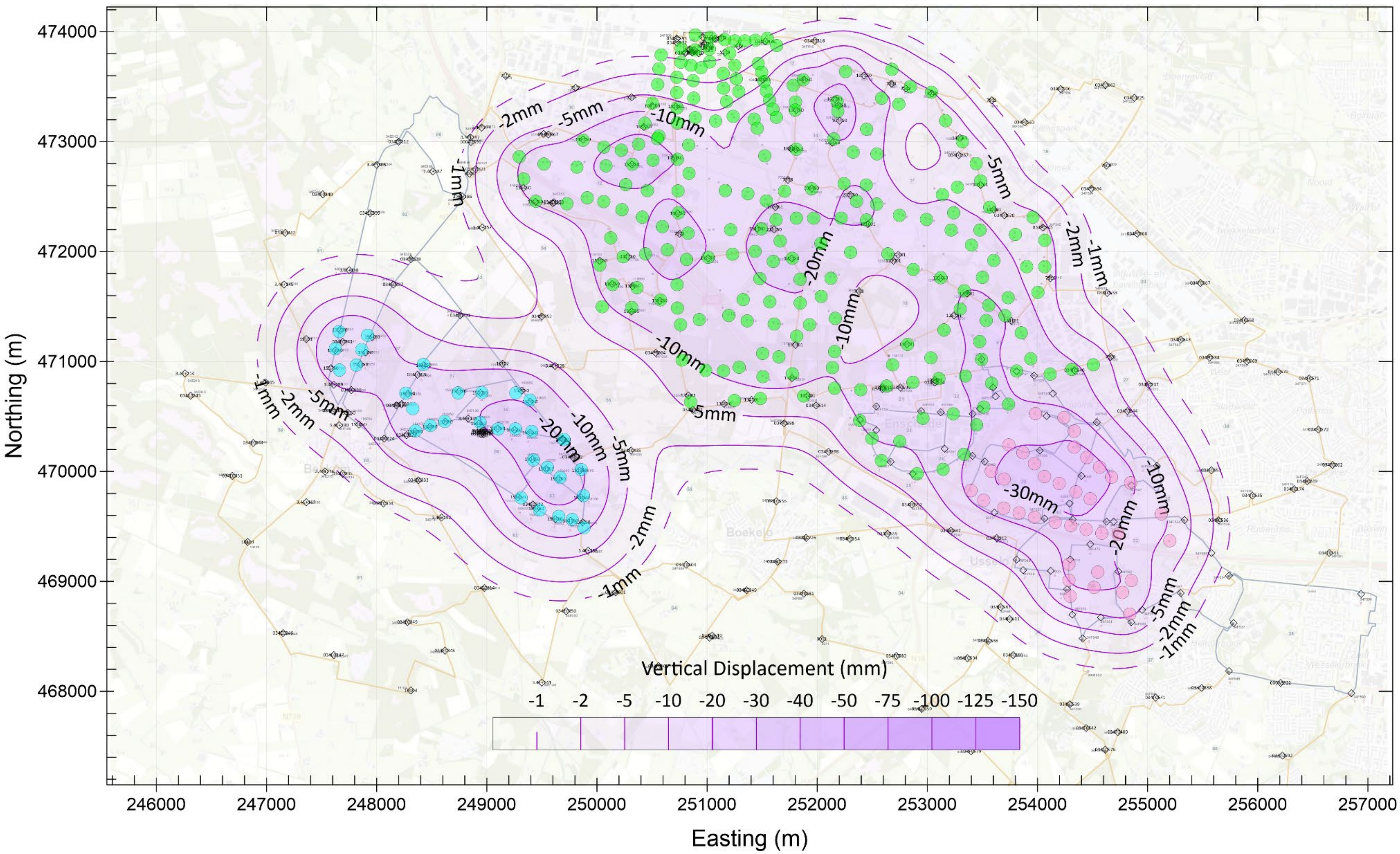

Figure 3-3. Vertical Displacement (Millimeters) Predicted Over the Hengelo, Usseler Es, and Ganzebos Brinefields in Year 2050.

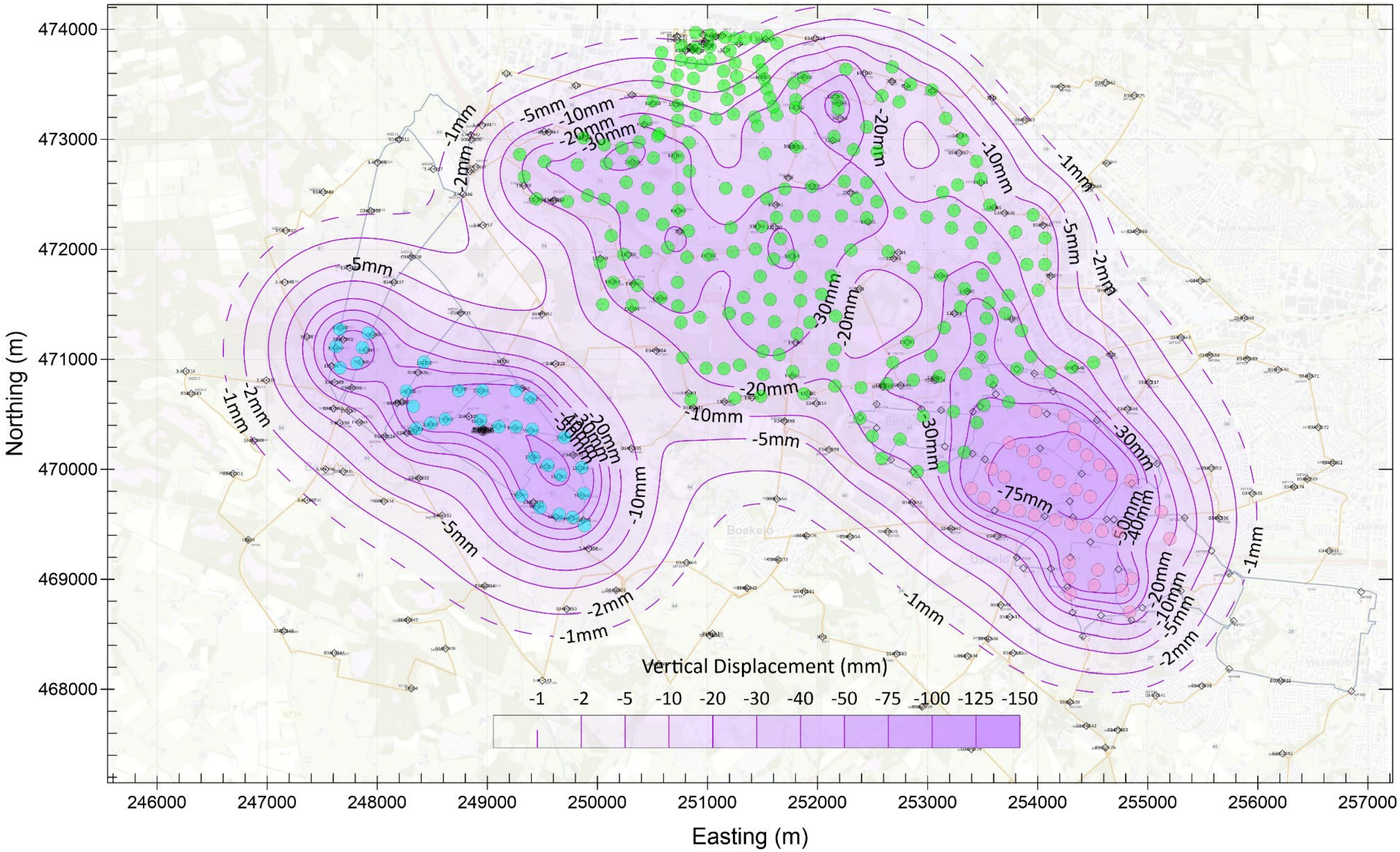

Figure 3-4. Vertical Displacement (Millimeters) Predicted Over the Hengelo, Usseler Es, and Ganzebos Brinefields in Year 2100.

Figures 3-5 and 3-6 show contours of the predicted extensional and compressional strains (microstrain). These figures also illustrate the impact that the current brinefield solution-mining plan will have on the ground surface in Years 2050. The smallest contour in each figure is 10 microstrain, which is an arbitrary cutoff of the actual strain distribution. An examination of the contours reveals that the greatest extensional strains (blue contour lines) occur around the perimeter of the brinefield and the greatest compressional strains (yellow contour lines) occur near the center of the brinefield. The maximum predicted extensional strain in Year 2050 is 24 microstrain and occurs south of the Phase I caverns, while the maximum compressional strain of –51 microstrain is predicted east of the Phase I caverns. These horizontal strain magnitudes are less than the established threshold level, indicating negligible-to-slight damage to surface structures and infrastructure (1,000 microstrain).

Figures 3-7 and 3-8 show contours of the predicted extensional and compressional strains (microstrain). These figures also illustrate the impact the current brinefield solution-mining plan will have on the ground surface in Years 2100. At Year 2100, the maximum predicted extensional and compressional strains are 50 microstrain and -105 microstrain, respectively. The location of the maximum extensional strain is predicted to occur on the surface overlying the Usseler Es brinefield. The maximum compressional occurs over the Ganzebos brinefield. These results suggest that the horizontal extensional and compressional strains that will accumulate in Year 2100 from the continued closure of the brinefield caverns are less than the threshold for negligible-to-light damage (±1,000 microstrains) and not expected to impact the surface structures and infrastructures.

3.1.3 GROUND-SURFACE TILT

Ground-surface tilt occurs from nonuniform surface displacement and is generally greatest near the underground mine perimeter. The tilt of tall structures with narrow foundation widths relative to their heights (e.g., towers) may cause a lateral shift in the center of gravity, which could cause load redistribution over the supporting foundation. Ground-surface tilt may also cause asymmetric loading on sensitive machinery, altering the grade and drainage in buried water, sewer, and pipelines.

The contours of the predicted tilts (mm/km) attributed to the continued convergence of the current brinefield solution-mining plan in Years 2050 and 2100 are shown in Figures 3-9 and 3-10, respectively. The smallest contour in each figure is 20 mm/km, which is an arbitrary cutoff of the actual tilt distribution. The maximum tilt predicted in Year 2050, attributed to the current brinefield solution-mining plan, is 66 mm/km. At Year 2100, the maximum tilt magnitude increases to 179 mm/km, which is significantly less than the established threshold of negligible-to-slight damage (2,000 mm/km). *These results suggest that the surface tilts expected to accumulate in Year 2100 from the continued closure of the brinefield caverns are unlikely to cause negligible-to-slight damage to surface structures and infrastructure.*

3.2 CONTRIBUTION OF THE USSELER ES AND GANZEBOS BRINEFIELDS

The previous section presented the total subsidence that is anticipated to accumulate on the surface from the continued convergence of the current and future caverns since mining began in 1935. To illustrate the impact that the Usseler Es and Ganzebos brinefields will have on the subsidence

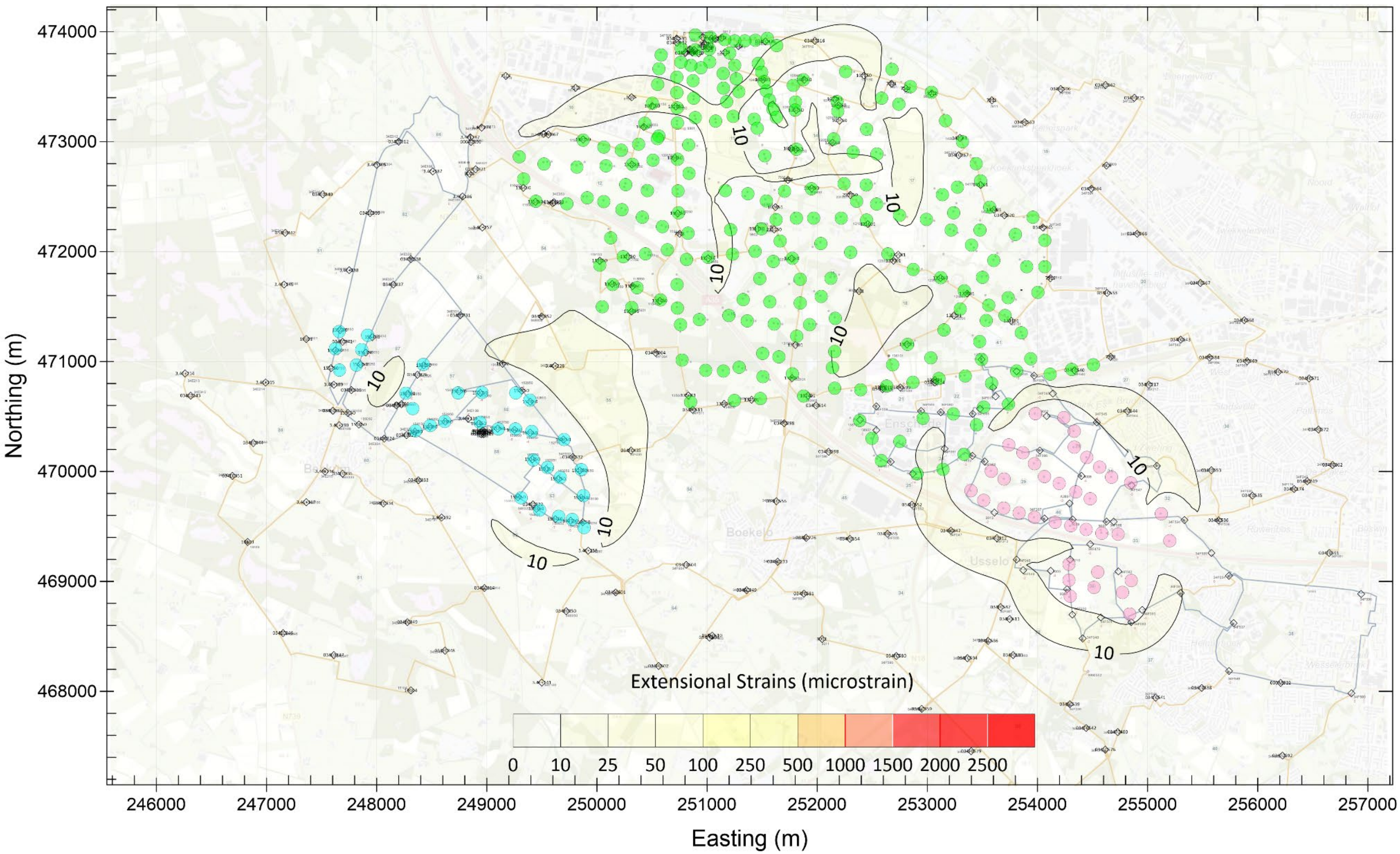

Figure 3-5. Horizontal Extensional Strain (Microstrain) Predicted Over the Hengelo, Usseler Es, and Ganzebos Brinefields in Year 2050.

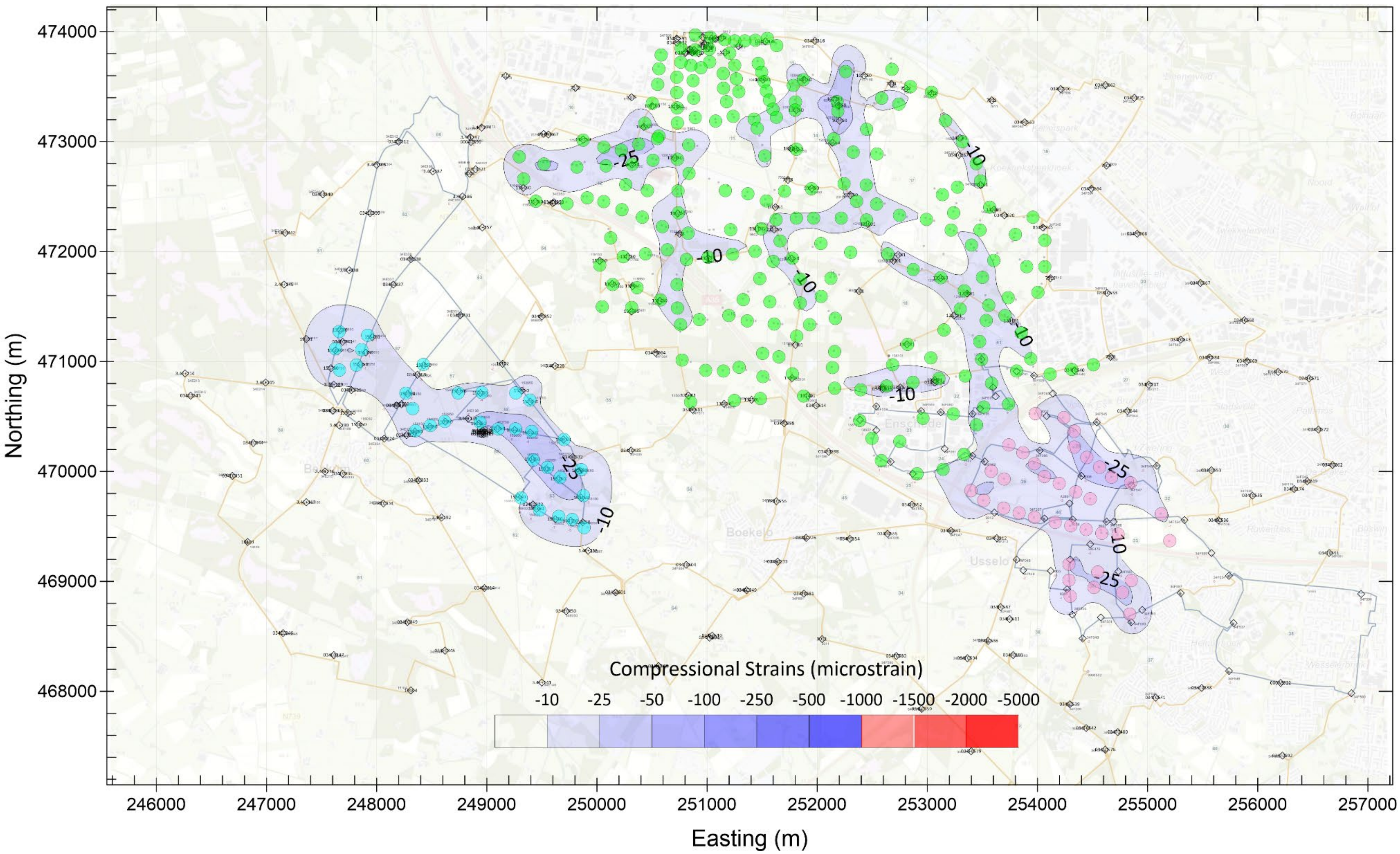

Figure 3-6. Horizontal Compressional Strain (Microstrain) Predicted Over the Hengelo, Usseler Es, and Ganzebos Brinefields in Year 2050.

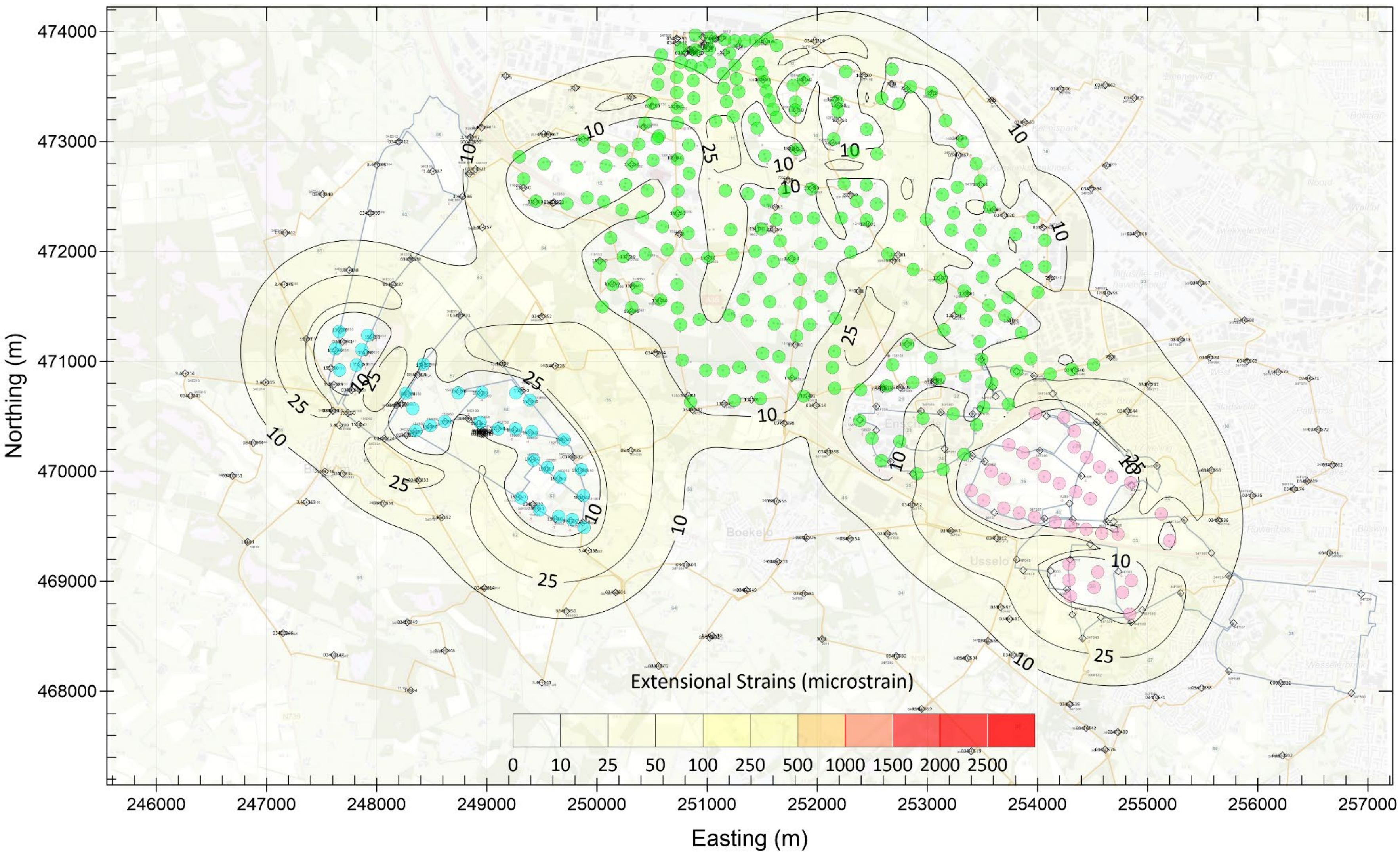

Figure 3-7. Horizontal Extensional Strain (Microstrain) Predicted Over the Hengelo, Usseler Es, and Ganzebos Brinefields in Year 2100.

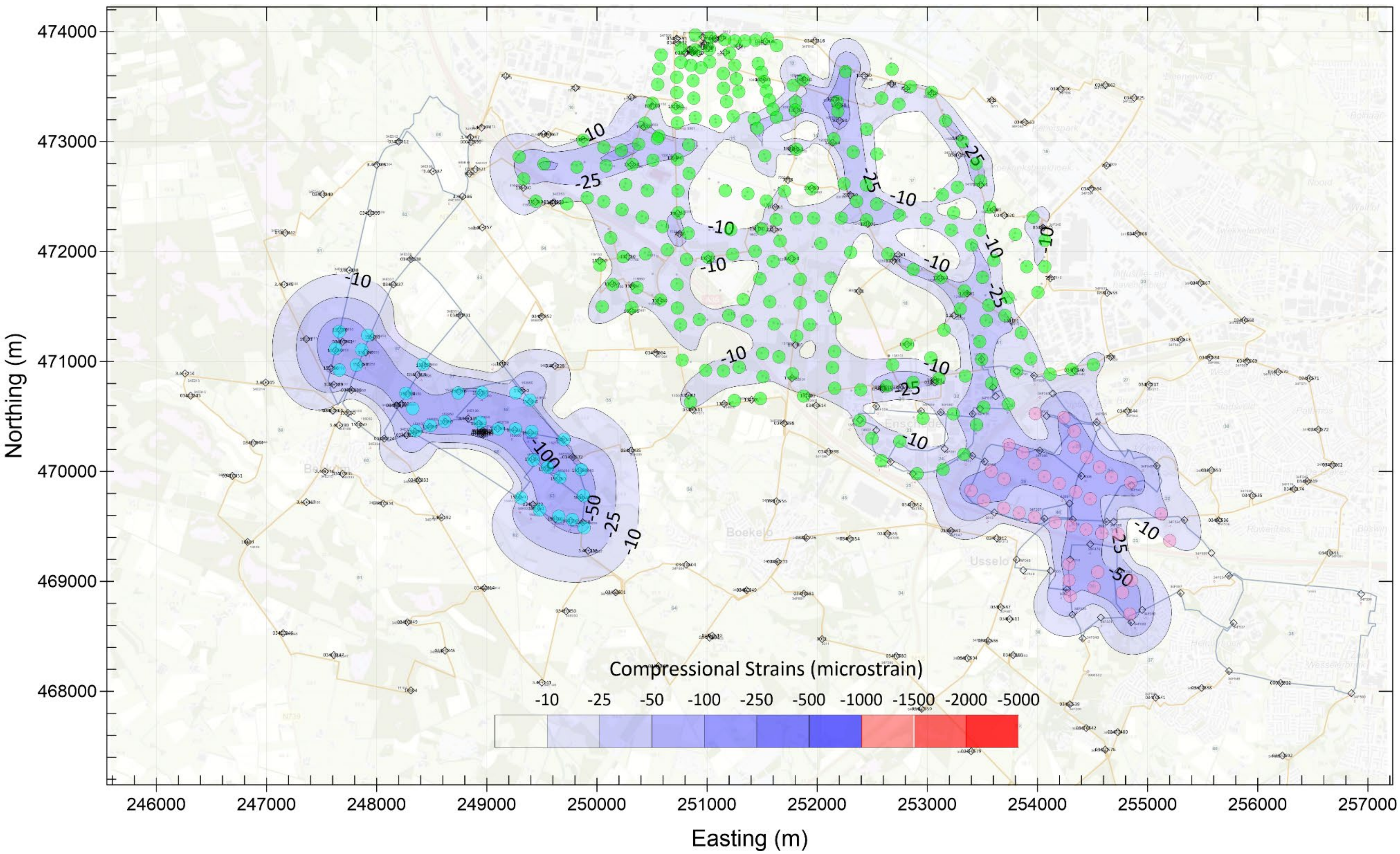

Figure 3-8. Horizontal Compressional Strain (Microstrain) Predicted Over the Hengelo, Usseler Es, and Ganzebos Brinefields in Year 2100.

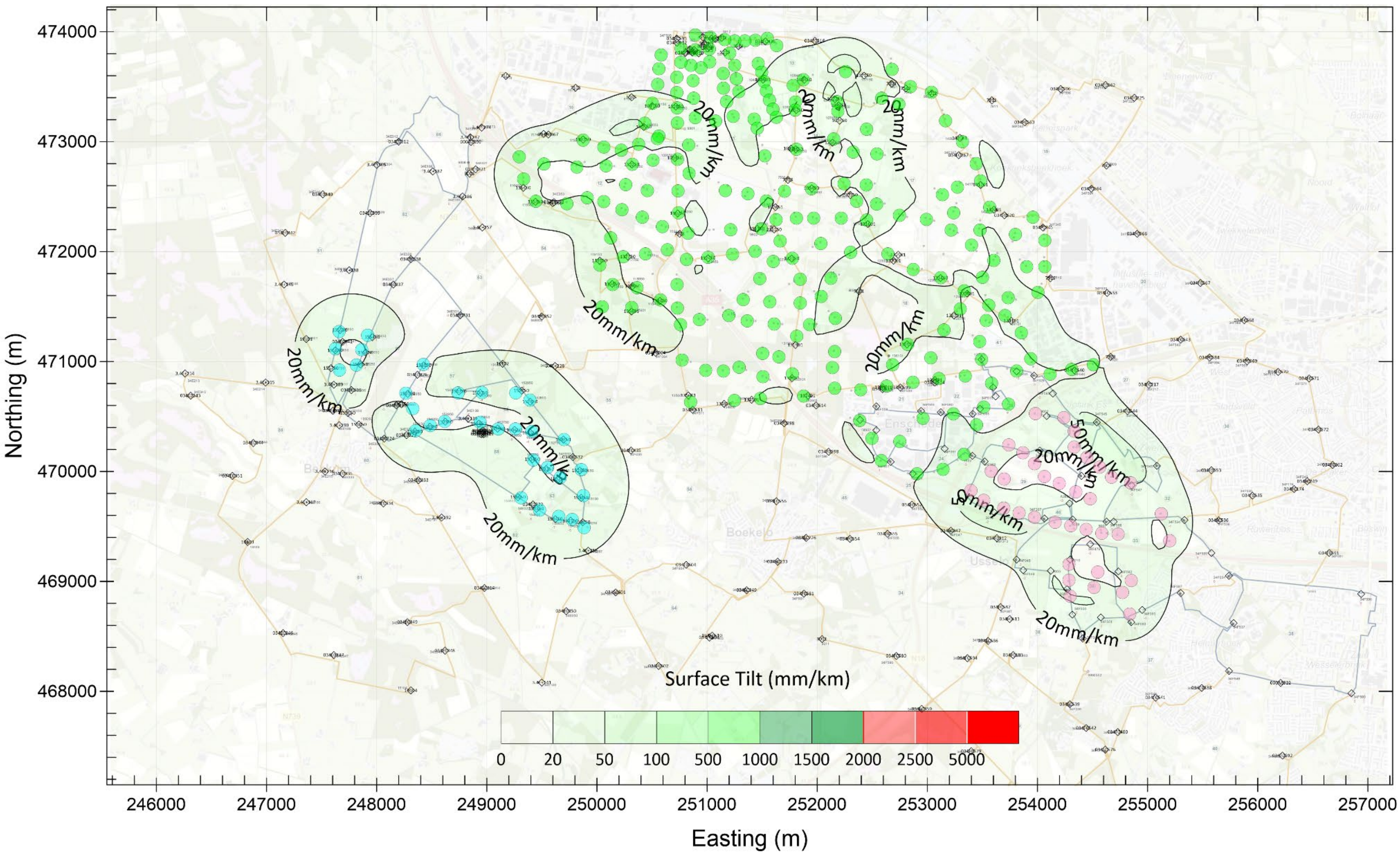

Figure 3-9. Ground-Surface Tilt (Millimeter per Kilometer) Predicted Over the Hengelo, Usseler Es, and Ganzebos Brinefields in Year 2050.

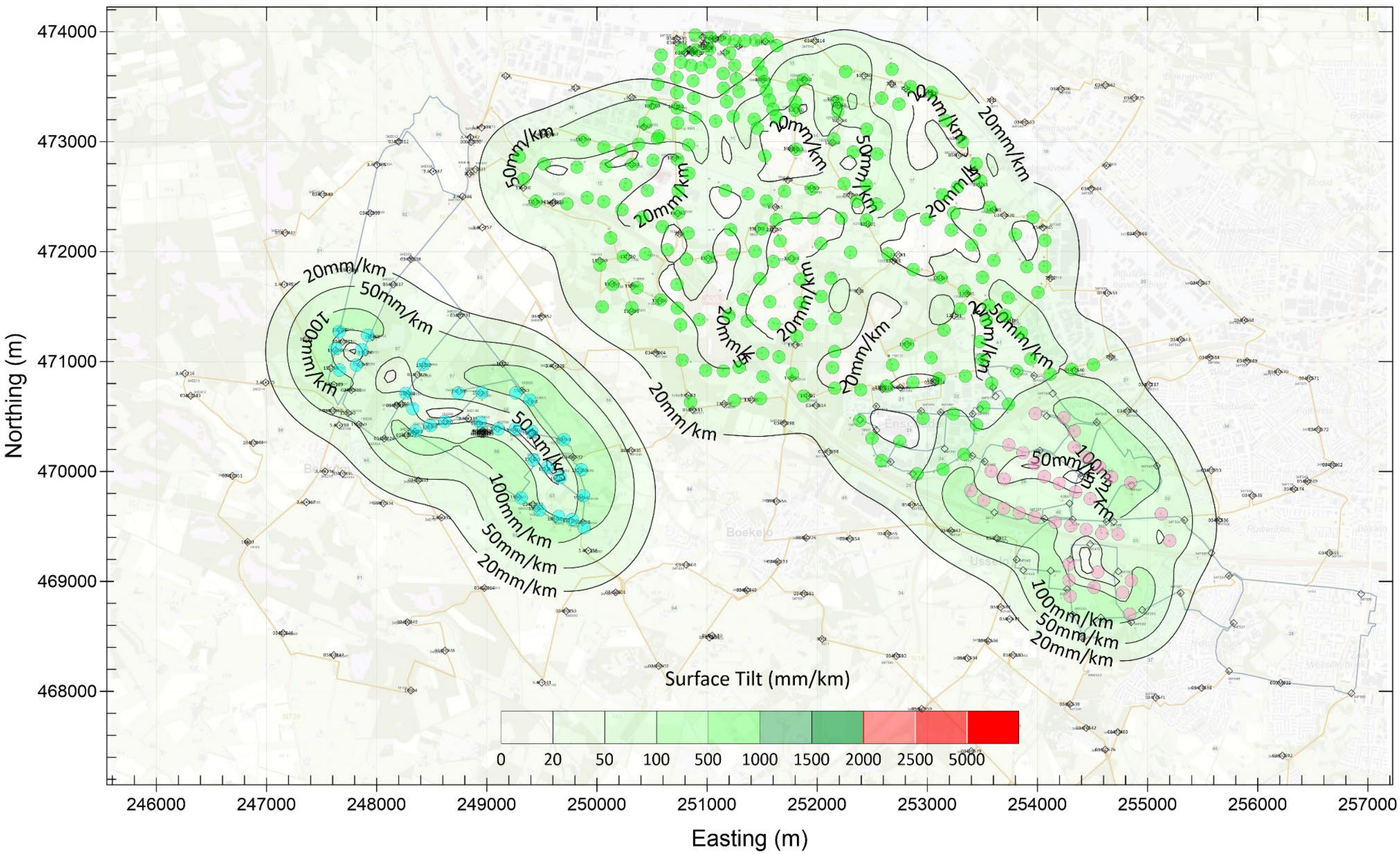

Figure 3-10. Ground-Surface Tilt (Millimeter per Kilometer) Predicted Over the Hengelo, Usseler Es, and Ganzebos Brinefields in Year 2100.

distribution, the following results discuss the incremental increase in subsidence and subsidence rate that can likely be only attributed to the continued convergence of the Usseler Es and Ganzebos brinefields.

3.2.1 USSELER ES BRINEFIELD

Figures 3-11 and 3-12 show the incremental vertical displacement (millimeters) that is only attributed to the development of the Usseler Es brinefield in Years 2050 and 2100, respectively; the subsidence attributable to other brinefields was disregarded. These results suggest that the maximum incremental subsidence that can likely be attributed to the Usseler Es brinefield in Year 2050 is 35 mm, occurs on the surface directly overlying Usseler Es brinefield, and diminishes radially away from the cavern locations. The predicted maximum vertical displacement that will likely accumulate in 2100 can be attributed to the Usseler Es brinefield approaches 95 millimeters.

Figures 3-13 and 3-14 show contours of the predicted incremental vertical displacement rate (mm/yr) attributed to the Usseler Es brinefield in Years 2050 and 2100, respectively. The figures illustrate the impact that the Usseler Es brinefield will have on the response of the ground surface. The smallest contour of vertical displacement is 0.1 mm/yr, which is an arbitrary cutoff of the actual vertical displacement distribution. As expected, the surface regions with the greatest subsidence rates correspond to areas above the cavern field where the greatest salt volume will have been extracted. If all of the 37 Usseler Es caverns are developed, the maximum predicted subsidence rate in Year 2050 will be 1.2 mm/yr and is nearly identical to the maximum subsidence rate predicted in Year 2100, which is 1.2 mm/yr.

3.2.2 GANZEBOS BRINEFIELD

Figures 3-15 and 3-16 show the incremental vertical displacement (in mm) that is only attributed to the development of the Ganzebos brinefield in Years 2050 and 2100, respectively; the subsidence attributable to other brinefields was disregarded. These results suggest that the maximum incremental subsidence that can likely be attributed to the Ganzebos brinefield in Year 2050 is 27 mm, occurring on the surface directly overlying Ganzebos brinefield, and diminishes radially away from the cavern locations. The predicted maximum vertical displacement that will likely accumulate in 2100 that can be attributed to the Ganzebos brinefield approaches 80 millimeters.

Figures 3-17 and 3-18 show contours of the predicted incremental vertical displacement rate (mm/yr) attributed to the Ganzebos brinefield in Years 2050 and 2100, respectively. The figures illustrate the impact that the Ganzebos brinefield will have on the response of the ground surface. The smallest contour of vertical displacement is 0.1 mm/yr, which is an arbitrary cutoff of the actual vertical displacement distribution. As expected, the surface regions that have the greatest subsidence rates correspond to areas above the cavern field where the greatest salt volume will have been extracted. If all of the 37 Ganzebos caverns are developed, the maximum predicted subsidence rate in Year 2050 will be 1 mm/yr, which is nearly identical to the maximum subsidence rate predicted in Year 2100, which is 1 mm/yr.

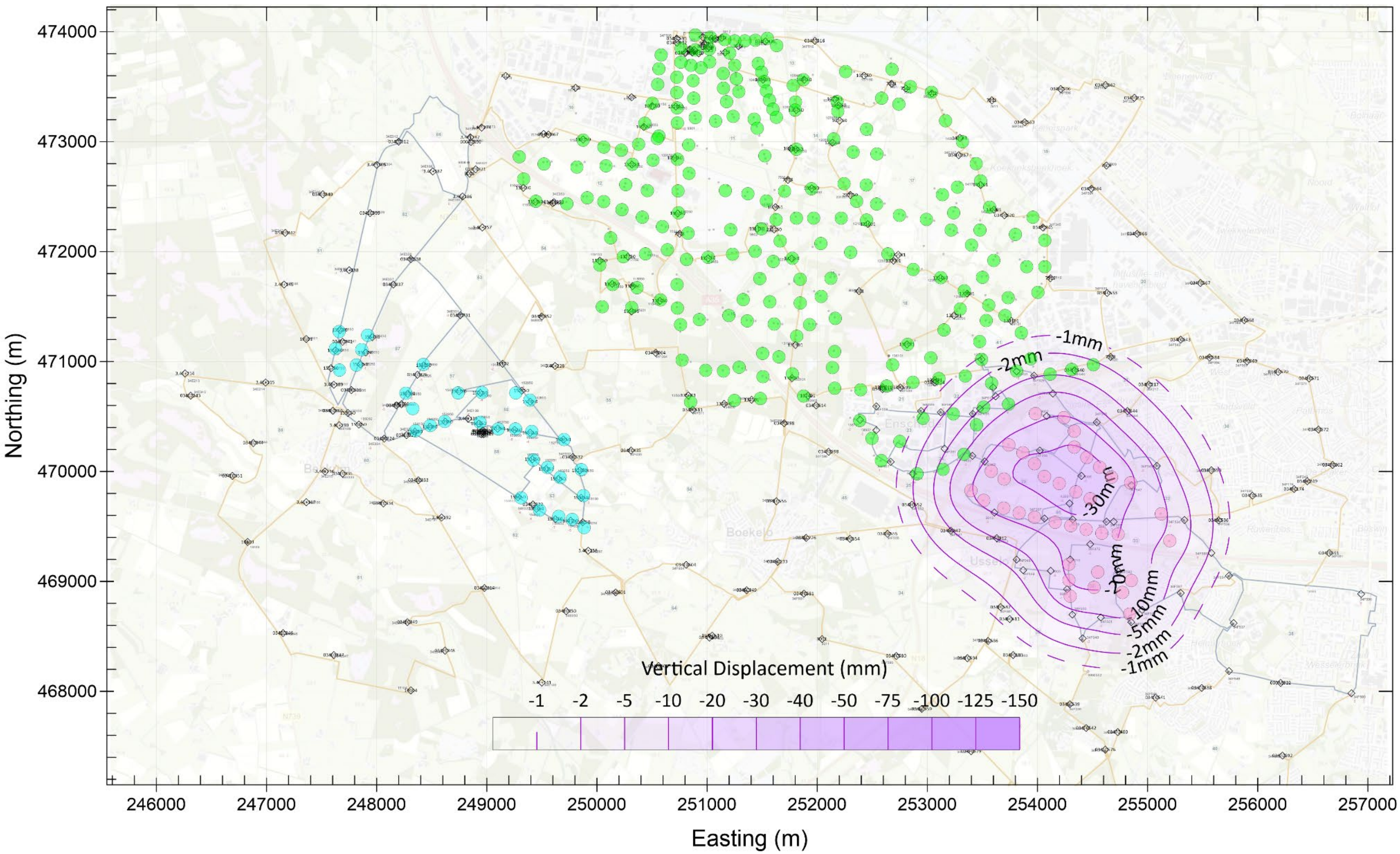

Figure 3-11. Incremental Vertical Displacement (Millimeters) Attributed to the Usseler Es Caverns in Year 2050.

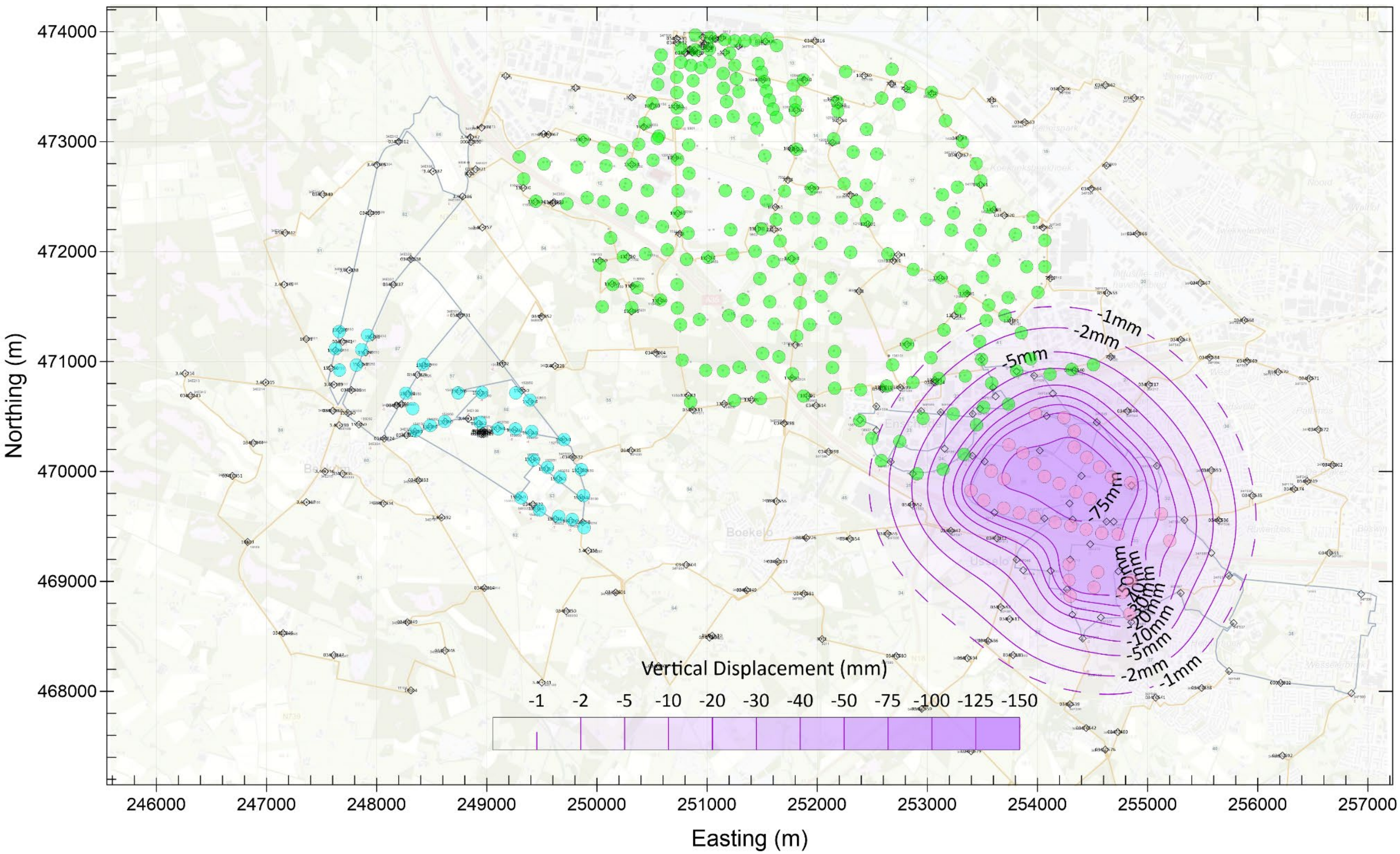

Figure 3-12. Incremental Vertical Displacement (Millimeters) Attributed to the Usseler Es Caverns in Year 2100.

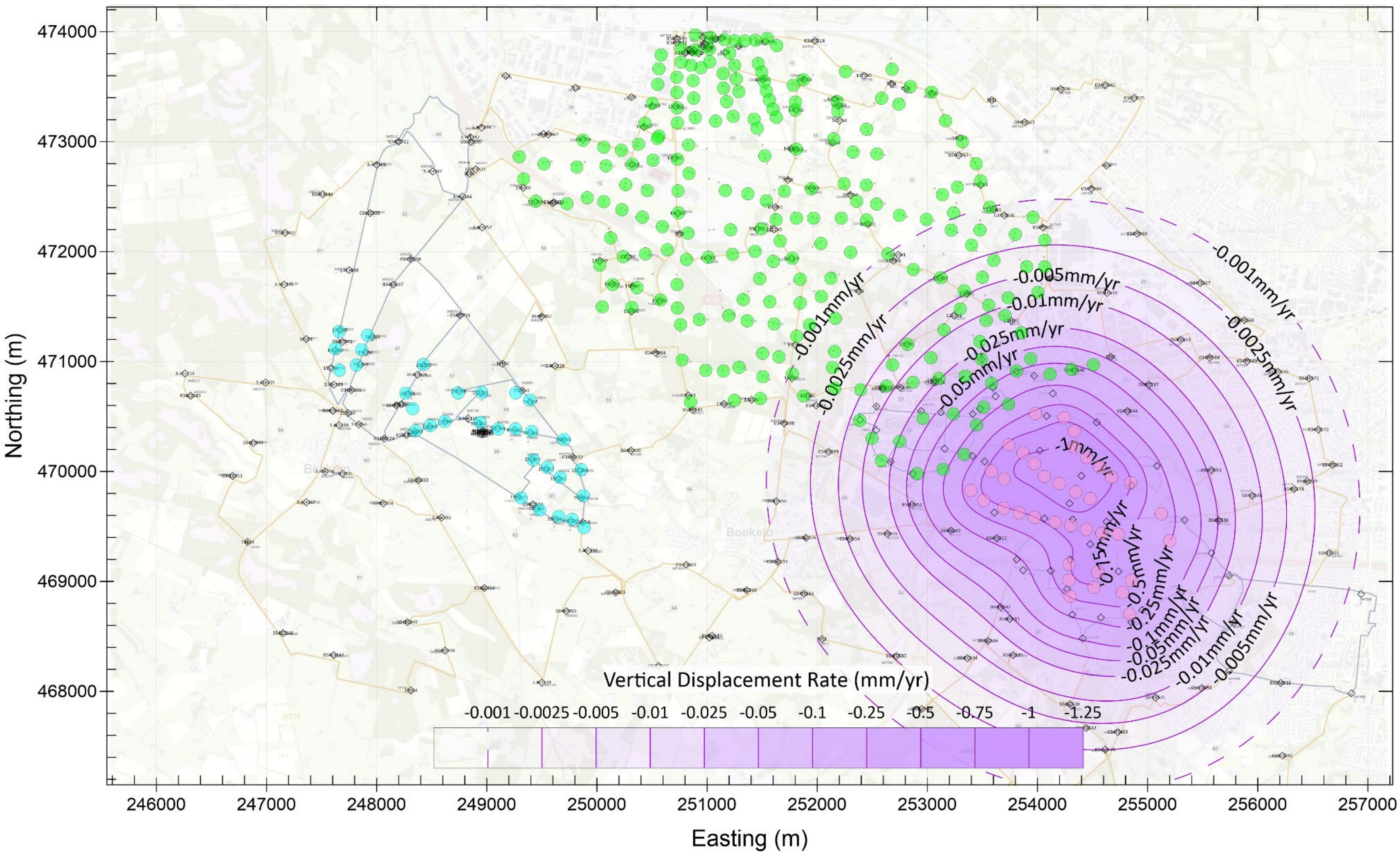

Figure 3-13. Incremental Vertical Displacement Rate (Millimeters per Year) Attributed to the Usseler Es Caverns in Year 2050.

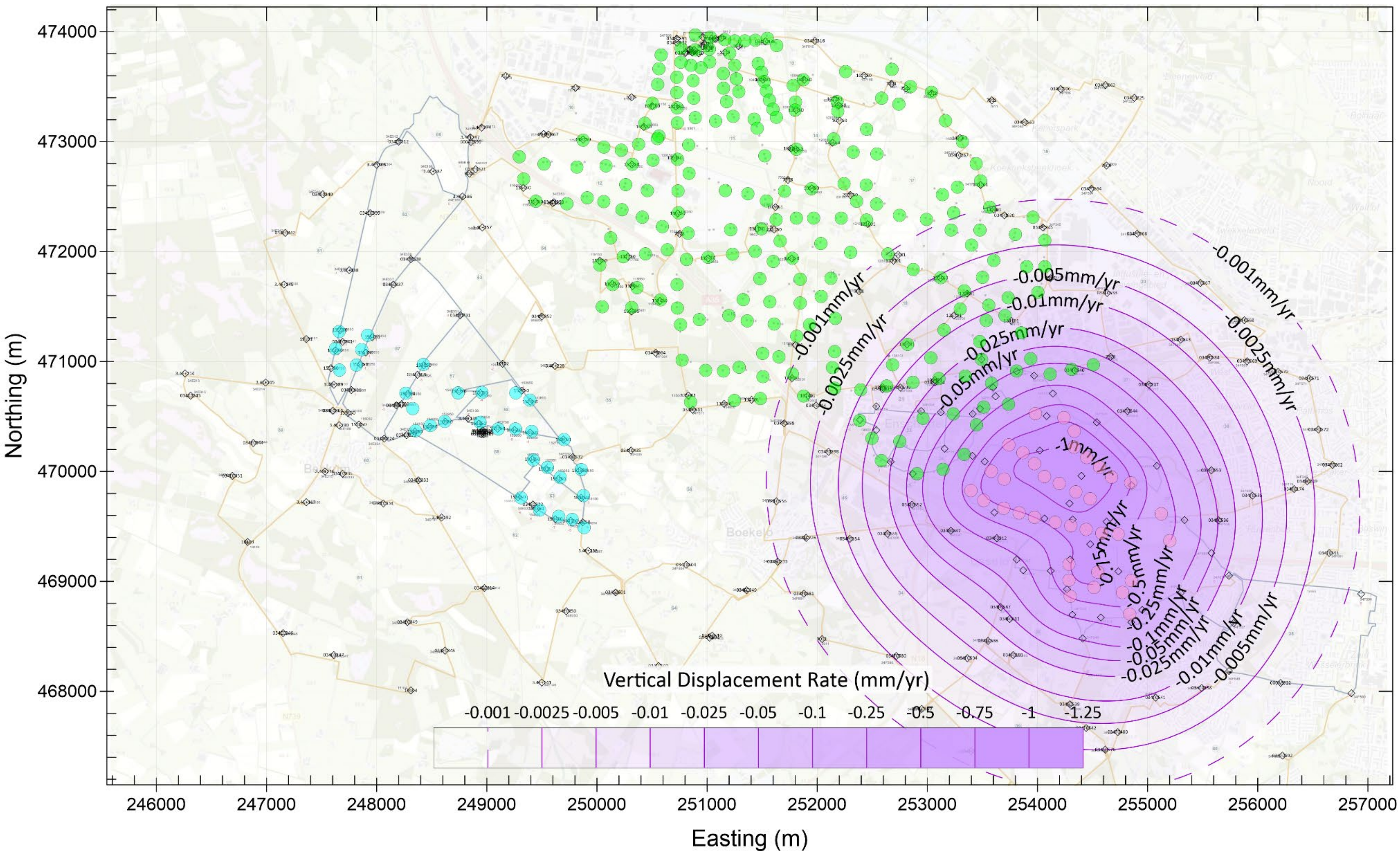

Figure 3-14. Incremental Vertical Displacement Rate (Millimeters per Year) Attributed to the Usseler Es Caverns in Year 2100.

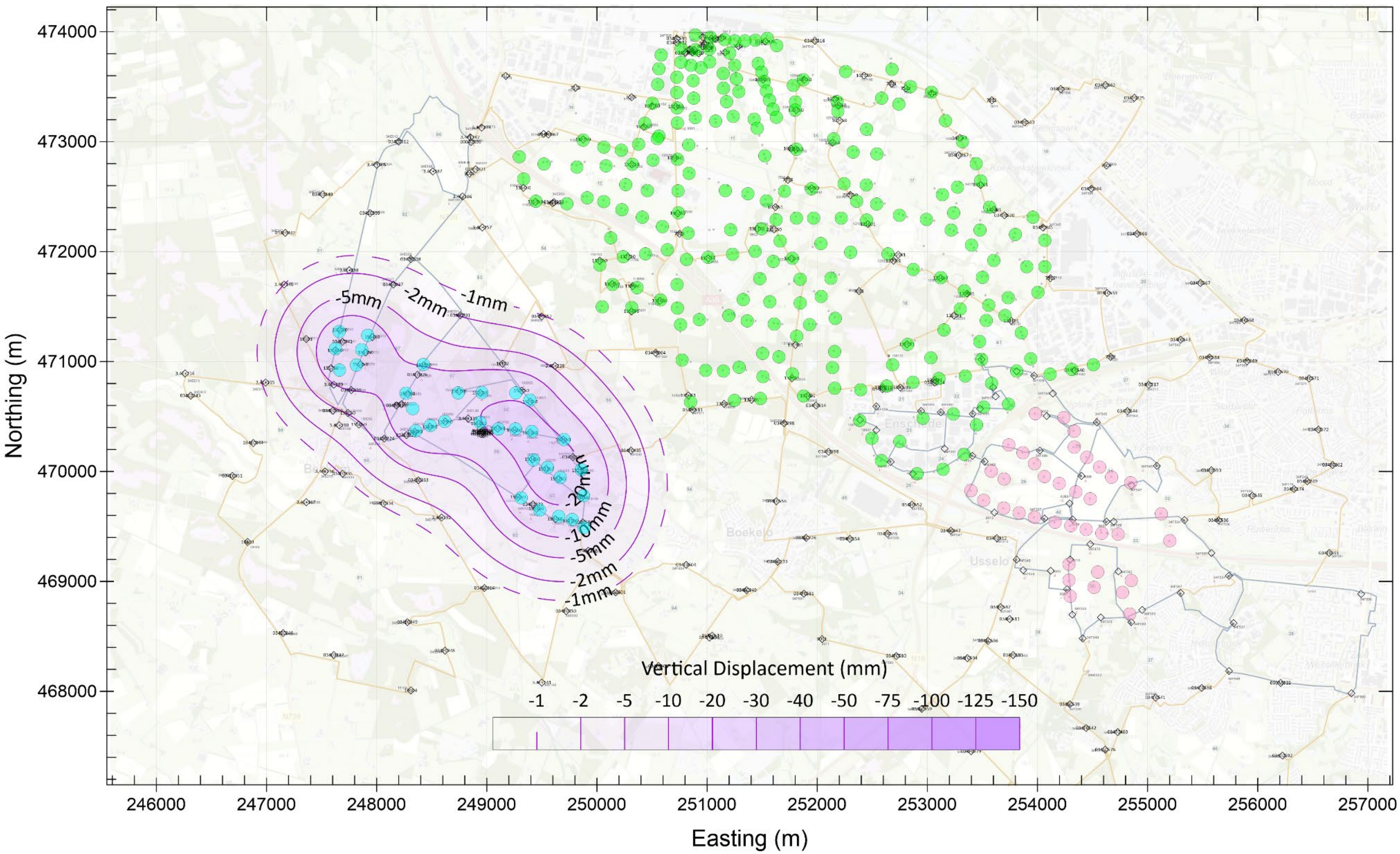

Figure 3-15. Incremental Vertical Displacement (Millimeters) Attributed to the Ganzebos Caverns in Year 2050.

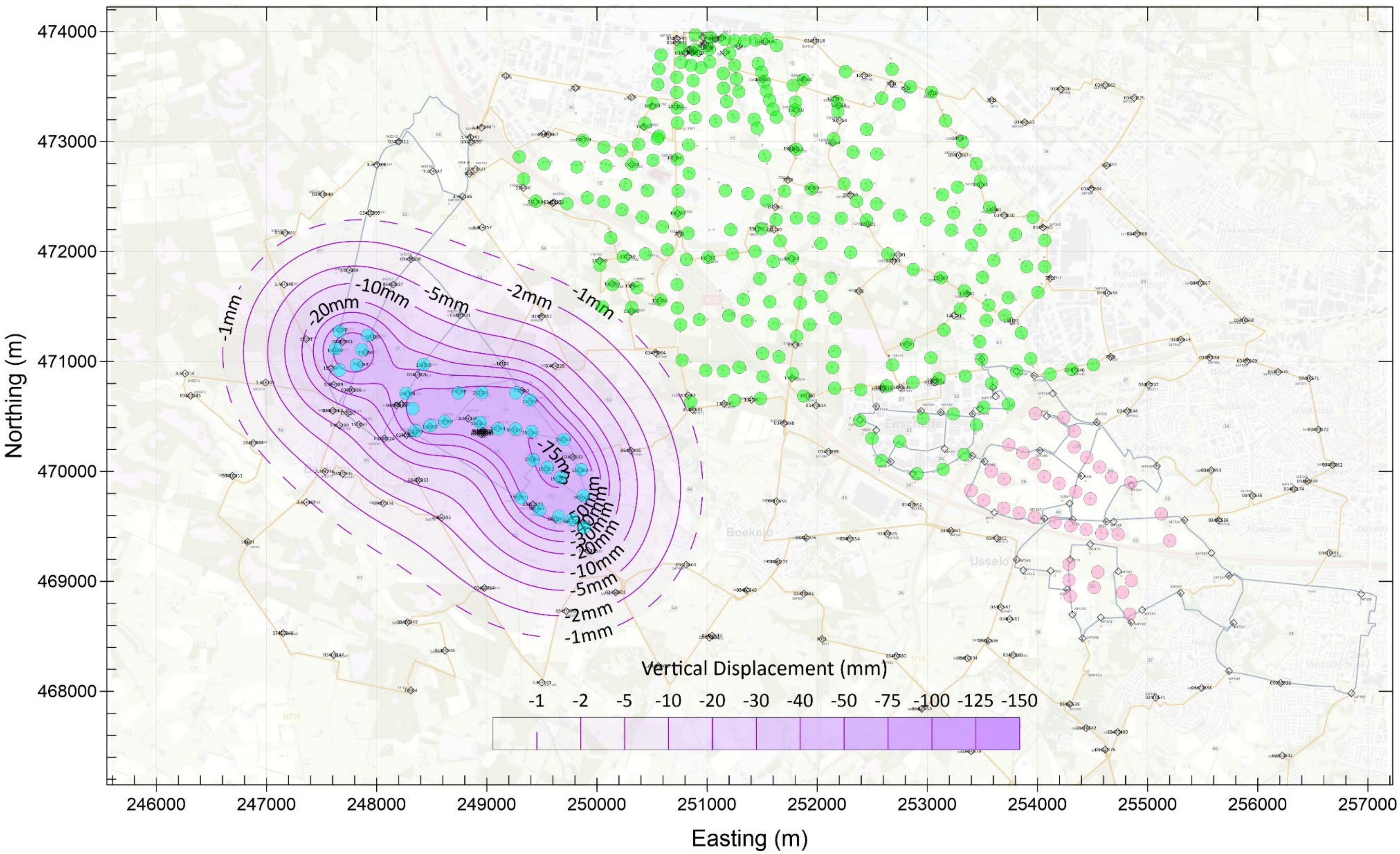

Figure 3-16. Incremental Vertical Displacement (Millimeters) Attributed to the Ganzebos Caverns in Year 2100.

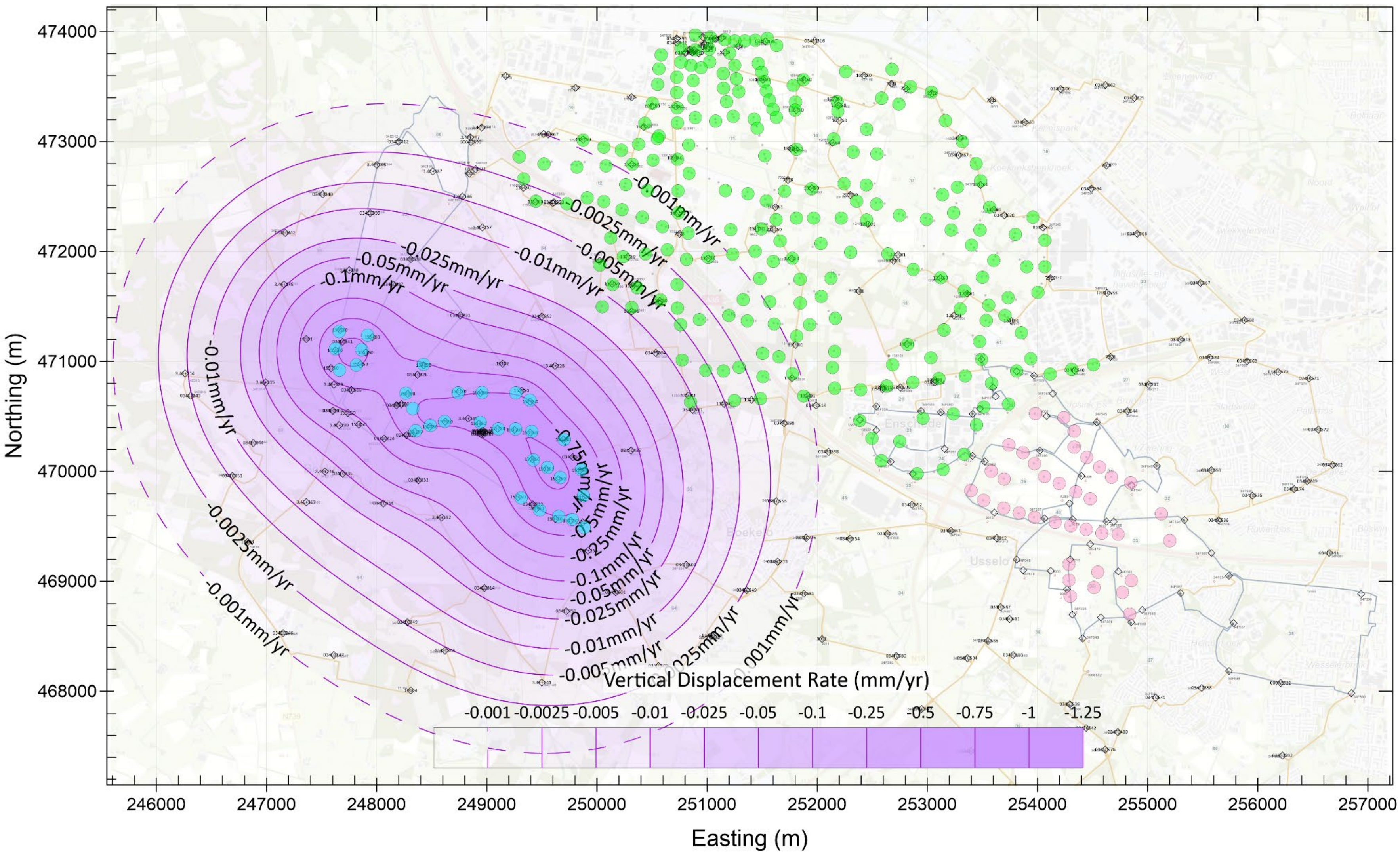

Figure 3-17. Incremental Vertical Displacement Rate (Millimeters per Year) Attributed to the Ganzebos Caverns in Year 2050.

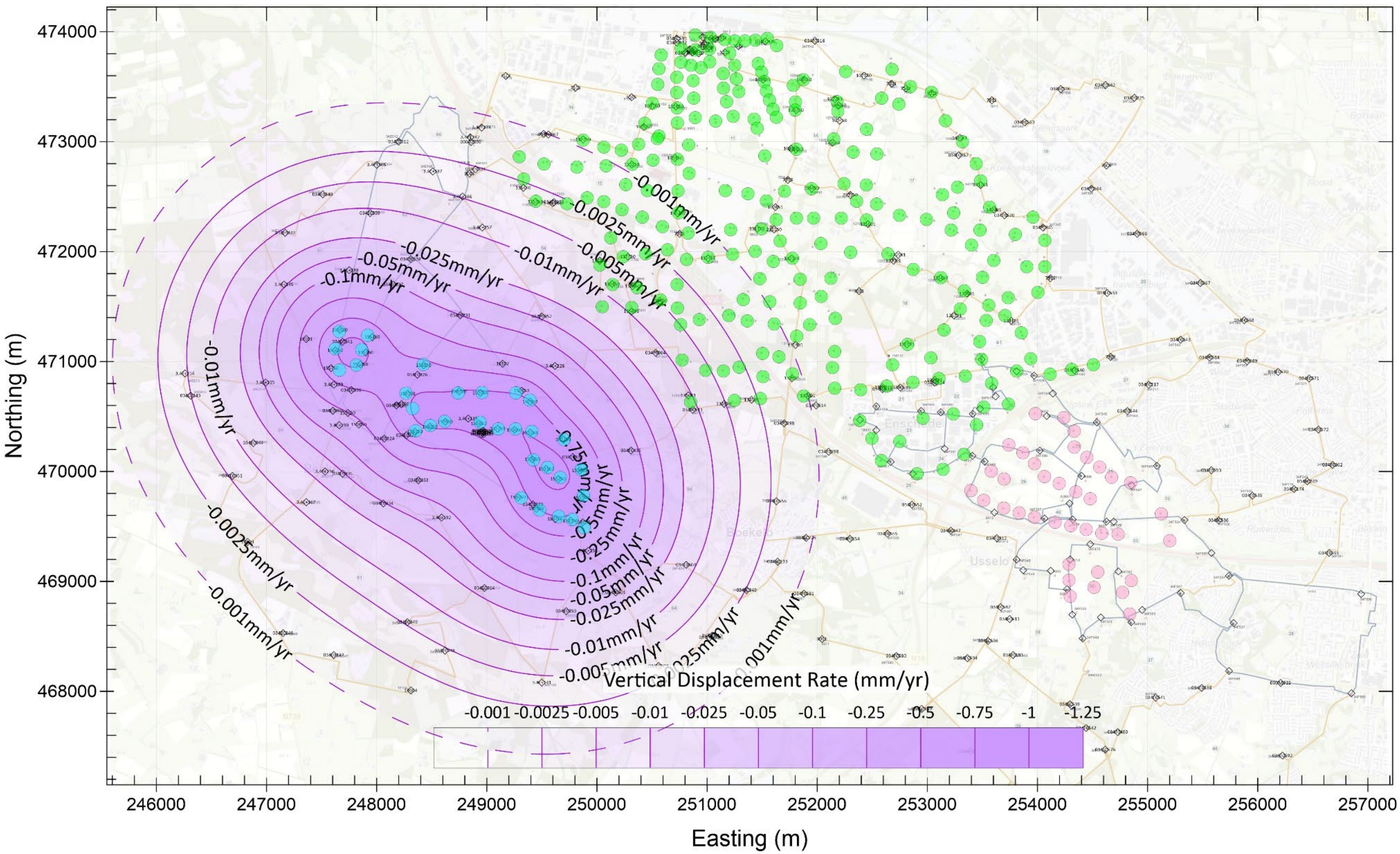

Figure 3-18. Incremental Vertical Displacement Rate (Millimeters per Year) Attributed to the Ganzebos Caverns in Year 2100.

4.0 SUMMARY AND CONCLUSIONS

The primary objective of this subsidence study was to reevaluate the closure model parameter values for the Hengelo, Usseler Es, and Ganzebos brinefields to more accurately represent the short-term subsidence attributed to the closure of the brine caverns and the long-term, steady-state closure rate that have been proven over the Hengelo brinefield. Subsidence calculations represented the progressive development of the Hengelo, Usseler Es, and Hengelo brinefields annually based on actual mining dates and cavern volume growth rates. However, the Phase 1 caverns (i.e., 1 through 50) at the Hengelo brinefield were excluded because other processes (i.e., cavern migrations) are having a greater influence on the subsidence that manifests on the surface that typical cavern convergence attributed to salt creep. The simulations then calculated the ground-surface response that could be attributed to mine closure until Year 2125. Tables 4-1, 4-2, and 4-3 provide the maximum predicted subsidence values overlying the Hengelo, Usseler Es, and Ganzebos brinefields, respectively. The predicted values of vertical displacement, ground-surface tilt, and horizontal strain were compared to established damage-avoidance threshold values to assess the potential impact that mining-induced subsidence will have on the ground-surface response and delineate regions on the surface that may suffer adversely from continual convergence of the mine.

Table 4-1. Subsidence Component Maximum Value Predicted in 2025, 2050, 2075, 2100, and 2125 Over the Hengelo Brinefield

Year	Vertical Displacement (mm)	Vertical Displacement Rate (mm/yr)	Extensional Horizontal Strain (microstrain)	Compressional Horizontal Strain (microstrain)	Ground Surface Tilt (mm/km)
2025	–18	–0.4	16	–33	43
2050	–27	–0.4	24	–51	64
2075	–37	–0.4	32	–67	86
2100	–46	–0.4	40	–84	107
2125	–55	–0.4	47	–101	130

Table 4-2. Subsidence Component Maximum Value Predicted in 2025, 2050, 2075, 2100, and 2125 Over the Usseler Es Brinefield

Year	Vertical Displacement (mm)	Vertical Displacement Rate (mm/yr)	Extensional Horizontal Strain (microstrain)	Compressional Horizontal Strain (microstrain)	Ground Surface Tilt (mm/km)
2025	–7	–1.0	3	–5	12
2050	–35	–1.2	18	–33	66
2075	–66	–1.2	34	–62	122
2100	–96	–1.2	50	–91	179
2125	–126	–1.2	65	–120	235

Table 4-3. Subsidence Component Maximum Value Predicted in 2025, 2050, 2075, 2100, and 2125 over the Ganzebos Brinefield

Year	Vertical Displacement (mm)	Vertical Displacement Rate (mm/yr)	Extensional Horizontal Strain (microstrain)	Compressional Horizontal Strain (microstrain)	Ground Surface Tilt (mm/km)
2025	–3	–0.5	3	–3	5
2050	–27	–1.1	16	–35	49
2075	–53	–1.1	32	–69	98
2100	–80	–1.1	47	–105	148
2125	–107	–1.1	62	–138	198

The following significant conclusions were made from this study:

- **The ground-surface tilts predicted to accumulate at Year 2100 from the continued convergence of the Hengelo, Usseler Es, and Ganzebos brinefields are not expected to have an adverse effect on sensitive surface structures and infrastructure.** The maximum ground-surface-tilt magnitudes predicted surrounding the underground workings at Year 2100 is 179 mm/km. These values are less than the 2,000 mm/km threshold limit for negligible-to-slight damage, suggesting that the continued development and convergence of the brinefields are not expected to impact sensitive surface structures and infrastructure in 2100.
- **The extensional and compressional strains predicted to accumulate at Year 2100 from the continued convergence of the Hengelo, Usseler Es, and Ganzebos brinefields are not expected to have an adverse effect on sensitive surface structures and infrastructure.** The maximum extensional and compressional strains predicted to occur on the surface are less than 50 and –105 microstrain, respectively. The strains are well below a damage threshold limit of 1,000 microstrain, suggesting that the continued development and convergence of the brinefields are not expected to impact surface structures, such as buildings, roads, and pipelines, in 2100.
- **The total vertical displacements that are predicted to accumulate at Year 2100 from the continued convergence of the Hengelo, Usseler Es, and Ganzebos brinefields may approach 96 mm, but are not expected to have an adverse effect on surface drainage.** The predicted vertical displacements that overlie the brinefields had a maximum vertical displacement approaching 96 mm over the Usseler Es brinefield in Year 2100. The continued convergence of the Usseler Es and Ganzebos brinefields are expected to result in incremental vertical displacements on the surface that approach 95 and 80 mm, respectively. These displacement magnitudes are less than the damage threshold limit of 150 mm, suggesting that the continued convergence of the brinefields is not expected to impact surface drainage in 2100.

As with any excavation in an evaporite medium, the subsidence amount that manifests on the surface will be a function of the amount of removed salt, the volumetric-closure rate of the caverns, and the elapsed time. The simulations in this study assumed that the caverns would continue to close after mining ceases, while the actual subsidence that manifests on the surface will depend on the chosen abandonment plans after mining has ceased. The abandonment plan could significantly reduce the predicted magnitudes presented. Additionally, no provision was made to reduce the reported cavern volume to account for insoluble material that partially filled the cavern void space. Furthermore, subsequent elevation data collected over the Ganzebos brinefield may indicate a long-term behavior that is typical of other brinefields in the area. Thus, the total subsidence distribution may change, and the presented results will likely overestimate the actual subsidence distributions.

5.0 REFERENCES

Nieland, J. D. and L. L. Van Sambeek, 2010. *SALT_SUBSID, Version 2.0 User's Manual*, Research Report RR2009-02, prepared by RESPEC, Rapid City, SD, and POD, Inc., Albuquerque, NM, for Solution Mining Research Institute, Clarks Summit, PA.

Van Sambeek, L. L., 2008. *Selection of y_{ss} Parameter for SALT_SUBSID*, External memorandum RSI(RCO)-1477/6-08/2 to W. Paar, Akzo Nobel Chemicals, Hengelo, Netherlands, from L. Van Sambeek, RESPEC, Rapid City, SD, United States, June 6.

Vining, C.A. and N. Gupta, 2021a. *Reassessment of the Ganzebos Brinefield*, RSI(RCO)-M0030.21001/8-21/3, prepared by RESPEC, Rapid City, SD, United States, for Els Wijermars, Nobian, Hengelo, Netherlands, August 4.

Vining, C.A. and N. Gupta, 2021b. *Surface Subsidence Investigation of the Usseler Es Brinefield*, RSI(RCO)-M0030.21001/8-21/17 prepared by RESPEC, Rapid City, SD, United States, for Els Wijermars, Nobian, Hengelo, Netherlands, August 11.

APPENDIX A

TECHNICAL INFORMATION SUPPORTING THE SUBSIDENCE EVALUATION OF THE HENGELO, USSELER ES, AND GANZEBOS BRINEFIELD

RESPEC

APPENDIX A: TECHNICAL INFORMATION SUPPORTING THE SUBSIDENCE EVALUATION

The following sections briefly discuss (1) the surface-subsidence components and their potential effects on surface structures and surface and subsurface infrastructure, (2) the damage-avoidance criterion used to assess the potential impacts of ground-surface subsidence, and (3) the development of the subsidence model used to predict the ground-surface response over the Hengelo, Usseler Es, and Ganzebos brinefields.

A.1 GROUND-SURFACE SUBSIDENCE AND THE ASSOCIATED MOVEMENTS

Ground-surface subsidence is a natural, normal, and unavoidable movement of the earth's surface in response to fluids or solids being removed from underground. The term surface subsidence implies the total phenomenon of surface and subsurface movements, which includes vertical and horizontal displacements and the associated forms of ground movement that result from differential (nonuniform) ground. The relationship between the different subsidence components' movement overlying an idealistic opening underground is illustrated in Figure A-1.

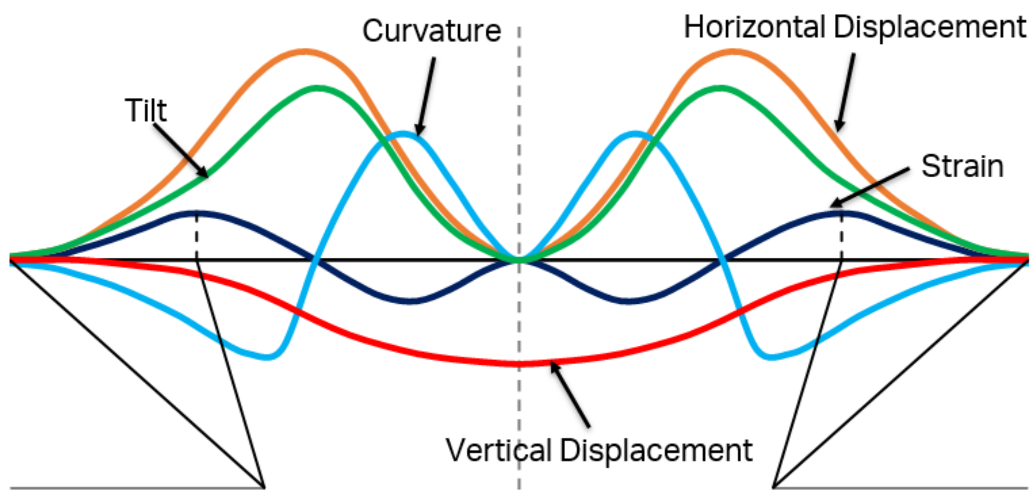

Figure A-1. Components of Ground Movement.

In addition to vertical displacement, additional components include ground-surface tilt, ground-surface curvature, and horizontal extensional and compressional strains. All of these components can affect surface features in different ways. The following sections briefly describe the components and the potential effect on surface structures and surface subsurface infrastructures.

A.1.1 VERTICAL DISPLACEMENT

As shown in Figure A-1, the greatest vertical displacements generally occur at the midspan of the brinefield. The lateral extent of the vertical displacements (i.e., the subsidence bowl) is defined by the angle of draw that is generally a percentage of the ultimate subsidence. For opening in evaporite settings, the volume of the subsidence bowl that manifests on the surface often approaches the volume of ore extracted underground. Vertical displacements of the ground surface have the potential to affect surface-drainage patterns for unfavorable surface topographies and cause rivers to overflow and water to collect in low areas.

A.1.2 GROUND-SURFACE TILT, ANGULAR DISTORTION, AND CURVATURE

Ground-surface tilt is caused by the nonuniform displacement of the surface and is expressed as a change in elevation per horizontal unit length (i.e., slope). As shown in Figure A-1, tilt values are generally the greatest near the perimeter of the brinefields, and the point of maximum tilt occurs where the vertical displacement is approximately one-half of its maximum and is the smallest near the center of the subsidence bowl. Tall structures with narrow foundation widths relative to their heights (e.g., towers) are most sensitive to ground-surface tilt. Tilt of tall structures has the potential to cause a significant lateral shift in the center of gravity, which may cause load redistribution over the supporting foundation. Ground-surface tilt also has the potential to cause asymmetric loading on sensitive machinery (i.e., the mine hoist) within the structures and alter the grade and drainage in buried water, sewer, and pipelines.

Differential vertical displacements have the potential to cause an angular distortion of a structure's walls (i.e., racking) that may cause brickwork, drywall, and plaster to crack; door and window frames to distort; stair-steps to crack; and floors to shift. The severity of the damage will depend on the walls' orientation, with the greatest distortion occurring when the wall is parallel to the direction of maximum slope (on a dip), while walls that are orientated perpendicular to the direction of maximum slope (on strike) may experience little or no distortion. Buildings have a certain amount of rigidity that provides some resistance to angular distortion; however, this benefit is difficult to estimate and is conservatively ignored in this analysis. Therefore, the angular distortion is assumed to be the same as the predicted tilt, which limits the need for two separate criteria.

A change in the slope along the subsidence bowl profile will warp the ground surface from its original shape to a curved profile. Positive curvature (concave upward) may cause stiff foundations to become mostly supported at their ends and relatively unsupported in their centers. Negative curvature (convex upward) may cause stiff foundations to become supported at their centers and relatively unsupported at their ends. Other types of ground movement, especially horizontal strains, often cause damage before curvature, which limits the requirement for separate curvature criteria.

A.1.3 HORIZONTAL DISPLACEMENT

As shown in Figure A-1, horizontal displacements reach a maximum on the surface just inside the perimeter of the brinefield, at the point where the vertical displacement is approximately one-half the maximum value and no horizontal displacements occur at the midspan of the underground workings. Horizontal displacements have the potential to create frictional forces that affect elongated buildings, railways, and buried pipeline and utility cables. The shifting ground may also alter the passive earth pressures on deep foundations. Rather than considering a maximum magnitude of horizontal displacement, a generally accepted practice for assessing potential damage is to consider the induced horizontal strains.

A.1.4 HORIZONTAL EXTENSIONAL AND COMPRESSIONAL STRAINS

Differential horizontal displacement causes a lengthening and shortening of the ground surface (i.e., horizontal strains). As shown in Figure A-1, a lengthening of the ground surface occurs where the ground surface becomes convex along the perimeter of the brinefield, and a shortening of the ground surface occurs where the surface becomes concave (near the midspan of the brinefield). The transition from extensional to compressional strain occurs just inside the perimeter of the brinefield (at the point where the horizontal displacements are greatest). Horizontal strains can potentially damage linear structures (e.g., elongated buildings, roads, and pipelines) that are unfavorably orientated by stretching (extensional strains) or compressing (compressional strains) the structure. As the strains are transferred to the structures, surface cracks may form in high extensional strain zones, and bulging may occur in high compression areas.

A.2 DAMAGE-AVOIDANCE CRITERIA

Selecting an appropriate damage-avoidance criterion for each subsidence-related type of damage is not straightforward. The type of damage and severity level depends on the specific subsidence effect and structure type. The factors that describe the structure type as they influence the subsidence-induced damage include the following:

- Foundation (e.g., concrete slab or piles and footings)
- Soil-to-structure interaction (e.g., footings and piles)
- Structural rigidity (e.g., frame type and building materials)
- Structure use and crack/distortion tolerance (e.g., residential versus office or factory).

The severity of the structural damage is generally classified as follows:

- **Architectural:** Architectural damage affects appearance and is usually related to hairline cracks or separations in panel walls, floors, and finishes. Architectural damage is especially noticeable in plaster and wall boards, but the damage does not affect functional use or structural stability.
- **Functional:** Functional damage affects the routine use of the structure, as exemplified by jammed doors and windows, extensively cracked walls, and tilting floors. The damage does not affect the structural stability.
- **Structural:** Structural damage affects the stability of the structure and is usually related to loss of strength or functionality in beams, columns, load-bearing walls, and foundations. Repairs require replacement rather than just straightening, adjusting, or covering over.

The degree of damage is generally classified as follows:

- **Negligible to very slight.** This degree of damage includes hairline cracks that are easily repaired during routine redecoration. Slight redecoration is warranted because of the damage, cracks are easily filled, exterior cracks are visible in brickwork and slabs, or some binding occurs in windows and doors.
- **Moderate.** A moderate degree of damage consists of reoccurring cracks after fixing and may even require removing or replacing damaged portions of walls and floors. Doors and windows stick tightly but can still be moved. Utility services to the structure (e.g., water, electrical, and sewer) may be interrupted.

- **Severe.** A severe degree of damage requires extensive repair that involves removing and replacing sections of walls and floors. Windows and door frames may be distorted and only partially functional, and floors may noticeably slope. Walls may lean or bulge, and beams may become partially dislocated. Utility services are disrupted (e.g., broken water lines or stretched electrical lines).
- **Very severe (intolerable).** Very severe damage requires major repairs that involve partial to complete reconstruction. Beams may no longer rest on bearing surfaces, and walls may require shoring to arrest leaning. Windows may be frozen, and glass may be broken by distortion. Strong perception of instability is noted even if the structure still stands.

For this study, threshold values that have been developed to indicate the onset of negligible-to-slight damage were used to delineate regions on the surface where mining-induced subsidence may adversely affect surface structures and surface and subsurface. The threshold values that indicate the onset of negligible-to-slight damage are given in Table A-2. Surface-water drainage will begin to be affected by elevation change after approximately 0.15 m of subsidence [Van Sambeek, 2000]. As a result, water may collect in areas that were previously drained. Absolute horizontal strain values, expressed as a change in length per unit length, greater than 0.001 (e.g., 1 millimeter per meter [mm/m] or 0.001 strain equals 1 millistrain or 1,000 microstrains) can cause negligible-to-slight damage to structures by stretching (extensional strains) or compressing (compressional strains) the structure [Kratzsch, 1983]. For linear structures designed to accommodate subsidence, the strain damage threshold increases to 0.002 [Kratzsch, 1983]. Surface-tilt values (expressed as the change in elevation per horizontal unit length) of less than 0.002 meter per meter (m/m) are not expected to cause significant damage to buildings, roads, and pipelines [Kratzsch, 1983]. Vertical displacement, horizontal strain, and tilt values that exceed these limits may result in negligible-to-very-slight damage.

Table A-1. Damage-Avoidance Criteria Values

Zone Description	Unit	Damage-Avoidance Value
Vertical Displacement	m	0.15
Absolute Horizontal Strain	(—)	0.001 to 0.002
Ground-Surface Tilt	m/m	0.002

A.3 SUBSIDENCE-MODEL APPROACH

To better understand future subsidence distribution, ground-displacement predictions were made using the Solution Mining Research Institute (SMRI) computer program SALT_SUBSID [Nieland and Van Sambeek, 2010]. Predicting surface subsidence requires understanding the relationship between the volume of the underground openings, rate of material movement into the openings, and spatial limits and proportional volume of surface movement. Consequently, the parameter values required for calculating ground displacement included the mined geometries and mined depths, mined dates, volumetric-closure parameters, and parameters that define the properties of the isotropic material that was used to model subsidence over the brinefields. The following sections describe the subsidence software and subsidence model representing the Nobian brinefields.

A.3.1 SUBSIDENCE-PREDICTION SOFTWARE

SALT_SUBSID is a three-dimensional (3D) computer program developed to simulate ground subsidence above solution-mined caverns or dry mines in salt, salt, and trona deposits. The methodology used in SALT_SUBSID is based on the analytical solution for a "closing" parallelepiped opening in a homogeneous material. Subsidence is estimated in SALT_SUBSID using influence functions to relate the convergence of underground openings to surface displacements. The ultimate subsidence from the complete convergence of an underground opening is estimated by integrating the influence function over the volume of the opening. The subsidence at a specific time is determined by multiplying the ultimate subsidence by the fractional closure of the opening at a chosen time. The solutions for each opening are superimposed to obtain an approximation for the total displacements at the ground surface.

The surface subsidence, S_j, at a given horizontal location $P(x,y)$ with respect to the global coordinate system, at time t can be expressed as follows:

$$S_j\left(x, y, t\right) = \sum_{i=1}^{n}\left(C_i(t) \times \int_V f_j\left(x'_i, y'_i, z'_i\right) dv\right) \qquad \text{(A-1)}$$

where:

n = number of underground openings

$C_i(t)$ = fractional closure of underground opening i at time t

$f_j\left(x'_i, y'_i, z'_i\right)$ = ultimate subsidence from complete closure of opening i relative to the opening center

j = subsidence component $(x, y, \text{or } z)$

x'_i, y'_i, z'_i = relative coordinates from $P(x, y)$ to center of underground opening i.

The influence function used to simulate the mine is based on the closure of openings in an isotropic elastic half-space described by Maruyama [1964]. Thus, this model assumes that the rock mass that hosts the underground openings is an isotropic elastic material, and the solution assumes a Poisson's ratio of 0.25, which is suitable for most rocks. The influence function for vertical surface displacements calculated with this model is given by:

$$f_z\left(x', y', z'\right) = \frac{-3}{2\pi\left(\rho^2+1\right)^{2.5}} \qquad \text{(A-2)}$$

where:

x', y', z' = coordinates to the center of the opening with respect to the point at which subsidence is calculated

$$\rho^2 = \frac{x'^2 + y'^2}{z'^2}.$$

The influence functions for the horizontal displacements of this model are given by:

$$
\begin{aligned}
f_x\left(x', y', z'\right) &= f_z\left(x', y', z'\right) \\
f_y\left(x', y', z'\right) &= f_z\left(x', y', z'\right)
\end{aligned}
\tag{A-3}
$$

The horizontal surface strains and surface tilt are calculated from the surface displacements $\left(S_x, S_y, \text{and } S_z\right)$ as follows:

$$
\begin{aligned}
\text{Horizontal strain in Easting } (x) \text{ direction} &= \varepsilon_x = \frac{d}{dx} S_x \\
\text{Horizontal strain in Northing } (y) \text{ direction} &= \varepsilon_y = \frac{d}{dy} S_y \\
\text{Surface shear strain} &= \gamma_{xy} = \frac{d}{dx} S_y + \frac{d}{dy} S_x \\
\text{Tilt in the Easting } (x) \text{ direction} &= T_x = \frac{d}{dx} S_z \\
\text{Tilt in the Northing } (y) \text{ direction} &= T_y = \frac{d}{dy} S_z
\end{aligned}
$$

For conventional dry mines, the fractional closure as a function of time, $C\left(t\right)$, is:

$$
C\left(t\right) = y_{ss} t + y_0 \left(1 - e^{\frac{-\beta_C t}{(1-E)^n}}\right) \tag{A-4}
$$

where:

$$
\begin{aligned}
y_{ss}, y_0, \beta_c, \text{and } n &= \text{model parameters} \\
E &= \text{extraction ratio of the mine} \\
t &= \text{time since opening was created.}
\end{aligned}
$$

The closure model in SALT_SUBSID (Equation A-4) includes four parameters that control the steady-state volumetric-closure rate $\left(y_{ss}\right)$, the transient volumetric-closure rate $\left(y_0\right)$, the transient closure rate exponential decay factor $\left(\beta\right)$, and the stress concentration influence of the extraction ratio on the subsidence rate $\left(n\right)$. The closure of an opening, $C\left(t\right)$, is not allowed to exceed a value of 1. When $C\left(t\right)$ is equal to 1, the opening has completely closed. Predictions at $C\left(t\right) = 1$ (when all mined openings are fully closed) in SALT_SUBSID are referred to as the ultimate subsidence values.

A.3.2 SUBSIDENCE MODEL

The subsidence model represented all current and proposed caverns in the Hengelo, Usseler Es, and Hengelo brinefields, except for the Phase 1 caverns (i.e., 1 through 50) at the Hengelo brinefield. The Phase 1 cavern was excluded because other processes (i.e., cavern migrations) have a greater influence on the subsidence that manifests on the surface than typical cavern convergence attributed to salt creep. Removing Phase 1 from the simulation will have a negligible impact on the predicted subsidence overlying the Phase 3 Hengelo caverns and the Ussler Es and Ganzebos brinefields. These caverns are believed to be sufficiently removed, so any influence on the subsidence distribution overlying the Phase 3 caverns is negligible.

The remaining caverns were explicitly represented based on the location, cavern depth, cavern height, and cavern volume over time, based on the updated solution-mining plan Nouryon provided RESPEC. The solution-mining plan provided each cavern's well location, initial and final mining dates, roof and floor depths, and final volume in cubic meters [m^3]). Tables A-1, A-2, and A-3 provide the information for the Hengelo, Usseler Es, and Gazebos brinefields, respectively. The caverns that are represented in the subsidence model included 218 Phase 2 and Phase 3 caverns at the Hengelo brinefield, 37 Phase 4 caverns at the Usseler Es brinefield, and 31 caverns at the Ganzebos brinefield.

A.3.3 SUBSIDENCE PARAMETER VALUES

The speed at which the surface subsides and the ultimate magnitude depend on the amount of salt removed, cavern depth and height, internal cavern pressures, and the salt-creep characteristics surrounding the caverns. The cavern volumetric-closure rate will be greater early on as the cavern volume increases from mining; however, with time, salt creep will redistribute the stresses in the salt surrounding the caverns and the volumetric convergence rate will slow, approaching a steady-state long-term convergence rate. This process may occur over several decades.

Considering the Usseler Es and Ganzebos brinefields are relatively young, the long-term volumetric-closure rates were estimated based on the Hengelo brinefield by adjusting the subsidence parameter value (Yss) to account for the greater depth at the Usseler Es and Ganzebos brinefield. To estimate the influence that the cavern depth has on the creep rate of the salt surrounding the caverns, RESPEC used analytical equations that define stationary stress distribution around a circular hole [Van Sambeek, 1993] to estimate the volumetric-closure rate for a typical Ganzebos cavern where the creep of salt was represented by a creep law of:

$$\dot{\varepsilon}^{c}_{ij} = \frac{d\varepsilon^{c}_{ij}}{dt} = A\exp\left(\frac{-Q}{RT}\right)\sigma_{\text{eff}}^{n-1}\left(\frac{3}{2}S_{ij}\right) \tag{A-5}$$

where

$\dot{\varepsilon}^{c}_{ij}$ = the creep strain rate tensor

ε^{c}_{ij} = the creep strain tensor

S_{ij} = the deviatoric stress tensor

σ_{eff} = effective stress

= $\sqrt{3J_2}$, where J_2 is the second invariant of S_{ij}

$\left(\frac{Q}{R}\right)$ = collectively is a thermal activation energy

T = temperature

A and n = material constants.

Table A-2. Hengelo Brinefield Information (Page 1 of 6)

Well Number	Well I.D.	Easting (m)	Northing (m)	Start Mining (date)	Complete Mining (date)	Cavern Roof Depth (m)	Cavern Floor Depth (m)	Expected Volume (m^3)
Hengelo_1	1	251439	473923	4/2/1935	8/9/1960	336	360	84,100
Hengelo_2	2	251342	473917	6/17/1935	1/31/1955	336	360	124,400
Hengelo_3	3	251250	473916	9/2/1935	1/31/1955	336	360	42,500
Hengelo_4	4	251161	473929	11/11/1935	1/30/1955	336	360	168,700
Hengelo_5	5	251028	473951	1/11/1936	10/1/1959	336	360	64,700
Hengelo_6	6	250894	473972	4/4/1936	10/1/1959	336	360	158,300
Hengelo_7	7	251019	473842	8/15/1939	10/1/1959	336	360	73,300
Hengelo_8	8	251025	473725	11/3/1939	10/1/1959	336	360	96,800
Hengelo_9	9	250945	473673	6/26/1940	10/1/1959	336	360	74,100
Hengelo_10	10	250853	473696	4/4/1941	10/1/1959	336	360	131,600
Hengelo_11	11	250762	473722	5/12/1941	5/10/1959	336	360	89,600
Hengelo_12	12	251547	473941	11/28/1947	1/31/1955	336	360	65,600
Hengelo_13	13	251632	473873	3/8/1948	1/31/1955	336	360	109,800
Hengelo_14	14	250892	473833	7/6/1948	2/1/1960	336	360	81,600
Hengelo_15	15	250765	473847	10/14/1948	2/7/1968	281	288	191,200
Hengelo_16	16	251205	473806	2/15/1949	11/1/1959	336	360	40,200
Hengelo_17	17	251252	473695	5/19/1949	1/7/1959	336	360	120,700
Hengelo_18	18	251266	473573	9/1/1949	11/1/1959	336	360	136,800
Hengelo_19	19	251287	473454	11/28/1949	11/1/1959	336	360	178,100
Hengelo_21	21	251146	473621	6/12/1950	11/1/1959	336	360	70,900
Hengelo_22	22	251147	473487	9/28/1950	11/1/1959	336	360	92,500
Hengelo_23	23	251176	473366	4/11/1951	5/1/1962	336	360	116,500
Hengelo_25	25	251236	473231	6/23/1951	5/1/1962	336	360	137,600
Hengelo_27	27	250724	473586	8/22/1952	11/1/1962	336	360	86,700
Hengelo_28	28	250726	473447	11/25/1952	11/11/1962	336	360	125,700
Hengelo_29	29	250728	473307	3/13/1953	11/1/1964	336	360	153,100
Hengelo_30	30	250731	473170	7/8/1953	11/1/1964	336	360	187,100
Hengelo_32	32	250874	473556	3/1/1954	4/1/1962	336	360	71,300
Hengelo_33	33	250880	473396	7/3/1954	4/30/1964	336	360	189,700
Hengelo_35	35	250892	473218	12/20/1954	11/1/1964	336	360	244,800
Hengelo_37	37	250583	473788	7/16/1955	8/1/1979	349	383	65,900
Hengelo_38	38	250564	473663	10/15/1955	4/1/1975	336	360	144,700
Hengelo_39	39	250552	473521	2/8/1956	12/1/1978	336	360	122,100
Hengelo_40	40	250503	473349	5/23/1956	6/1/1979	336	360	191,600
Hengelo_42	42	251078	473187	12/8/1956	11/1/1964	336	360	158,800
Hengelo_44	44	251464	473712	6/13/1957	1/1/1973	336	360	30,000

Table A-2. Hengelo Brinefield Information (Page 2 of 6)

Well Number	Well I.D.	Easting (m)	Northing (m)	Start Mining (date)	Complete Mining (date)	Cavern Roof Depth (m)	Cavern Floor Depth (m)	Expected Volume (m^3)
Hengelo_45	45	251496	473631	9/23/1957	1/1/1973	336	360	68,000
Hengelo_46	46	251518	473546	11/30/1957	1/1/1973	336	360	93,100
Hengelo_47	47	251539	473461	2/7/1958	1/1/1973	336	360	50,800
Hengelo_48	48	251568	473378	5/1/1958	1/1/1973	336	360	86,100
Hengelo_49	49	251599	473296	8/1/1958	1/1/1973	343	371	73,800
Hengelo_50	50	251628	473222	10/16/1958	1/1/1973	343	368	103,400
Hengelo_51	51	251428	473204	12/18/1958	11/1/1963	345	369	54,700
Hengelo_52	52	251456	473121	2/16/1959	6/1/1978	340	357	316,200
Hengelo_55	55	251523	472870	10/27/1959	11/1/1986	343	400	321,300
Hengelo_57	57	250832	472970	11/4/1959	10/1/1977	392	434	408,000
Hengelo_60	62A	251166	472556	11/28/1959	12/1/1978	382	407	184,800
Hengelo_63	63	251782	473512	6/1/1961	6/1/1978	346	360	80,900
Hengelo_64	64	251873	473563	6/1/1961	6/1/1978	294	314	161,800
Hengelo_66	66	251802	473362	9/15/1961	3/1/1996	359	381	112,500
Hengelo_67	67	251799	473287	7/28/1961	12/1/1975	317	355	241,300
Hengelo_69	69	252258	473638	6/29/1962	12/1/1977	274	344	303,900
Hengelo_72	72	252181	473363	12/21/1962	1/2/2002	314	346	541,000
Hengelo_73	73	252188	473276	3/27/1962	10/7/1974	298	317	239,800
Hengelo_77	77	252586	473396	8/5/1962	6/1/1982	302	335	126,500
Hengelo_78	78	251704	472550	2/14/1963	6/1/1989	358	389	186,700
Hengelo_80	80	251539	472462	5/28/1963	2/18/1997	377	420	114,900
Hengelo_81	81	251813	472930	8/23/1963	12/1/1979	336	377	272,400
Hengelo_84	84	251949	472571	12/5/1963	4/29/1990	357	387	177,500
Hengelo_86	86	251371	472528	3/5/1964	12/1/1978	378	384	151,800
Hengelo_88	88	250835	472713	9/22/1964	5/1/1989	388	422	188,000
Hengelo_90	90	250730	472839	9/23/1964	6/1/1978	393	437	134,700
Hengelo_92	92	250564	473052	2/10/1965	6/1/1978	427	452	0
Hengelo_93	93	250548	473027	2/10/1965	6/1/1978	427	452	131,000
Hengelo_94	94	250436	473166	2/4/1965	4/1/1977	420	448	131,000
Hengelo_96	96	250377	472978	6/15/1965	5/1/1988	413	444	581,600
Hengelo_98	98	250509	472831	5/15/1965	5/1/1996	399	444	42,900
Hengelo_100	100	250736	472551	12/8/1965	11/1/1989	411	438	189,700
Hengelo_102	102	250738	472352	8/1/1965	11/24/1999	428	442	218,400
Hengelo_104	104	250826	472167	2/28/1966	6/29/1999	451	459	593,300
Hengelo_108	108	251214	472200	9/22/1965	2/1/1990	403	451	190,900
Hengelo_110	110	251494	472206	12/1/1965	8/24/1982	396	435	188,200

RESPEC

Table A-2. Hengelo Brinefield Information (Page 3 of 6)

Well Number	Well I.D.	Easting (m)	Northing (m)	Start Mining (date)	Complete Mining (date)	Cavern Roof Depth (m)	Cavern Floor Depth (m)	Expected Volume (m^3)
Hengelo_112	112	251626	472291	9/22/1966	4/1/1981	383	403	216,900
Hengelo_114	114	251811	472304	10/3/1966	4/1/1981	369	406	170,500
Hengelo_116	116	251663	472097	10/24/1966	8/1/1982	387	414	167,400
Hengelo_118	118	251601	471912	2/16/1967	1/11/1999	408	449	227,600
Hengelo_120	120	251479	471756	3/14/1967	1/20/1998	429	466	262,100
Hengelo_122	122	250813	471928	9/15/1967	1/24/2000	449	477	236,400
Hengelo_124	124	251010	471949	9/12/1967	7/1/1994	428	470	198,500
Hengelo_126	126	251231	471977	9/28/1967	1/1/1996	418	463	163,800
Hengelo_128	128	251435	472003	11/11/1967	2/13/1999	401	447	197,300
Hengelo_130	130	251967	472304	12/4/1967	8/4/2004	363	412	242,600
Hengelo_132	132	250321	472794	5/3/1968	5/18/2005	425	468	218,800
Hengelo_134	134	250263	472609	2/29/1968	11/1/1981	422	458	994,00
Hengelo_136	136	250227	472381	1/3/1968	11/1/1982	434	479	134,600
Hengelo_138	138	250413	472313	2/20/1968	3/30/1984	459	477	139,600
Hengelo_140	140	250594	472226	2/12/1968	4/1/1994	435	477	211,100
Hengelo_142	142	250223	472923	11/19/1968	7/19/2011	445	469	239,300
Hengelo_144	144	250063	472952	1/8/1969	7/1/1988	398	450	190,000
Hengelo_146	146	250459	472554	6/13/1968	2/1/1993	427	453	208,400
Hengelo_148	148	250062	472455	6/25/1968	10/14/1997	448	473	112,600
Hengelo_149	149	249912	472490	8/14/1968	2/1/1993	436	465	178,700
Hengelo_151	151	249728	472436	10/3/1968	5/15/1997	446	482	211,500
Hengelo_153	153	249446	472457	2/10/1969	4/1/1993	433	456	252,600
Hengelo_156	156	249819	472770	11/3/1969	2/9/2070	451	479	996,707
Hengelo_159	159	250083	472779	8/18/1969	11/22/2004	426	470	443,200
Hengelo_162	162	249336	472660	12/9/1969	2/1/1997	463	495	341,200
Hengelo_165	165	249296	472862	1/26/1970	5/1/1994	428	446	151,400
Hengelo_167	167	249519	472797	4/2/1970	9/26/2007	297	317	251,300
Hengelo_170	170	250729	471701	10/2/1969	10/15/1997	476	482	355,500
Hengelo_173	173	250124	472124	7/16/1970	3/1/2018	453	474	356,800
Hengelo_176	176	250240	471953	10/5/1969	5/1/1997	480	513	235,900
Hengelo_178	178	250439	471980	11/20/1969	3/1/2018	470	487	348,400
Hengelo_180	180	250640	472016	12/9/1969	5/27/1997	447	489	253,600
Hengelo_182	182	250731	471486	8/25/1969	7/3/1998	505	530	242,100
Hengelo_184	184	250576	471561	8/1/1970	4/16/1996	473	532	277,900
Hengelo_187	187	250364	471671	7/1/1970	4/16/1996	504	532	278,100
Hengelo_190	190	250025	471876	10/6/1970	4/1/1984	468	485	106,100

Table A-2. Hengelo Brinefield Information (Page 4 of 6)

Well Number	Well I.D.	Easting (m)	Northing (m)	Start Mining (date)	Complete Mining (date)	Cavern Roof Depth (m)	Cavern Floor Depth (m)	Expected Volume (m^3)
Hengelo_192	192	249873	473014	5/1/1970	2/1/1982	402	443	53,300
Hengelo_194	194	250142	471699	10/5/1970	6/15/1996	479	537	186,900
Hengelo_196	196	250049	471499	10/29/1970	11/2/1999	523	561	227,300
Hengelo_198	198	250760	471337	10/2/1970	11/15/2000	502	533	317,900
Hengelo_201	201	251329	471563	1/1/1971	8/1/1997	470	493	253,000
Hengelo_204	204	252151	473026	5/27/1971	10/10/2001	330	355	346,400
Hengelo_207	207	252327	472905	6/28/1971	3/3/2004	348	366	225,400
Hengelo_209	209	252243	472616	5/27/1971	10/7/1997	350	383	242,400
Hengelo_211	211	252358	472459	5/28/1971	11/18/1998	360	391	260,800
Hengelo_213	213	252217	472303	8/16/1971	5/7/2003	378	411	216,500
Hengelo_215	215	252448	472287	6/28/1971	9/1/1999	358	403	334,000
Hengelo_218	218	252304	471995	9/30/1971	2/5/2010	389	420	278,600
Hengelo_220	220	252034	472073	11/23/1971	8/7/2009	393	415	354,000
Hengelo_223	223	251773	471941	6/20/1972	5/1/1997	399	446	250,700
Hengelo_225	225	251845	471749	4/15/1972	6/1/1997	419	442	316,900
Hengelo_228	228	252643	471981	8/1/1971	5/25/2013	379	408	338,300
Hengelo_231	231	252872	471837	11/1/1972	9/13/2013	384	408	364,200
Hengelo_234	234	253122	471764	11/12/1973	9/1/1996	364	422	273,500
Hengelo_237	237	253335	471644	2/1/1974	3/10/2004	387	418	282,600
Hengelo_239	239	253706	471418	6/27/1974	5/26/1999	390	433	320,400
Hengelo_242	242	253854	471261	12/1/1974	11/11/1999	398	443	273,900
Hengelo_245	245	253940	471025	6/15/1973	5/26/1999	443	462	305,900
Hengelo_248	248	253558	471511	3/10/1977	9/9/1989	387	426	256,200
Hengelo_251	251	253499	471765	9/28/1976	4/9/2010	374	398	227,900
Hengelo_253	253	252447	472608	3/4/1975	3/3/1998	355	380	231,400
Hengelo_256	256	252540	472433	6/23/1975	1/26/2001	355	386	204,000
Hengelo_259	259	252449	473114	2/5/1976	11/21/1995	321	347	269,000
Hengelo_262	262	252541	472889	7/21/1976	11/12/2003	351	367	105,300
Hengelo_265	265	253298	471477	6/15/1977	12/24/2003	393	421	361,300
Hengelo_268	268	253152	471288	8/29/1977	1/29/2009	413	441	313,700
Hengelo_270	270	253534	471372	12/2/1977	9/24/2003	397	432	252,700
Hengelo_272	272	253476	471182	3/1/1979	5/7/2009	407	441	386,300
Hengelo_275	275	253491	471018	8/30/1979	3/10/2004	428	453	295,000
Hengelo_278	278	253584	470802	4/16/1980	10/31/2006	428	459	388,900
Hengelo_281	281	254114	470887	10/10/1978	6/1/2005	431	463	174,200
Hengelo_283	283	254311	470928	5/29/1978	1/7/2010	433	465	198,200

RESPEC

Table A-2. Hengelo Brinefield Information (Page 5 of 6)

Well Number	Well I.D.	Easting (m)	Northing (m)	Start Mining (date)	Complete Mining (date)	Cavern Roof Depth (m)	Cavern Floor Depth (m)	Expected Volume (m^3)
Hengelo_285	285	254507	470970	2/24/1978	1/7/2010	423	461	248,000
Hengelo_287	287	253810	470914	1/25/1980	7/16/2003	447	465	213,800
Hengelo_290	290	253345	470869	1/26/1982	3/5/2010	426	456	370,300
Hengelo_293	293	253104	470845	7/3/1981	5/29/2013	416	450	395,000
Hengelo_296	296	252870	470810	1/21/1981	8/17/2011	422	455	413,900
Hengelo_299	299	252631	470776	7/1/1982	3/28/2013	422	449	441,300
Hengelo_302	302	252394	470742	4/14/1982	1/31/2008	446	464	301,000
Hengelo_305	305	251197	471419	9/2/1980	3/10/2004	491	507	150,500
Hengelo_308	308	251366	471369	2/9/1984	5/23/2051	475	503	606,915
Hengelo_311	311	251609	471341	3/20/1983	2/4/2021	448	466	338,800
Hengelo_314	314	251846	471533	5/15/1984	4/14/2011	428	460	297,100
Hengelo_317	317	251815	471229	10/1/1984	1/23/2019	438	475	305,900
Hengelo_320	320	251776	470888	3/26/1985	11/1/2010	453	482	339,500
Hengelo_323	323	251876	470686	9/11/1985	11/7/2001	452	486	106,200
Hengelo_325	325	251932	471336	12/23/1985	5/26/2004	435	463	179,400
Hengelo_328	328	252163	471393	1/29/1987	1/29/2016	432	459	263,000
Hengelo_331	331	252035	471591	9/1/1987	9/30/2010	422	440	251,200
Hengelo_334	334	252124	471759	9/1/1987	1/6/2010	420	440	318,500
Hengelo_337	337	251290	470947	5/24/1988	3/5/2010	513	528	244,500
Hengelo_340	340	251508	470862	2/15/1988	7/15/2010	481	512	228,700
Hengelo_343	343	251485	470663	11/4/1988	11/21/2013	506	520	177,700
Hengelo_346	346	251247	470646	4/4/1990	11/5/2000	532	540	50,400
Hengelo_347	347	250774	471015	11/30/1990	8/4/2008	509	553	206,300
Hengelo_349	349	250849	470631	7/30/1990	4/24/2009	533	564	293,500
Hengelo_352	352	250929	471380	1/10/1989	3/1/2018	496	501	275,600
Hengelo_355	355	250316	471493	5/23/1989	9/1/2009	517	549	217,700
Hengelo_358	358	252684	470972	11/24/1989	7/8/2010	439	459	235,900
Hengelo_361	361	252822	471156	8/9/1989	3/5/2010	427	443	267,200
Hengelo_364	364	253738	470611	5/21/1991	10/16/2014	431	469	264,900
Hengelo_367	367	253512	470587	4/16/1992	4/9/2051	444	472	604,469
Hengelo_369	369	253446	470424	3/21/1991	5/15/2056	441	469	710,622
Hengelo_372	372	253334	470156	6/12/1993	2/26/2055	444	472	685,369
Hengelo_375	375	253142	470021	9/2/1993	3/25/2008	445	468	263,600
Hengelo_378	378	252907	469981	2/24/1994	3/5/2010	458	467	186,600
Hengelo_381	381	252582	470098	6/23/1998	1/23/2019	453	468	155,600
Hengelo_384	384	252496	470301	6/13/1992	8/26/2015	432	457	338,500

Table A-2. Hengelo Brinefield Information (Page 6 of 6)

Well Number	Well I.D.	Easting (m)	Northing (m)	Start Mining (date)	Complete Mining (date)	Cavern Roof Depth (m)	Cavern Floor Depth (m)	Expected Volume (m^3)
Hengelo_387	387	252386	470465	1/7/1993	10/16/2014	435	466	257,500
Hengelo_390	390	252747	472329	11/24/1991	10/16/2014	371	390	254,600
Hengelo_393	393	252990	472293	9/2/1991	4/2/2010	369	387	242,200
Hengelo_396	396	253217	472195	2/10/1993	5/23/2012	361	390	252,300
Hengelo_399	399	253401	472060	8/2/1994	1/8/2010	363	391	284,300
Hengelo_402	402	253239	472352	7/4/1995	3/10/2004	376	385	39,900
Hengelo_405	405	253136	472519	11/24/1995	2/28/2011	351	371	216,100
Hengelo_408	408	253477	472197	2/13/1995	9/1/2004	370	387	143,700
Hengelo_411	411	253602	471919	6/2/1994	3/8/2011	377	401	274,400
Hengelo_414	414	253273	472587	3/4/1996	5/18/2005	355	370	59,900
Hengelo_416	416	253483	472644	10/14/1996	7/29/2021	342	361	259,900
Hengelo_419	419	253567	472404	4/24/1997	10/16/2014	357	373	139,100
Hengelo_422	422	253443	472799	12/2/1997	10/4/2017	335	352	226,700
Hengelo_425	425	253319	472999	6/30/1997	1/18/2017	328	342	172,400
Hengelo_428	428	253166	473190	4/7/1997	7/29/2021	321	334	258,100
Hengelo_431	431	253031	471034	4/20/2006	2/23/2017	432	454	134,200
Hengelo_432	432	253038	473449	4/9/1999	6/17/2015	320	335	148,300
Hengelo_434	434	252845	473502	7/14/1999	9/8/2004	338	350	431,00
Hengelo_437	437	252679	473659	1/11/2000	4/15/2016	321	335	119,000
Hengelo_440	440	252159	470756	1/17/2006	8/26/2015	454	478	155,100
Hengelo_441	441	252139	470945	2/15/2006	4/2/2015	455	477	161,900
Hengelo_442	442	252157	471090	1/17/2006	8/24/2016	446	472	173,500
Hengelo_443	443	252741	473341	8/23/2000	10/16/2014	314	331	144,200
Hengelo_445	445	251652	471043	6/1/2006	11/7/2018	467	498	198,300
Hengelo_446	446	251505	471074	6/1/2006	3/1/2018	477	508	236,400
Hengelo_447	447	250987	470920	12/20/2006	6/13/2044	516	544	462,381
Hengelo_448	448	253733	471581	9/15/2000	3/10/2004	428	430	9,600
Hengelo_451	451	254005	471628	8/1/2001	7/29/2021	404	417	144,900
Hengelo_454	454	253902	471863	11/30/2001	10/16/2014	384	404	149,900
Hengelo_457	457	254066	471862	6/28/2002	5/1/2019	386	402	141,000
Hengelo_460	460	254066	472102	9/11/2002	1/23/2019	368	383	173,500
Hengelo_463	463	253959	472313	3/11/2003	7/2/2034	349	377	255,278
Hengelo_466	466	253800	472155	9/15/2003	2/26/2019	372	387	105,000
Hengelo_469	469	253236	470524	6/25/1998	4/19/2050	439	467	584,249
Hengelo_472	472	252961	470483	4/6/1999	1/23/2019	450	466	165,000
Hengelo_475	475	252750	470273	5/18/2001	9/2/2046	439	467	508,630
Hengelo_478	478	251148	470915	12/20/2006	10/13/2045	507	535	490,170
Hengelo_479	479	251571	471544	11/20/2006	2/23/2018	455	481	207,200

Table A-3. Usseler Es Brinefield Information

Well I.D.	Well Number	Easting (m)	Northing (m)	Start Mining (date)	Complete Mining (date)	Cavern Roof Depth (m)	Cavern Floor Depth (m)	Expected Volume (m^3)
UsselorEs_480	480	253981	470526	2/9/2005	12/17/2021	450	479	263,300
UsselorEs_486	486	253580	470003	5/17/2008	9/22/2021	445	474	268,100
UsselorEs_487	487	253396	469825	5/17/2008	7/24/2035	438	466	522,574
UsselorEs_488	488	253511	469737	5/17/2008	1/6/2022	437	464	248,100
UsselorEs_489	489	253695	469667	7/1/2008	10/10/2018	435	465	223,400
UsselorEs_490	490	253833	469623	5/17/2008	1/11/2018	440	464	226,600
UsselorEs_491	491	253973	469583	7/1/2008	11/15/2017	439	466	224,600
UsselorEs_492	492	254160	469539	6/17/2009	2/21/2018	443	466	213,400
UsselorEs_493	493	254301	469508	6/17/2009	6/1/2018	444	470	221,800
UsselorEs_494	494	254442	469474	4/8/2009	1/6/2022	441	466	247,100
UsselorEs_495	495	254583	469440	1/27/2010	3/7/2018	437	463	203,600
UsselorEs_496	496	254733	469430	3/24/2010	2/12/2020	430	460	258,900
UsselorEs_497	497	254239	470489	3/21/2011	4/25/2033	450	478	485,556
UsselorEs_498	498	254333	470367	3/21/2011	9/22/2021	455	484	263,300
UsselorEs_499	499	254332	470220	9/5/2011	9/19/2033	459	487	490,170
UsselorEs_500	500	254449	470129	10/25/2011	10/8/2033	457	485	517,959
UsselorEs_501	501	254563	470040	11/14/2011	1/12/2022	455	487	275,800
UsselorEs_502	502	254673	469949	11/14/2011	4/16/2032	452	480	601,126
UsselorEs_503	503	254845	469898	11/21/2011	4/29/2032	449	477	554,878
UsselorEs_504	504	253740	470241	8/24/2010	8/18/2036	451	479	517,959
UsselorEs_505	505	253867	470171	5/26/2010	12/22/2021	449	480	307,000
UsselorEs_506	506	253974	470072	11/24/2010	1/2/2037	456	484	462,381
UsselorEs_507	507	254062	469954	4/23/2012	1/13/2022	452	482	267,900
UsselorEs_508	508	254196	469893	3/27/2012	5/12/2033	457	485	531,804
UsselorEs_509	509	254347	469813	10/17/2012	1/23/2039	457	485	416,233
UsselorEs_510	510	254479	469751	3/5/2012	2/28/2034	452	480	462,381
UsselorEs_511	511	253698	469931	1/12/2010	9/17/2036	446	474	485,556
UsselorEs_512	512	255125	469616	7/4/2011	7/11/2019	432	458	236,100
UsselorEs_513	513	255202	469369	3/23/2011	11/20/2017	424	443	152,600
UsselorEs_514	514	254286	469155	8/22/2013	2/18/2031	410	438	369,985
UsselorEs_516	516	254287	469010	8/22/2013	12/17/2030	391	419	323,737
UsselorEs_517	517	254296	468865	8/26/2013	3/2/2022	390	408	124,700
UsselorEs_520	520	254547	469085	3/10/2013	7/6/2031	400	428	369,985
UsselorEs_521	521	254513	468944	12/16/2013	2/12/2032	385	413	240,470
UsselorEs_523	523	254852	469008	12/10/2013	4/16/2030	390	418	342,196
UsselorEs_524	524	254771	468899	4/22/2014	10/8/2029	377	405	300,563
UsselorEs_525	525	254836	468704	1/2/2014	7/2/2034	359	387	184,993

m = meters

m^3 = cubic meters.

Table A-4. Ganzebos Brinefield Information

Well I.D.	Well Number	Easting (m)	Northing (m)	Start Mining (date)	Complete Mining (date)	Cavern Roof Depth (m)	Cavern Floor Depth (m)	Expected Volume (m^3)
GZB_f1_01	526	249858	470016	12/01/2014	12/01/2024	456	488	229,321
GZB_f1_02	527	249702	470290	04/01/2014	04/01/2024	460	491	223,795
GZB_f1_03	528	249392	470649	10/01/2017	10/01/2027	459	489	215,507
GZB_f1_04	529	249262	470714	11/01/2017	11/01/2027	462	492	216,198
GZB_f1_05	530	248956	470718	11/01/2017	11/01/2027	479	511	229,321
GZB_f1_06	531	249879	469780	02/01/2015	02/01/2025	473	507	241,753
GZB_f1_07	532	249667	469945	10/01/2014	10/01/2024	478	512	243,134
GZB_f1_08	533	249550	470038	10/01/2014	10/01/2024	484	518	245,897
GZB_f1_09	534	249423	470105	02/01/2014	02/01/2024	488	522	245,897
GZB_f1_10	535	249407	470363	09/01/2016	09/01/2026	481	514	238,299
GZB_f1_11	536	249260	470386	09/01/2016	09/01/2026	491	525	244,515
GZB_f1_12	537	249104	470386	07/01/2017	07/01/2027	489	523	242,443
GZB_f1_13	538	248939	470447	07/01/2017	07/01/2027	485	518	237,609
GZB_f1_14	539	248618	470456	11/01/2017	11/01/2027	494	528	243,134
GZB_f1_15	540	248487	470420	06/01/2017	06/01/2027	500	535	247,969
GZB_f2_16	541	248354	470371	11/01/2017	11/01/2027	507	543	254,185
GZB_f2_17	542	249882	469489	06/01/2018	06/01/2028	510	548	266,617
GZB_f2_18	543	249775	469563	06/01/2018	06/01/2028	515	553	268,689
GZB_f2_19	544	249653	469592	01/01/2019	01/01/2029	516	554	266,790
GZB_f2_20	545	249478	469649	05/01/2018	05/01/2028	518	556	266,790
GZB_f2_21	546	249311	469761	01/01/2020	01/01/2030	520	558	266,790
GZB_f3_01	547	248741	470716	01/01/2020	10/01/2030	511	546	266,790
GZB_f3_02	548	248424	470974	06/01/2020	06/01/2030	531	571	304,503
GZB_f3_03	549	248265	470712	06/01/2020	06/01/2030	511	546	266,790
GZB_f3_04	552	247816	470969	01/01/2021	01/01/2031	511	546	266,790
GZB_f3_05	553	247863	471109	01/01/2021	01/01/2031	511	546	266,790
GZB_f3_06	554	247919	471239	01/01/2021	01/01/2031	511	546	266,790
GZB_f3_07	555	247658	471272	01/01/2021	01/01/2031	506	546	304,503
GZB_f3_08	556	247624	471116	01/01/2021	01/01/2031	511	546	266,790
GZB_f3_09	557	247661	470923	01/01/2021	01/01/2031	491	521	229,076
GZB_f3_10	558	248328	470573	01/01/2020	01/01/2030	486	521	266,790

m = meters

m^3 = cubic meters.

And the effective stress measure is taken as the von Mises equivalent stress equal to:

$$\sigma_{eff} = \sqrt{3J_2} = \sqrt{\left\{\left(\sigma_1 - \sigma_2\right)^2 + \left(\sigma_2 - \sigma_3\right)^2 + \left(\sigma_3 - \sigma_1\right)^2\right\} / 2} \tag{A-6}$$

where $\sigma_1, \sigma_2,$ and σ_3 are principal stresses.

The stationary stress distribution for an axially constrained, hollow cylinder in a creeping medium that is subject to internal pressure $\left(P_i\right)$ and external pressure P_0 was estimated as:

$$\sigma_{rr} = -P_0 + \left(P_0 - P_i\right)\left[\frac{\left(b/r\right)^{2/n} - 1}{\left(b/a\right)^{2/n} - 1}\right] \tag{A-7}$$

$$\sigma_{\theta\theta} = -P_0 - \left(P_0 - P_i\right)\left[\frac{\left(\frac{2}{n} - 1\right)\left(b/r\right)^{2/n} + 1}{\left(b/a\right)^{2/n} - 1}\right] \tag{A-8}$$

$$\sigma_{zz} = -P_0 - \left(P_0 - P_i\right)\left[\frac{\left(\frac{1}{n} - 1\right)\left(b/r\right)^{2/n} + 1}{\left(b/a\right)^{2/n} - 1}\right]. \tag{A-9}$$

Substituting Equations 3 through 5 into Equation 2 gives:

$$\sigma_{eff} = \sqrt{3}/n\left[\frac{\left(P_0 - P_i\right)\left(b/r\right)^{2/n}}{\left(b/a\right)^{2/n} - 1}\right]. \tag{A-10}$$

Substituting Equation 6 into Equation 1 gives the velocity of a point in the radial direction $\left(\dot{u}\right)$ and can be described as:

$$\dot{u} = r\dot{\varepsilon}_{\theta\theta}. \tag{A-11}$$

$$\dot{u}/r = -A\left(\sqrt{3}/2\right)^{n+1}\left[\left(P_0 - P_i\right)\left\{\frac{\left(2/n\right)}{\left(b/a\right)^{2/n} - 1}\right\}\right]^n\left(b/r\right)^2. \tag{A-12}$$

For the special case where in the limit $b \to \infty$,

$$\dot{u}/r = -A\left(\sqrt{3}/2\right)^{n+1}\left[\left(P_0 - P_i\right)\left(2/n\right)\right]^n\left(a/r\right)^2. \tag{A-13}$$

This effort suggests that the Usseler Es and Ganzebos caverns' volumetric-closure rate may be greater than the volumetric-closure rate of the Hengelo Caverns, respectively. Therefore, this study used a y_{ss} parameter value of 0.0002 and 0.0005 to represent the Usseler Es and Ganzebos brinefield.

The parameter values used to describe the transient response (y_0 and β)of the volumetric-closure rate of the Hengelo, Usseler Es, and Ganzebos brinefields were derived from interpretations of subsidence rates based on benchmark measurements recorded above each of the brinefields by reducing the error between the predicted displacements from the simulation, which represented progressive development of the Hengelo, Usseler Es, and Hengelo brinefields and displacements calculated from the available benchmark-elevation surveys between 1935 and 2019. Table A-5 provides the input parameters that defined the closure model for the 975 Level, which were derived from the fitting process, and Figure A-2 illustrates the evolution of the volumetric convergence rates for each of the closure models. .

Table A-5. Subsidence-Model Closure Parameters for the Hengelo, Usseler Es, and Ganzebos Brinefields

Mine Block	y_{ss} (1/year)	y_0 (—)	β (1/year)	η (—)
Hengelo Brinefield	0.00008	0.0005	0.4	0.0168
Usseler Es Brinefield	0.00020	0.00055	0.4	0.0168
Ganzebos Brinefield	0.00050	0.001	0.4	0.0168

A.4 TIME-SERIES PLOTS OF THE MEASURED AND PREDICTED BENCHMARK DISPLACEMENTS

Figures A-3 through A-8 are time-series plots comparing the calculated displacements from the measured elevation surveys to the displacements predicted from the subsidence model at select locations overlying the brinefields.

A.5 REFERENCES

Kratzsch, H., 1983. *Mining Subsidence Engineering,* R. F. S. Fleming (translator), Springer-Verlag, Berlin, Germany.

Maruyama, T., 1964. "Statistical Elastic Dislocations in an Infinite and Semi-Infinite Medium," *Bulletin of the Earthquake Research Institute*, Tokyo University, Bunkyo, Tokyo, Japan, Vol. 42, pp. 289–368.

Nieland, J. D. and L. L. Van Sambeek, 2010. *SALT_SUBSID, Version 2.0 User's Manual*, Research Report RR2009-02, prepared by RESPEC, Rapid City, SD, and POD, Inc., Albuquerque, NM, for the Solution Mining Research Institute, Clarks Summit, PA.

Van Sambeek, L. L., 1993. *Stationary Stress Distributions Around a Circular Hole for a Multimechanism Creep Law*, RSI/SIR-93-06, prepared by RE/SPEC Inc., Rapid City, SD, December.

Van Sambeek, L. L., 2000. "An Introduction to Subsidence Over Salt and Salt Mining Facilities," *Solution Mining Research Institute Fall Meeting*, San Antonio, TX, October 15–18.

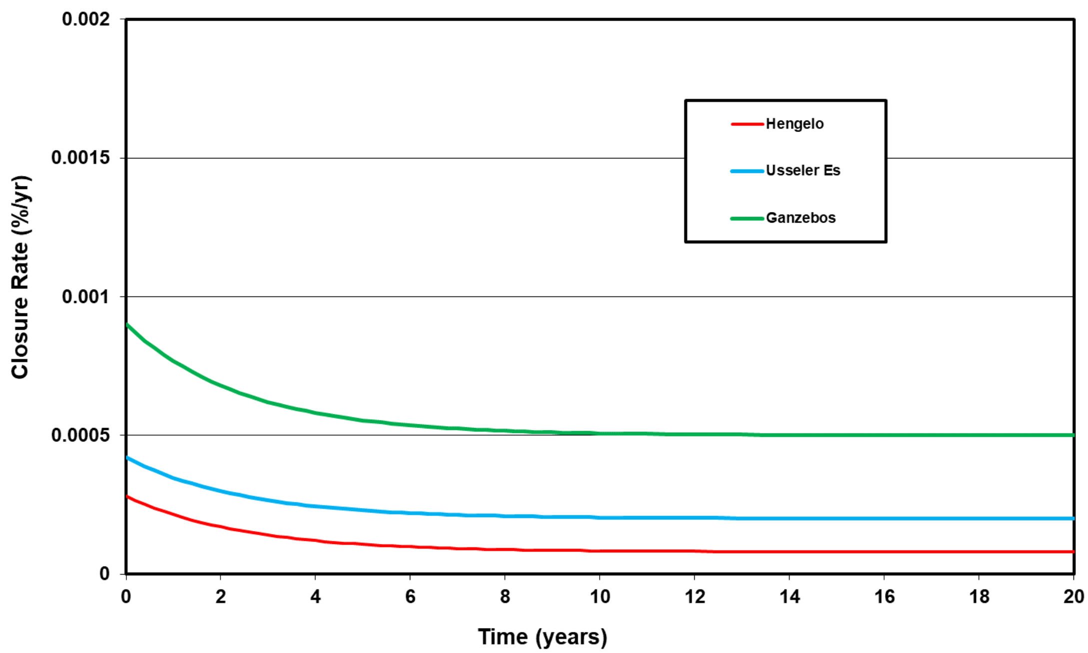

Figure A-2. Graphical Represenation of the Subsidence Closure Models Illustrating the Volumetric Cavern Convergence Rates Versus Time for the Hengelo, Usseler Es, and Ganzebos Brinefields.

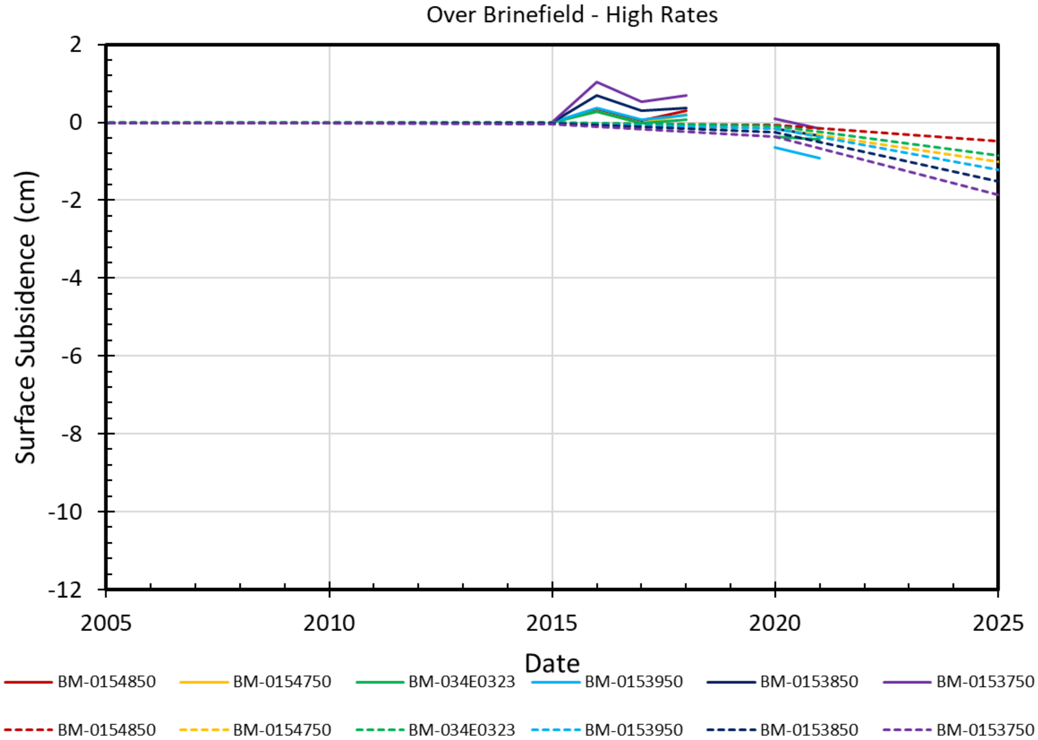

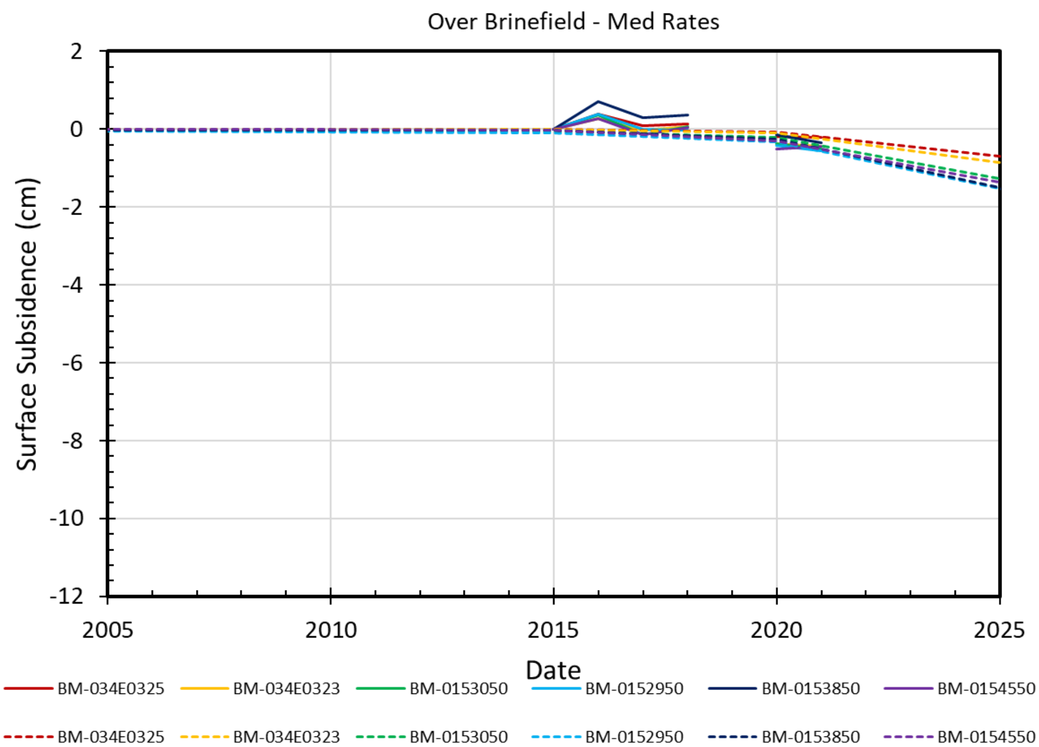

Figure A-3. Time-Series Plot Comparing the Measured and Predicted Ganzebos Benchmarks Located Over the Brinefield With Medium to High Measured Subsidence Rates.

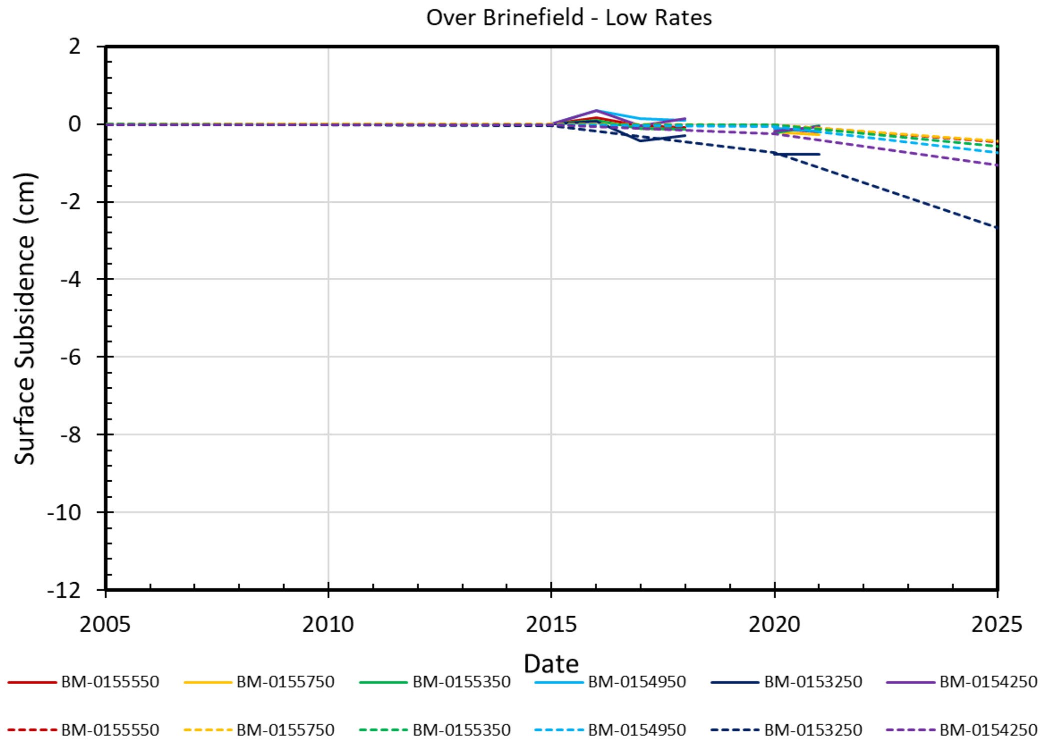

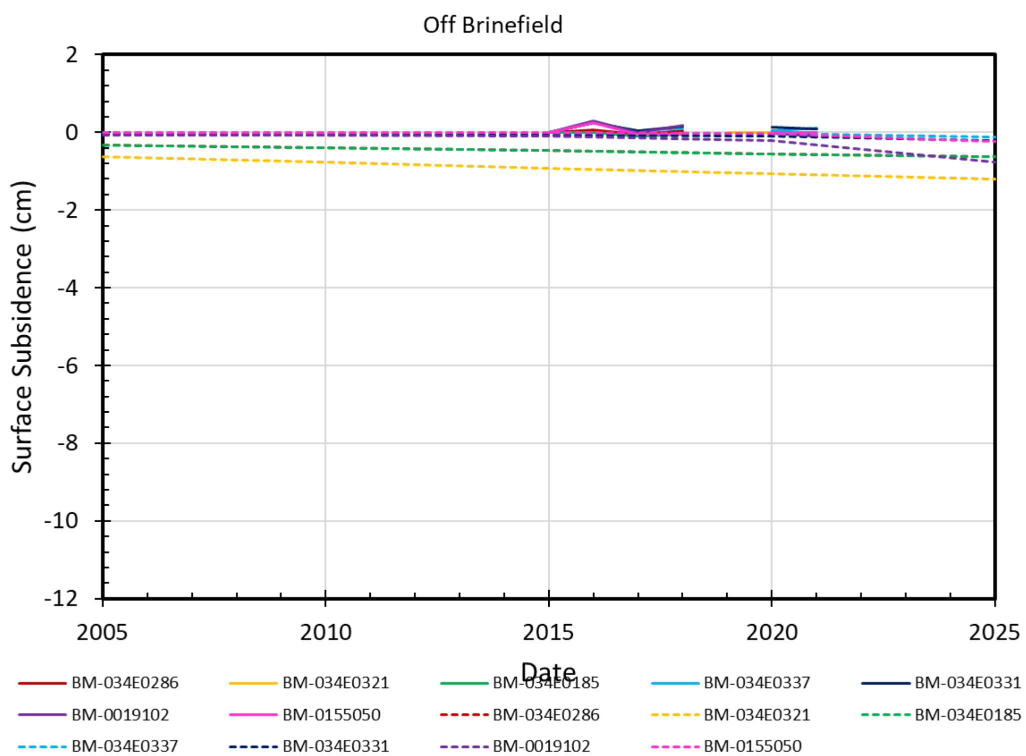

Figure A-4. Time-Series Plot Comparing the Measured and Predicted Ganzebos Benchmarks Located Off the Brinefield and Benchmarks Overlying the Brinefield With Low Measured Subsidence Rates.

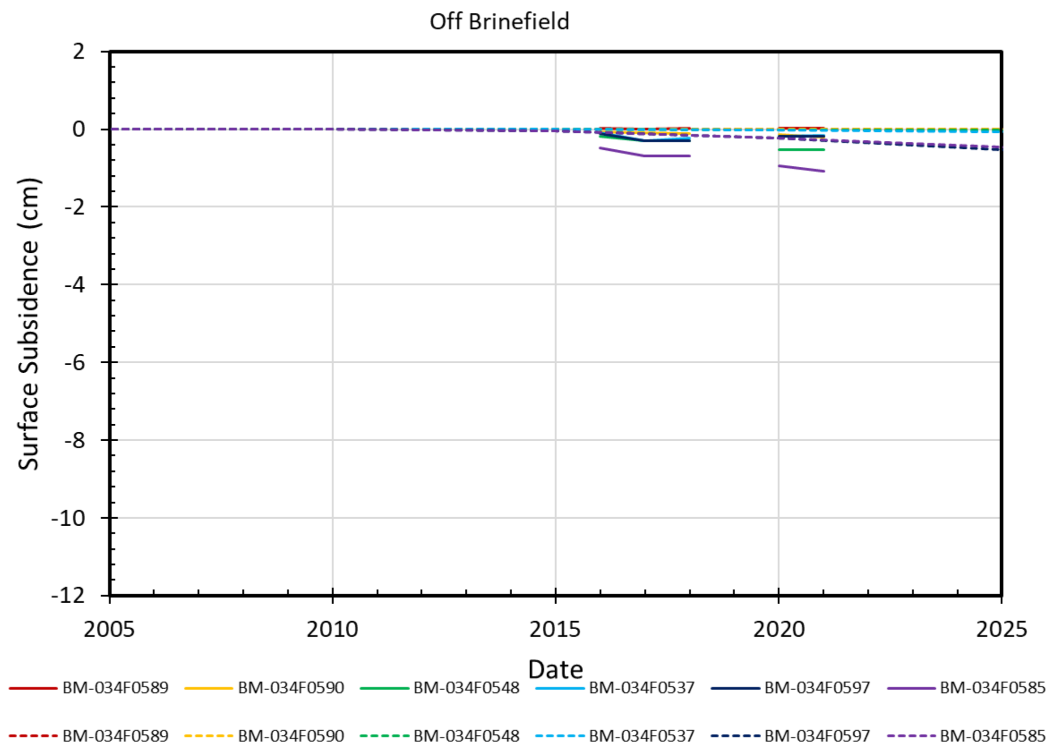

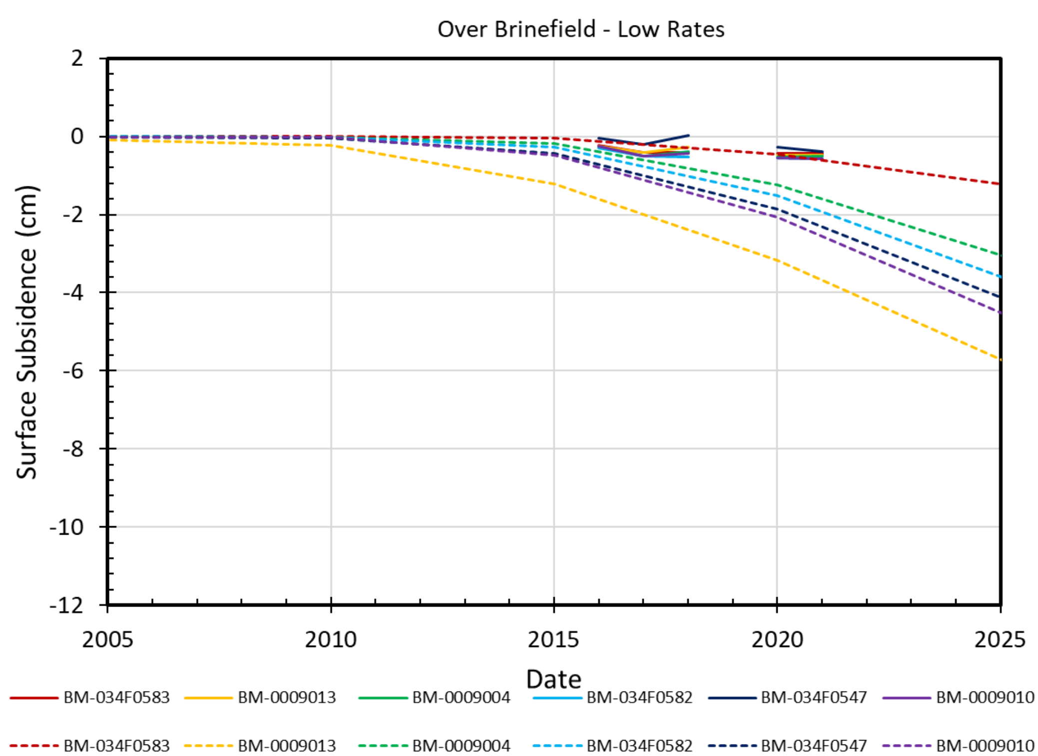

Figure A-5. Time-Series Plot Comparing the Measured and Predicted Usseler Es Benchmarks Located Off the Brinefield and Benchmarks Overlying the Brinefield With Low Measured Subsidence Rates.

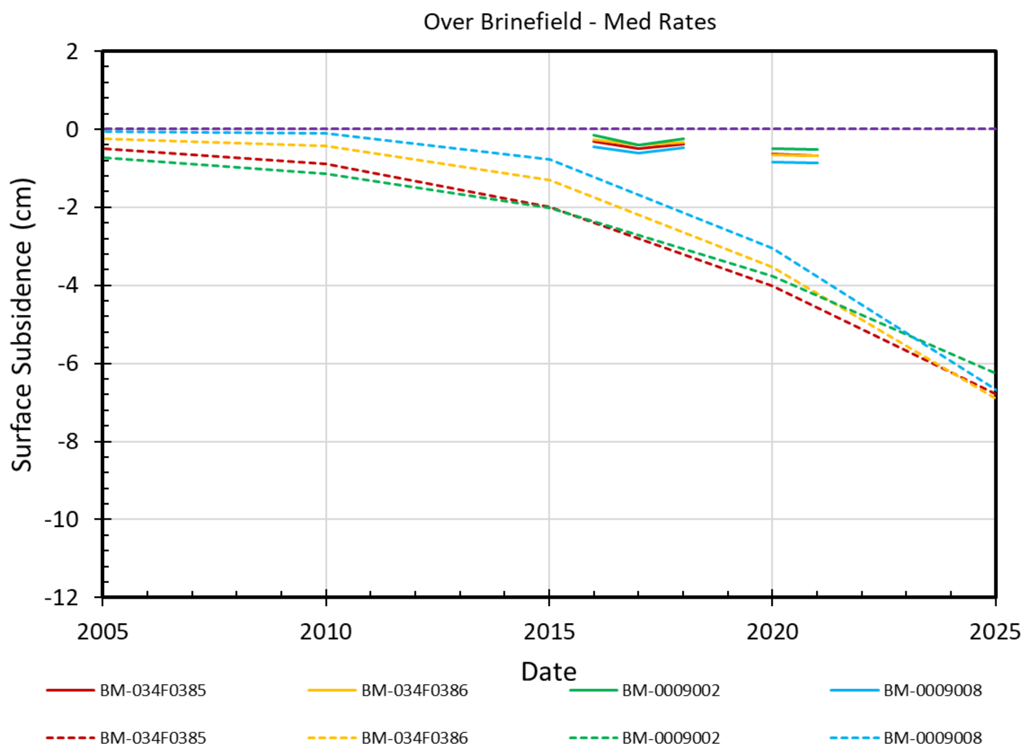

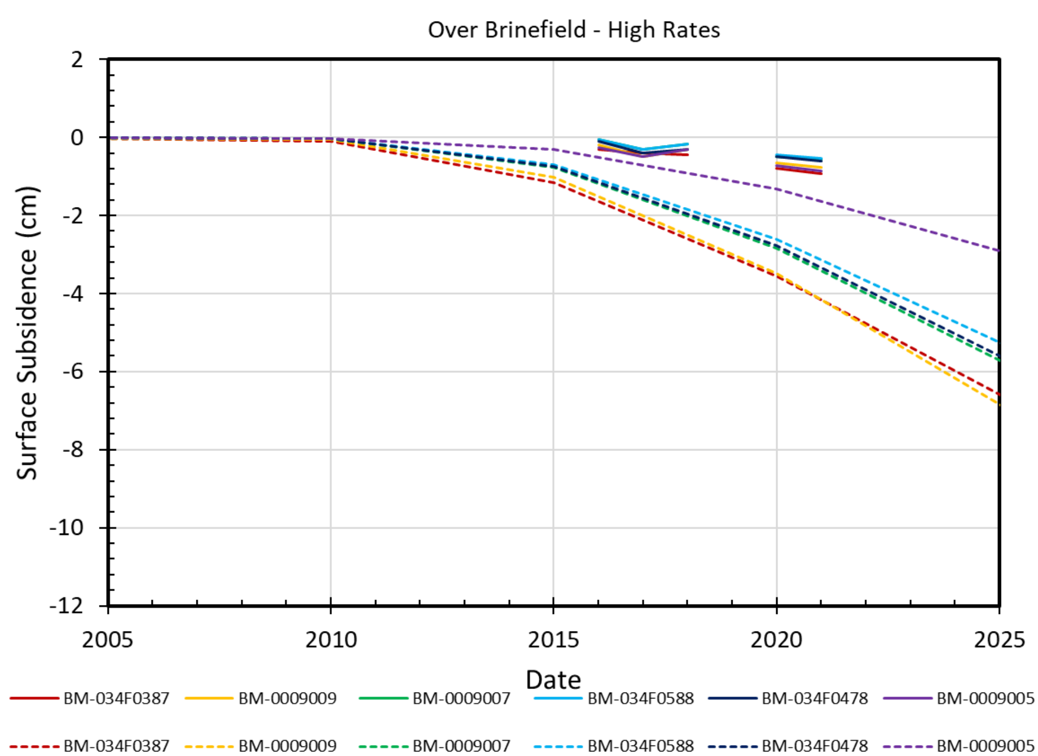

Figure A-6. Time-Series Plot Comparing the Measured and Predicted Ganzebos Benchmarks Located Over the Brinefield With Medium to High Measured Subsidence Rates.

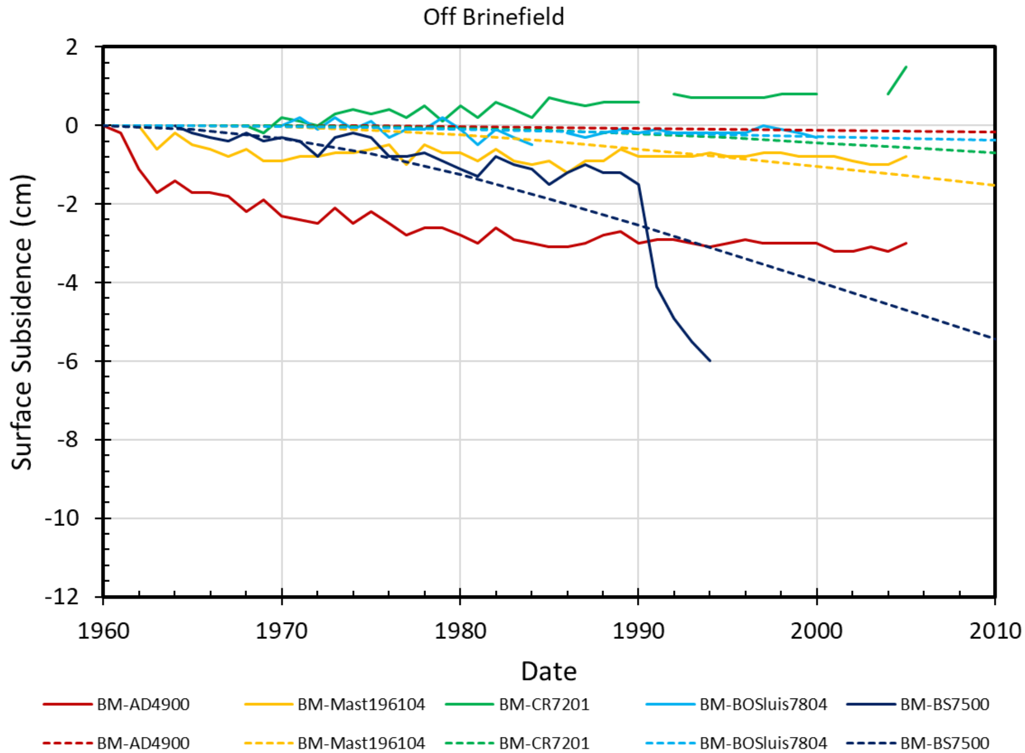

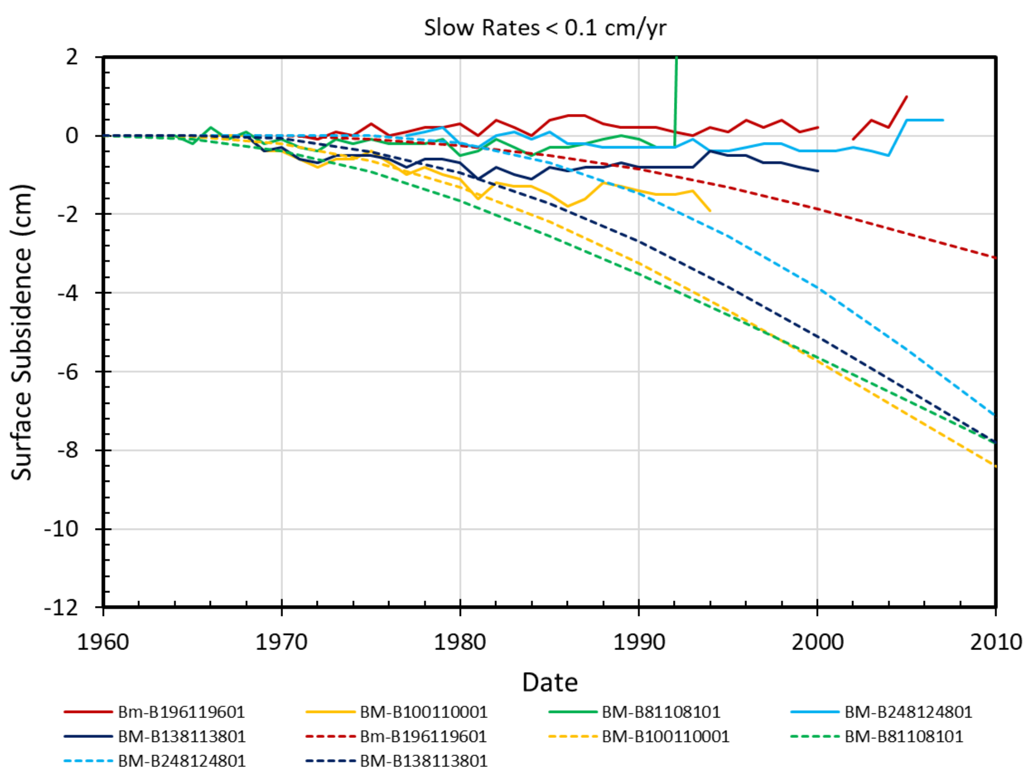

Figure A-7. Time-Series Plot Comparing the Measured and Predicted Hengelo Benchmarks Located Off the Brinefield and Benchmarks Overlying the Brinefield With Low Measured Subsidence Rates.

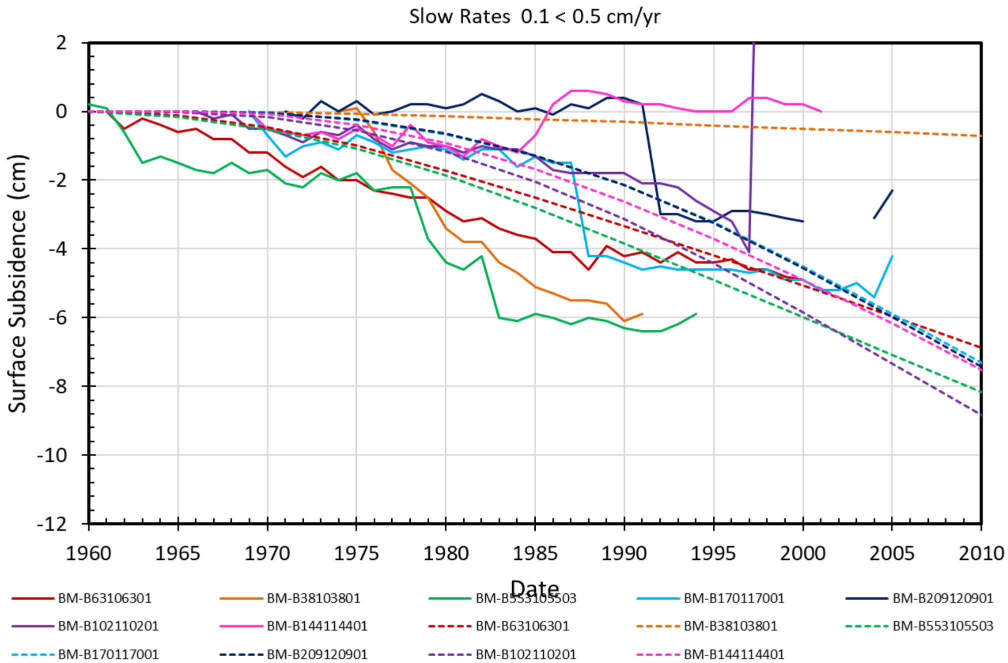

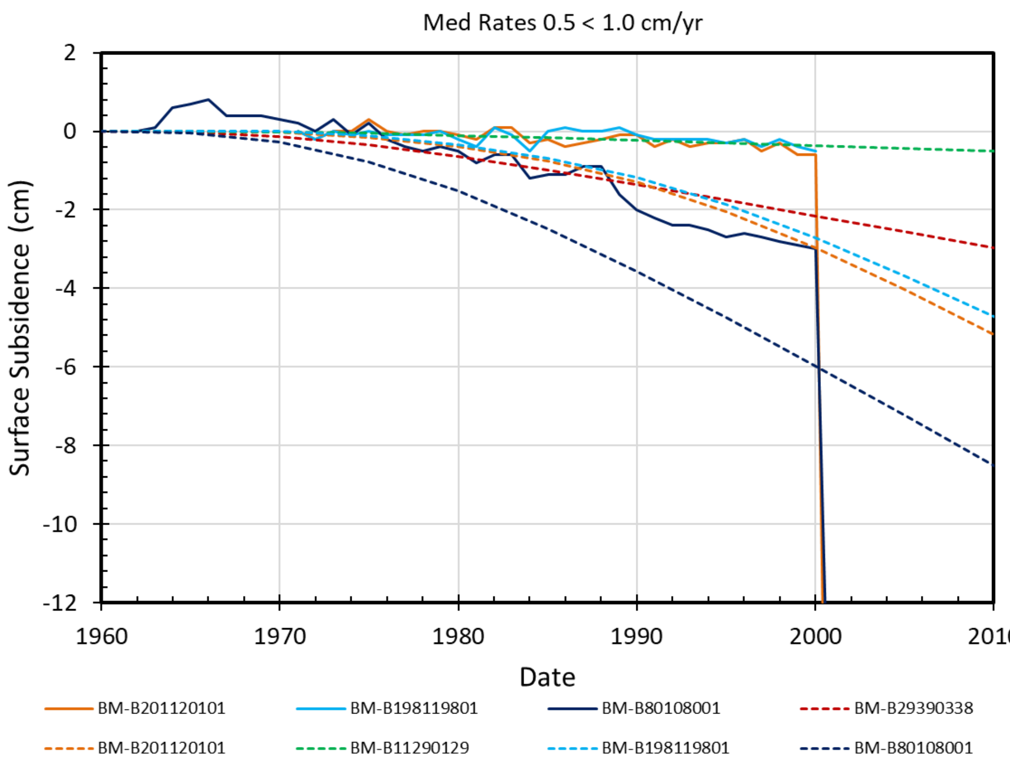

Figure A-8. Time Time-Series Plot Comparing the Measured and Predicted Hengelo Benchmarks Located Off the Brinefield and Benchmarks Overlying the Brinefield With Low Measured Subsidence Rates.

APPENDIX B

CONTOURS OF SUBSIDENCE DISTRIBUTION ATTRIBUTED TO ALL BRINEFIELDS IN 2025, 2050, 2075, 2100, AND 2125

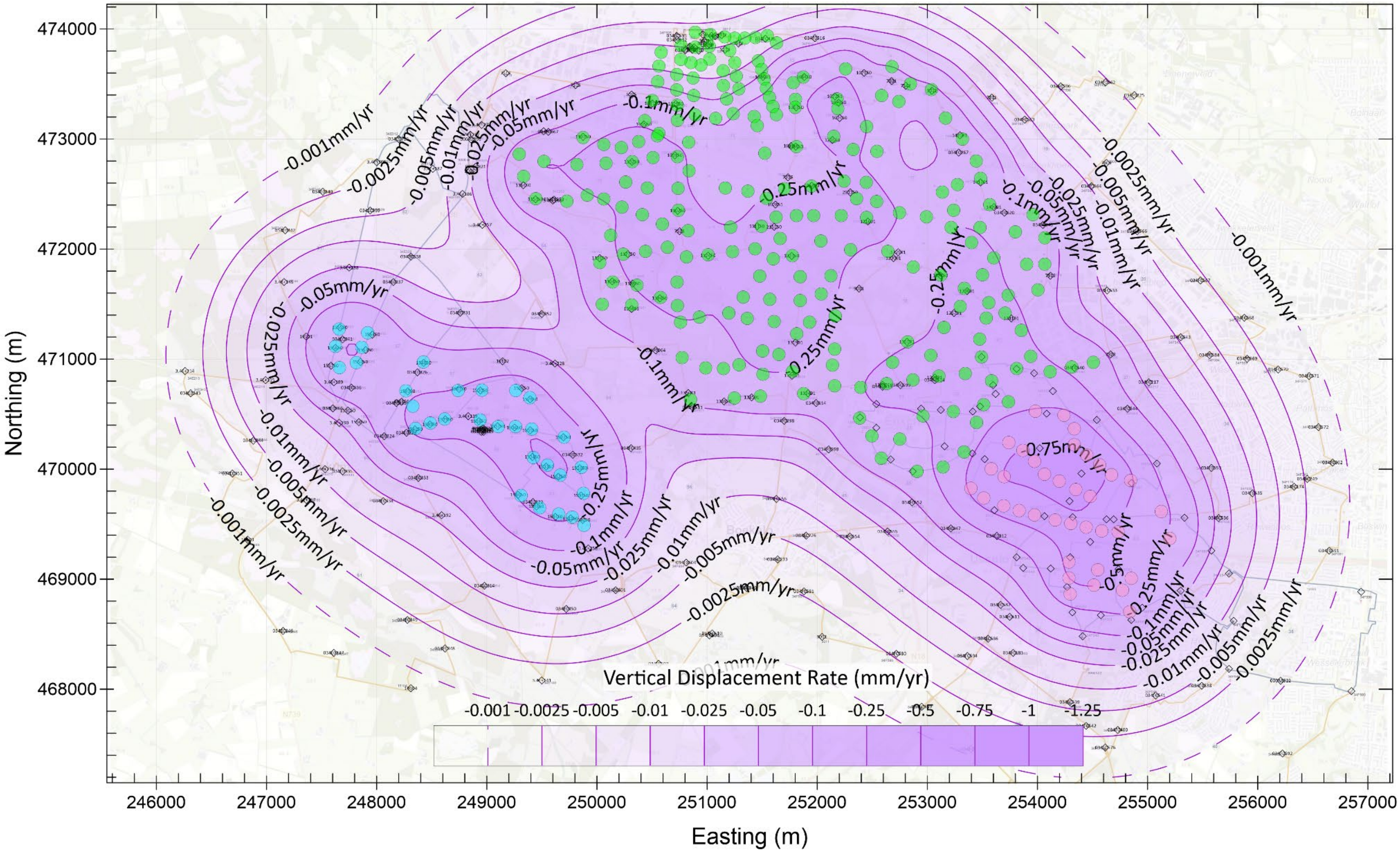

Figure B-1. Vertical Displacement Rate (Millimeters per Year) Predicted Over the Hengelo, Usseler Es, and Ganzebos Brinefields in Year 2025.

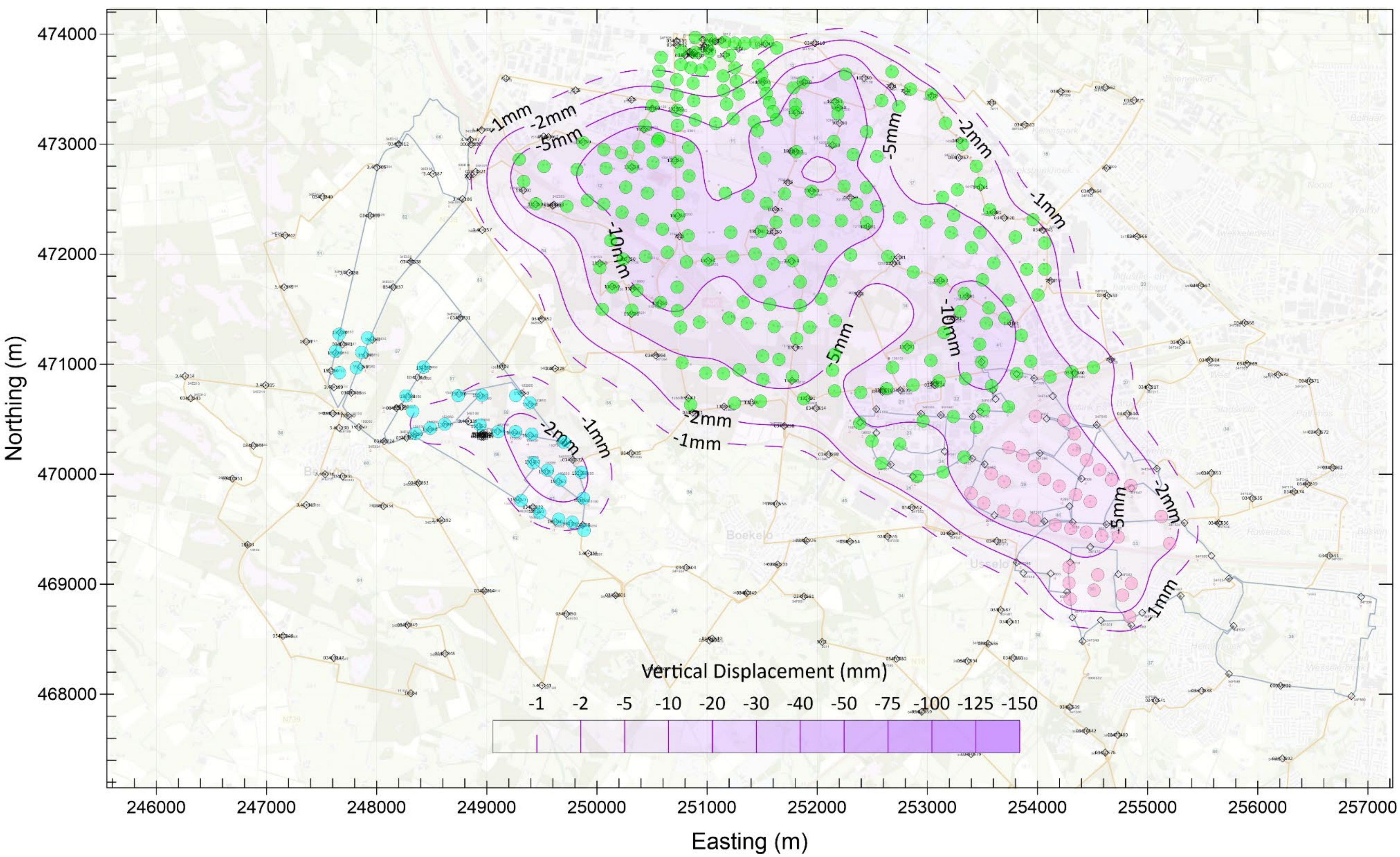

Figure B-2. Vertical Displacement (Millimeters) Predicted Over the Hengelo, Usseler Es, and Ganzebos Brinefields in Year 2025.

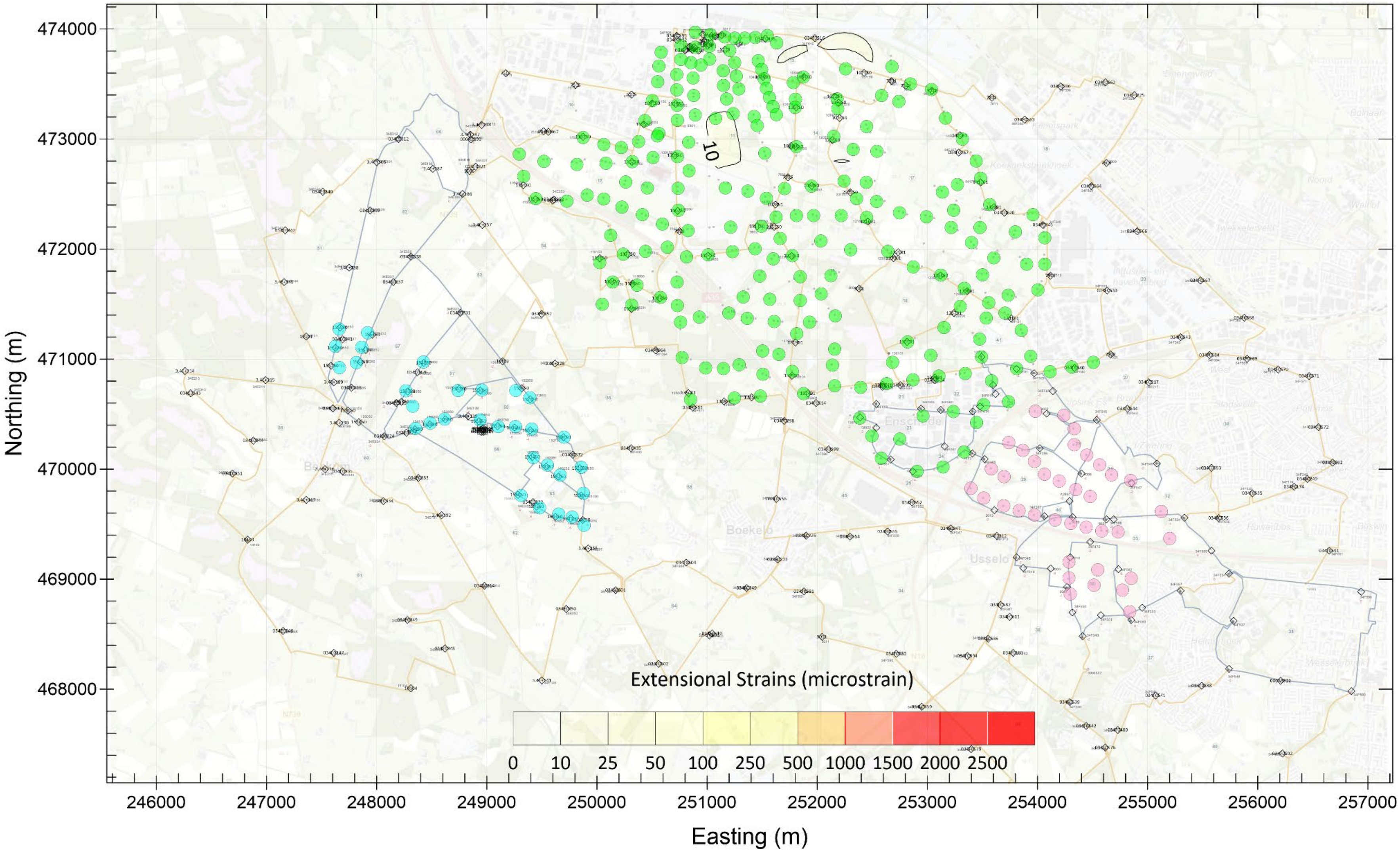

Figure B-3. Horizontal Extensional Strain (Microstrain) Predicted Over the Hengelo, Usseler Es, and Ganzebos Brinefields in Year 2025.

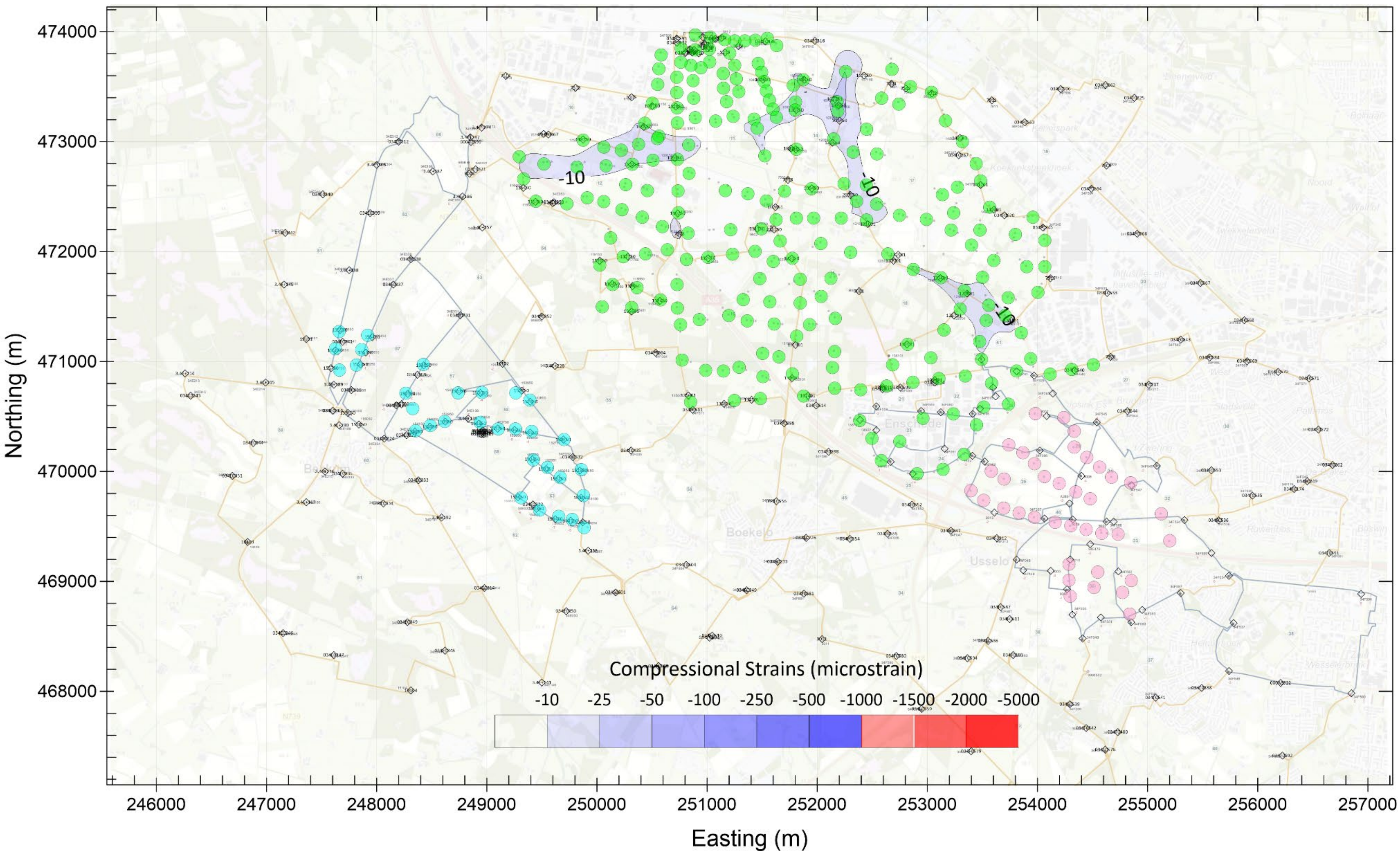

Figure B-4. Horizontal Compressional Strain (Microstrain) Predicted Over the Hengelo, Usseler Es, and Ganzebos Brinefields in Year 2025.

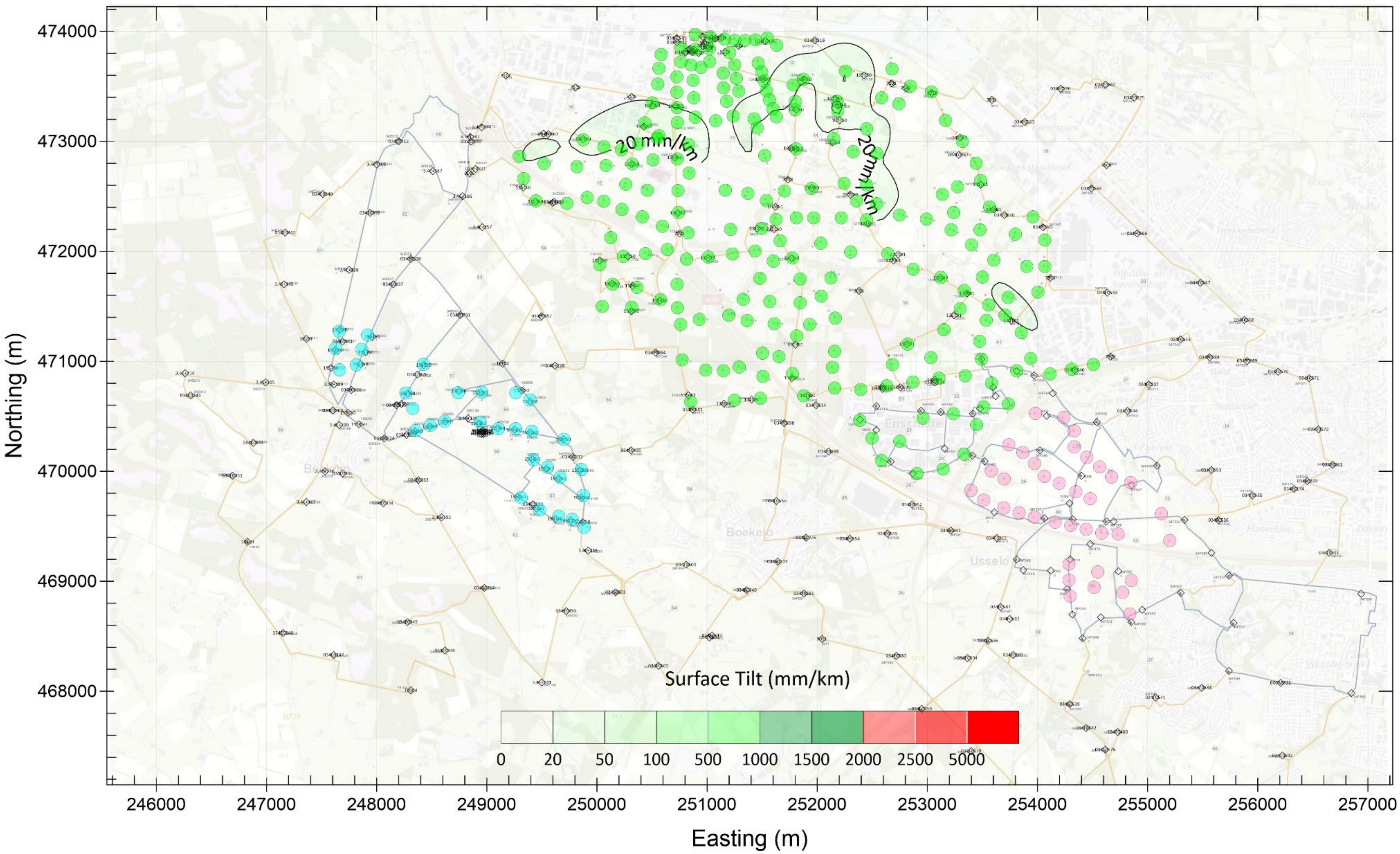

Figure B-5. Ground-Surface Tilt (Millimeters per Kilometer) Predicted Over the Hengelo, Usseler Es, and Ganzebos Brinefields in Year 2025.

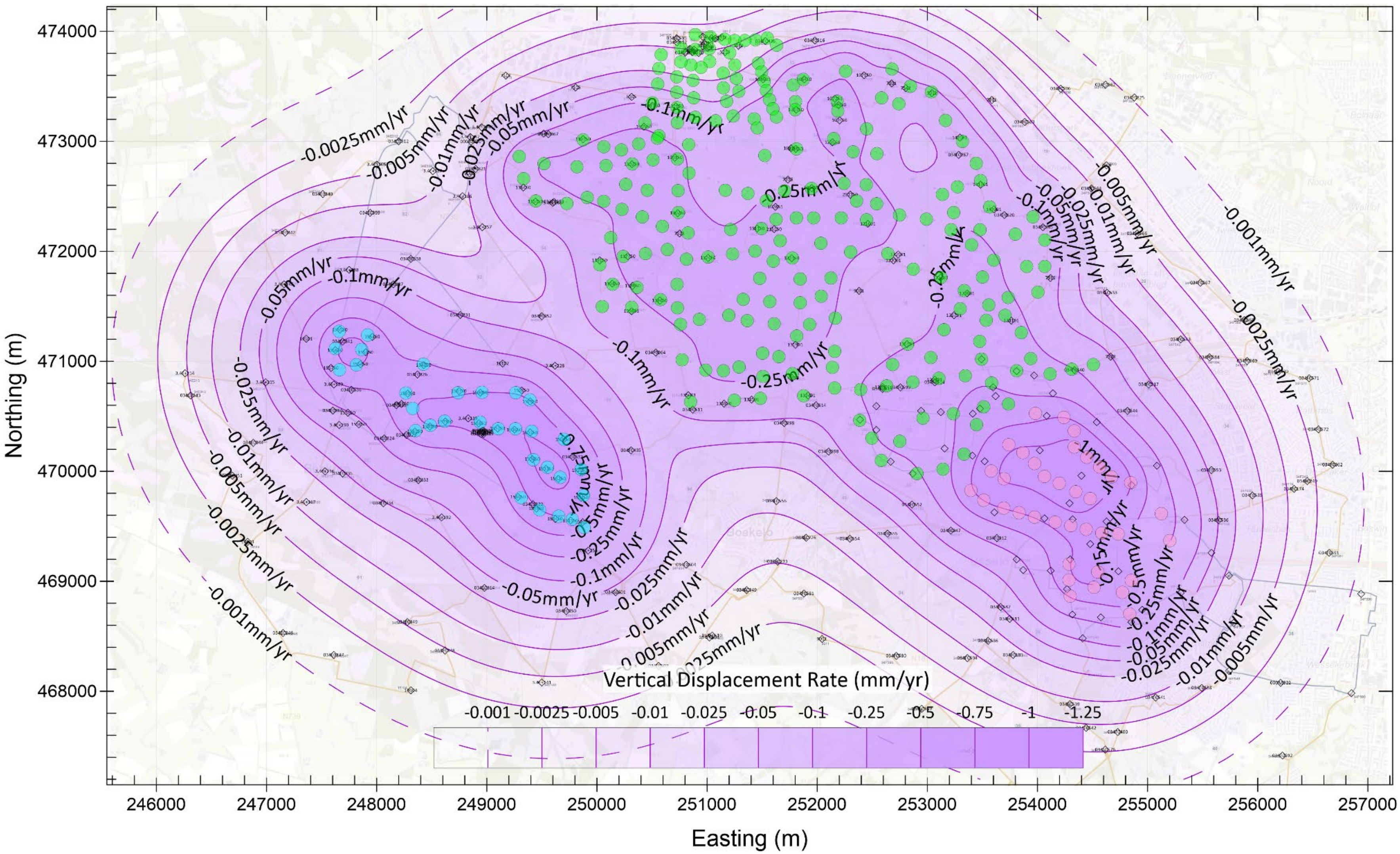

Figure B-6. Vertical Displacement Rate (Millimeters per Year) Predicted Over the Hengelo, Usseler Es, and Ganzebos Brinefields in Year 2050.

RESPEC

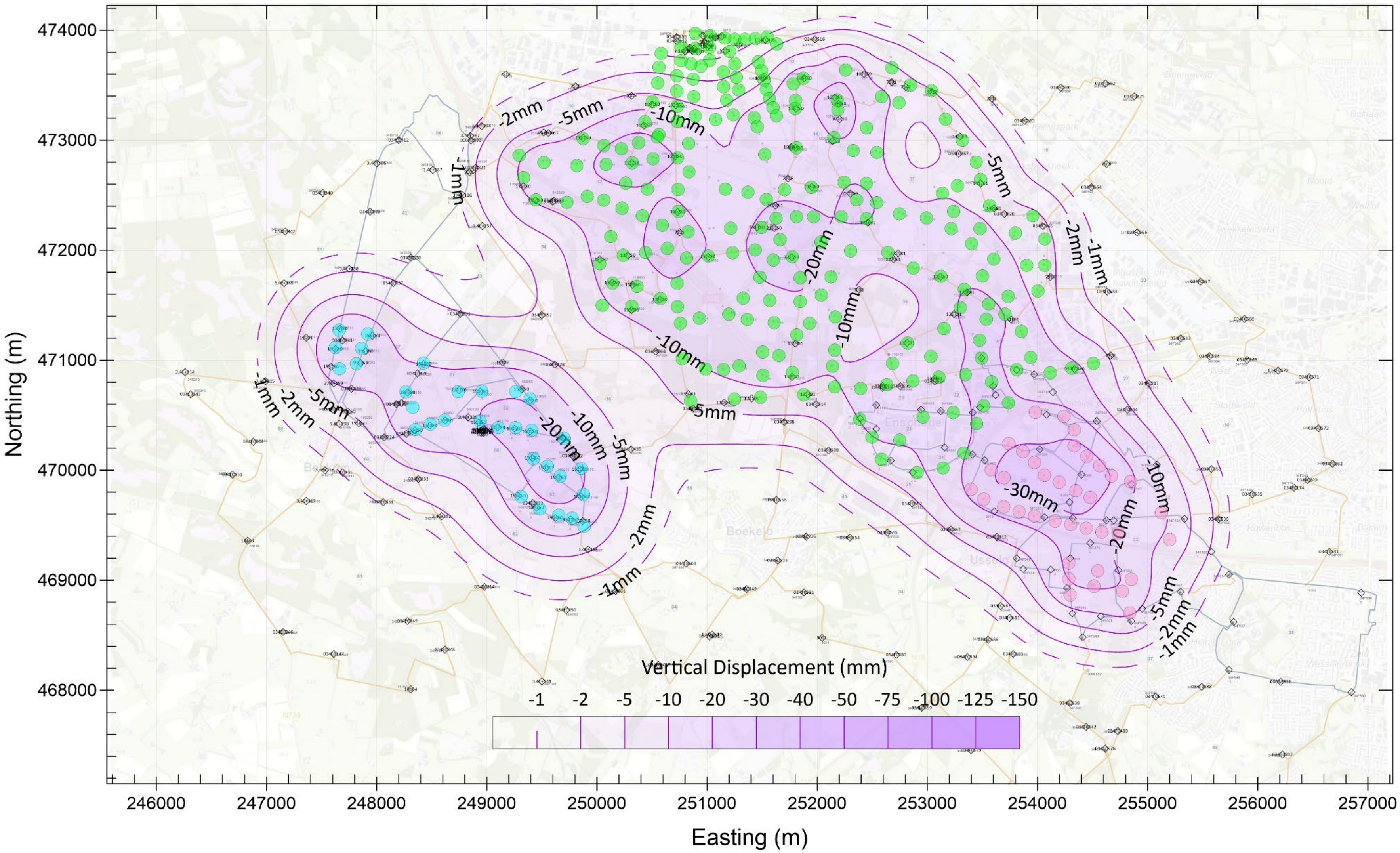

Figure B-7. Vertical Displacement (Millimeter) Predicted Over the Hengelo, Usseler Es, and Ganzebos Brinefields in Year 2050.

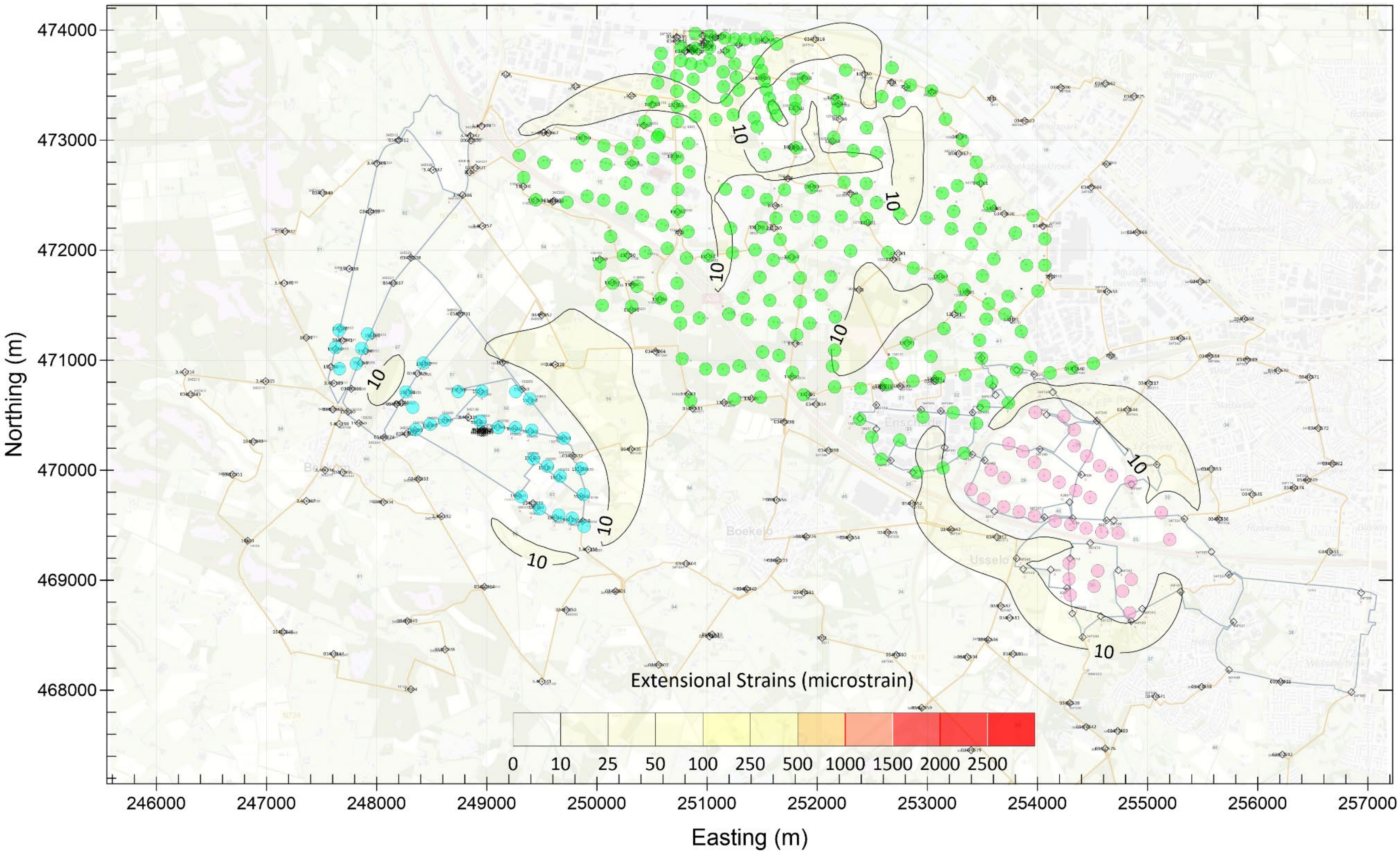

Figure B-8. Horizontal Extensional Strain (Microstrain) Predicted Over the Hengelo, Usseler Es, and Ganzebos Brinefields in Year 2050.

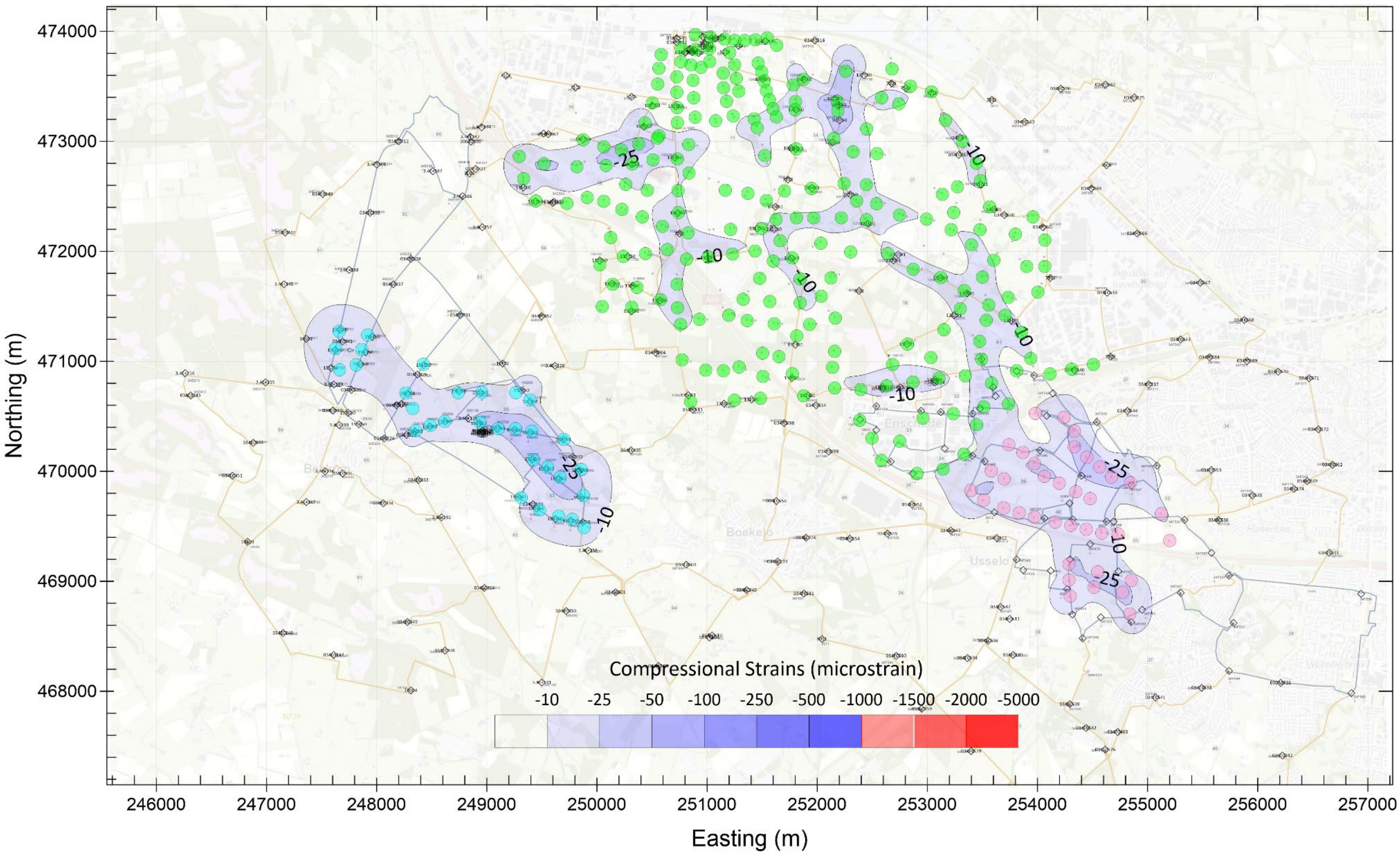

Figure B-9. Horizontal Compressional Strain (Microstrain) Predicted Over the Hengelo, Usseler Es, and Ganzebos Brinefields in Year 2050.

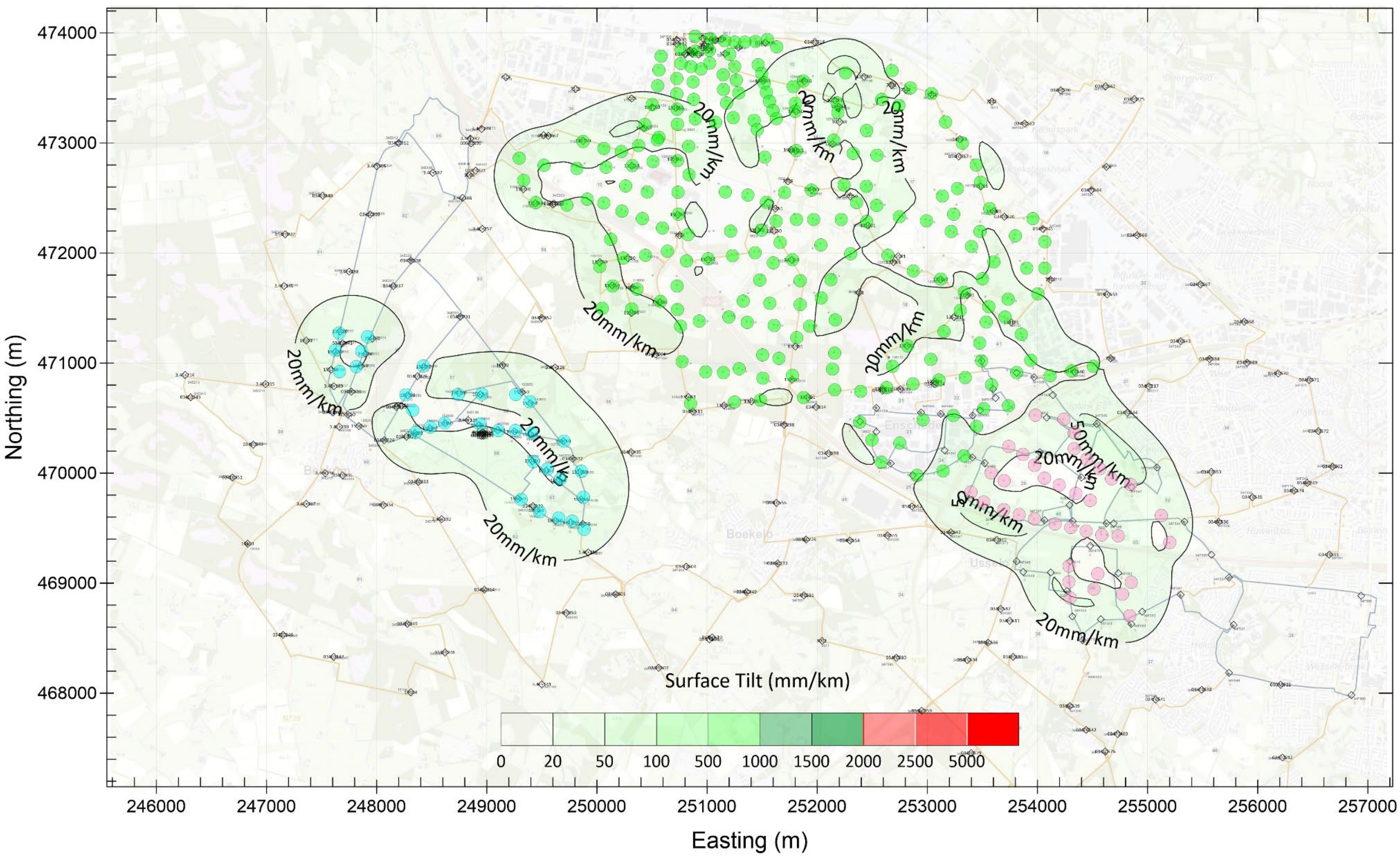

Figure B-10. Ground-Surface Tilt (Millimeters per Kilometer) Predicted Over the Hengelo, Usseler Es, and Ganzebos Brinefields in Year 2050.

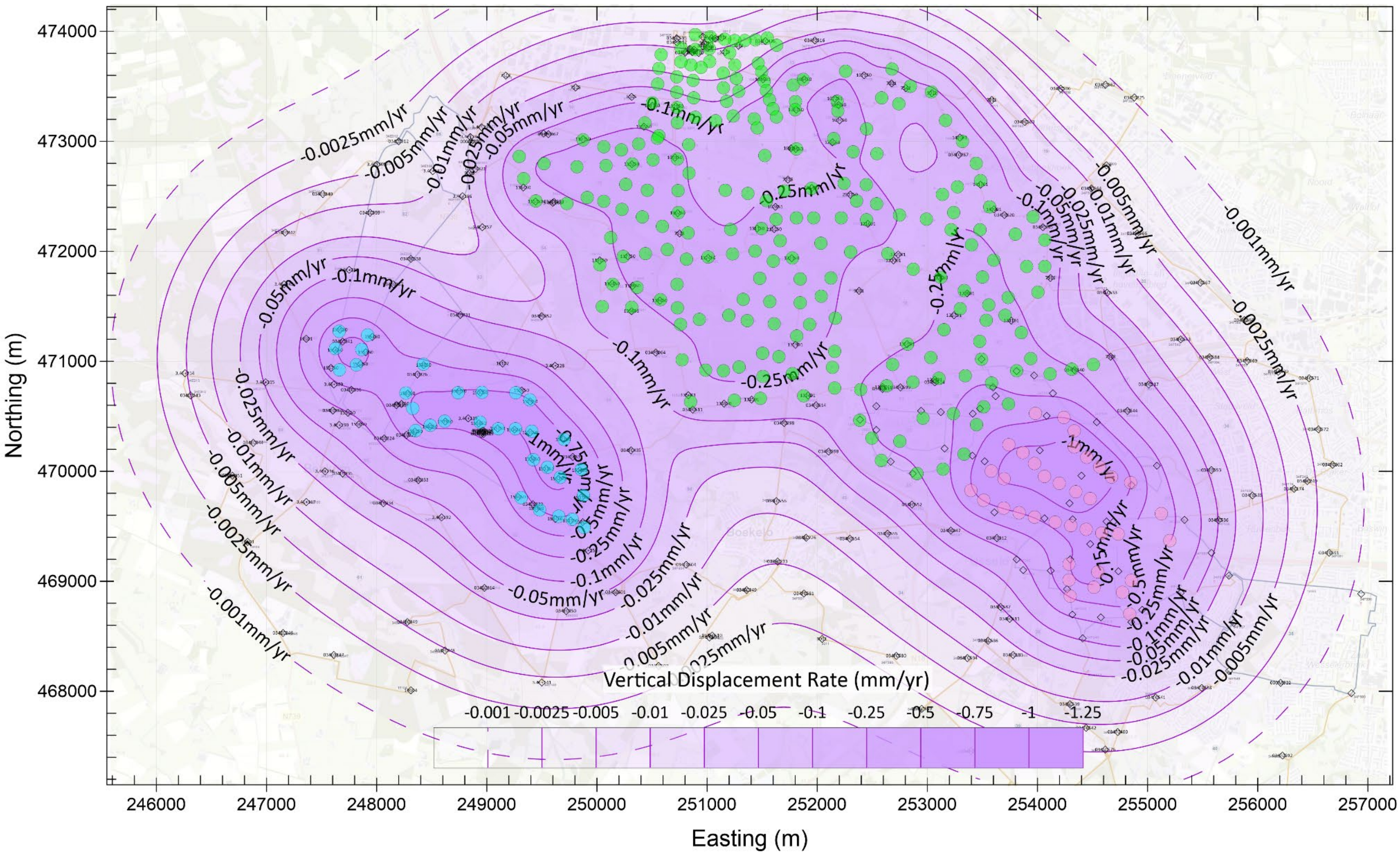

Figure B-11. Vertical Displacement Rate (Millimeters per Year) Predicted Over the Hengelo, Usseler Es, and Ganzebos Brinefields in Year 2075.

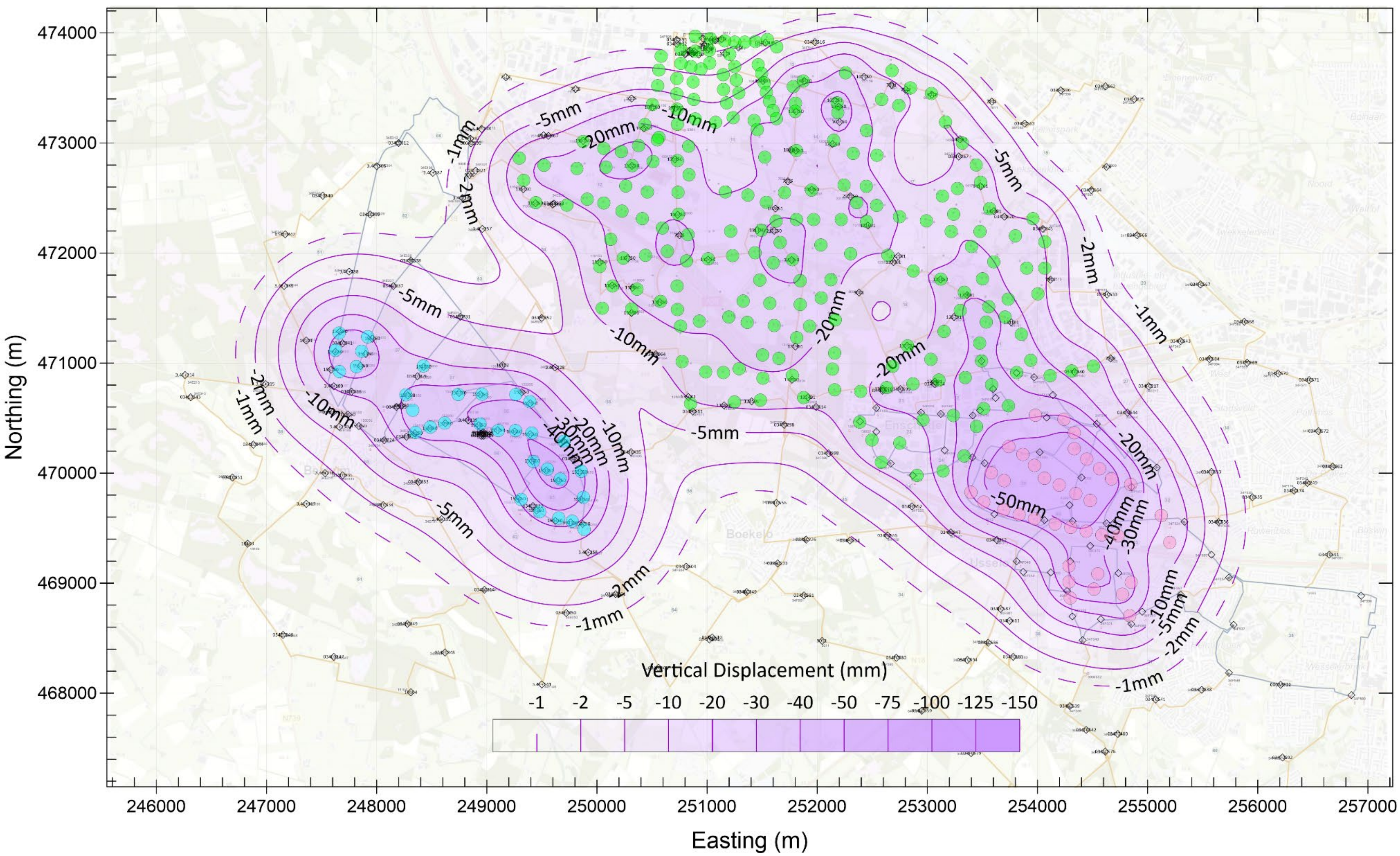

Figure B-12. Vertical Displacement (Millimeters) Predicted Over the Hengelo, Usseler Es, and Ganzebos Brinefields in Year 2075.

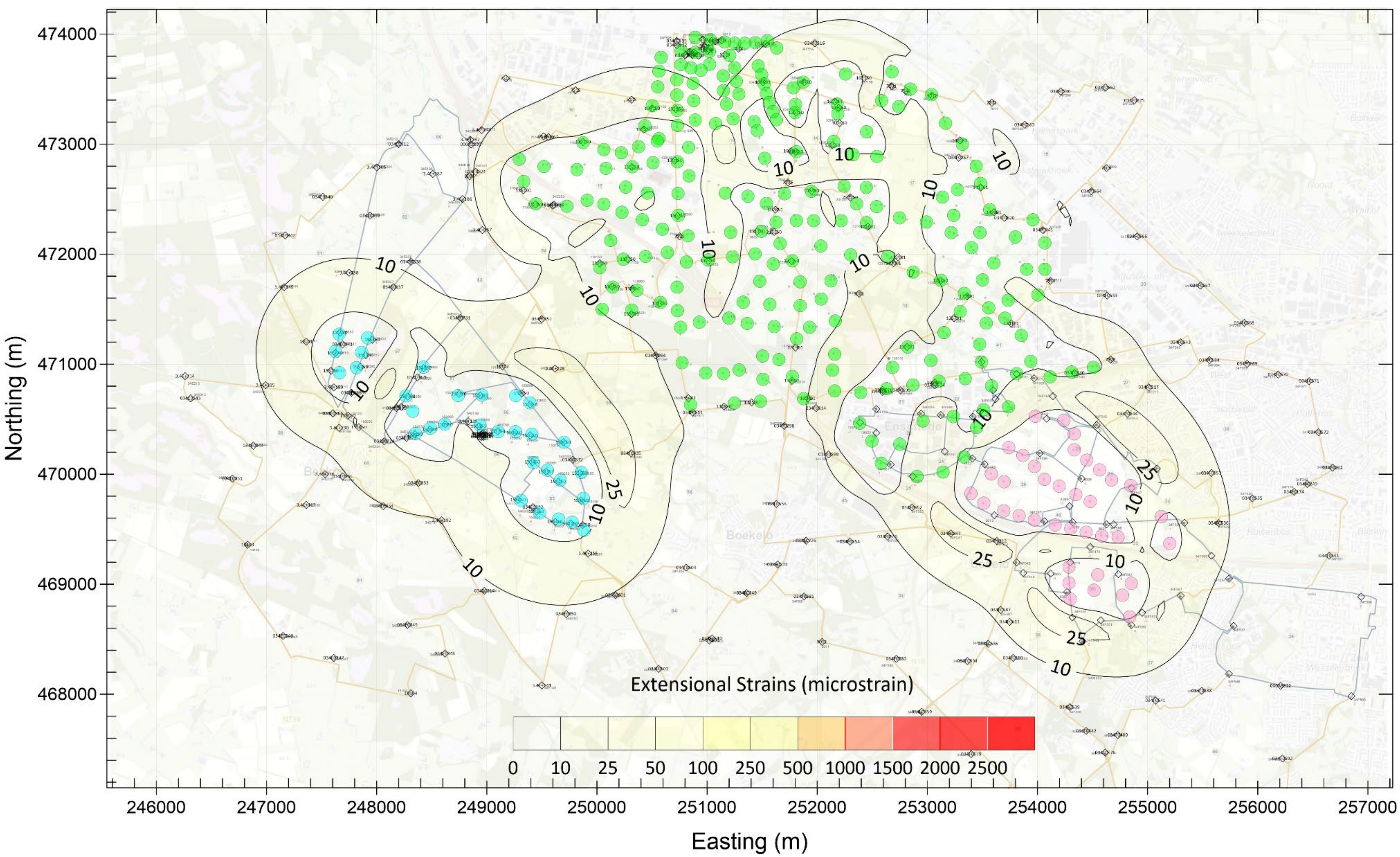

Figure B-13. Horizontal Extensional Strain (Microstrain) Predicted Over the Hengelo, Usseler Es, and Ganzebos Brinefields in Year 2075.

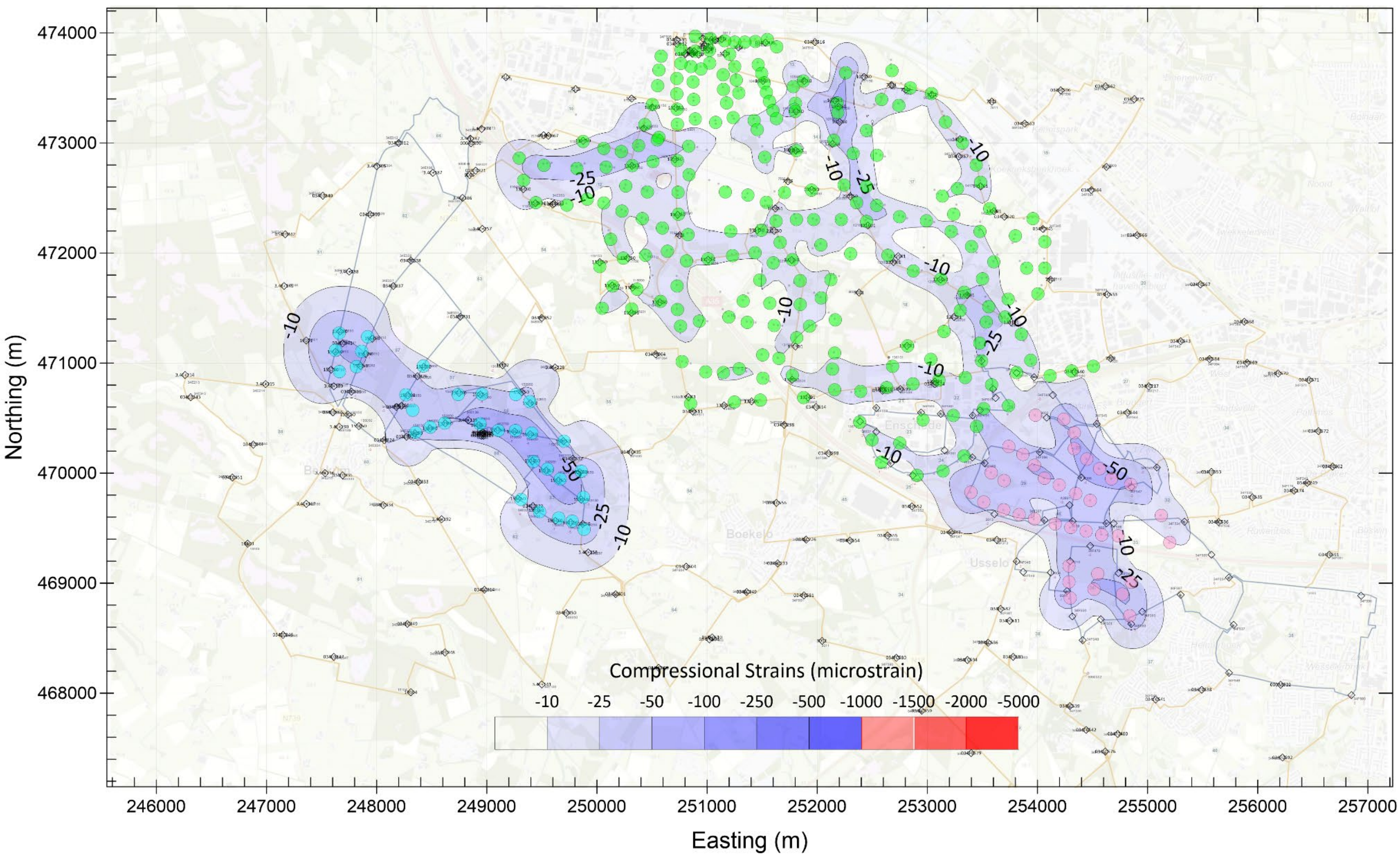

Figure B-14. Horizontal Compressional Strain (Microstrain) Predicted Over the Hengelo, Usseler Es, and Ganzebos Brinefields in Year 2075.

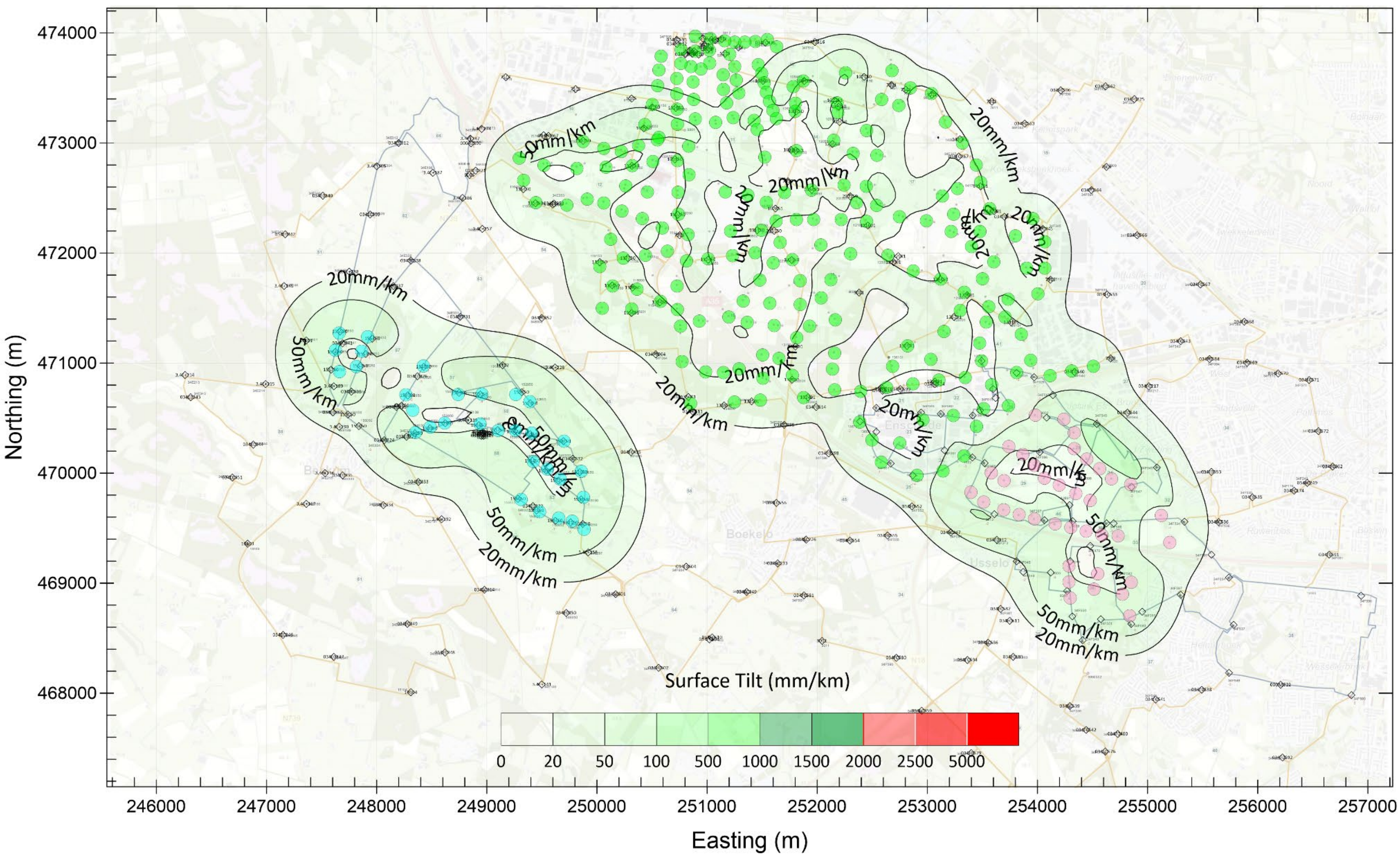

Figure B-15. Ground-Surface Tilt (Millimeters per Kilometer) Predicted Over the Hengelo, Usseler Es, and Ganzebos Brinefields in Year 2075.

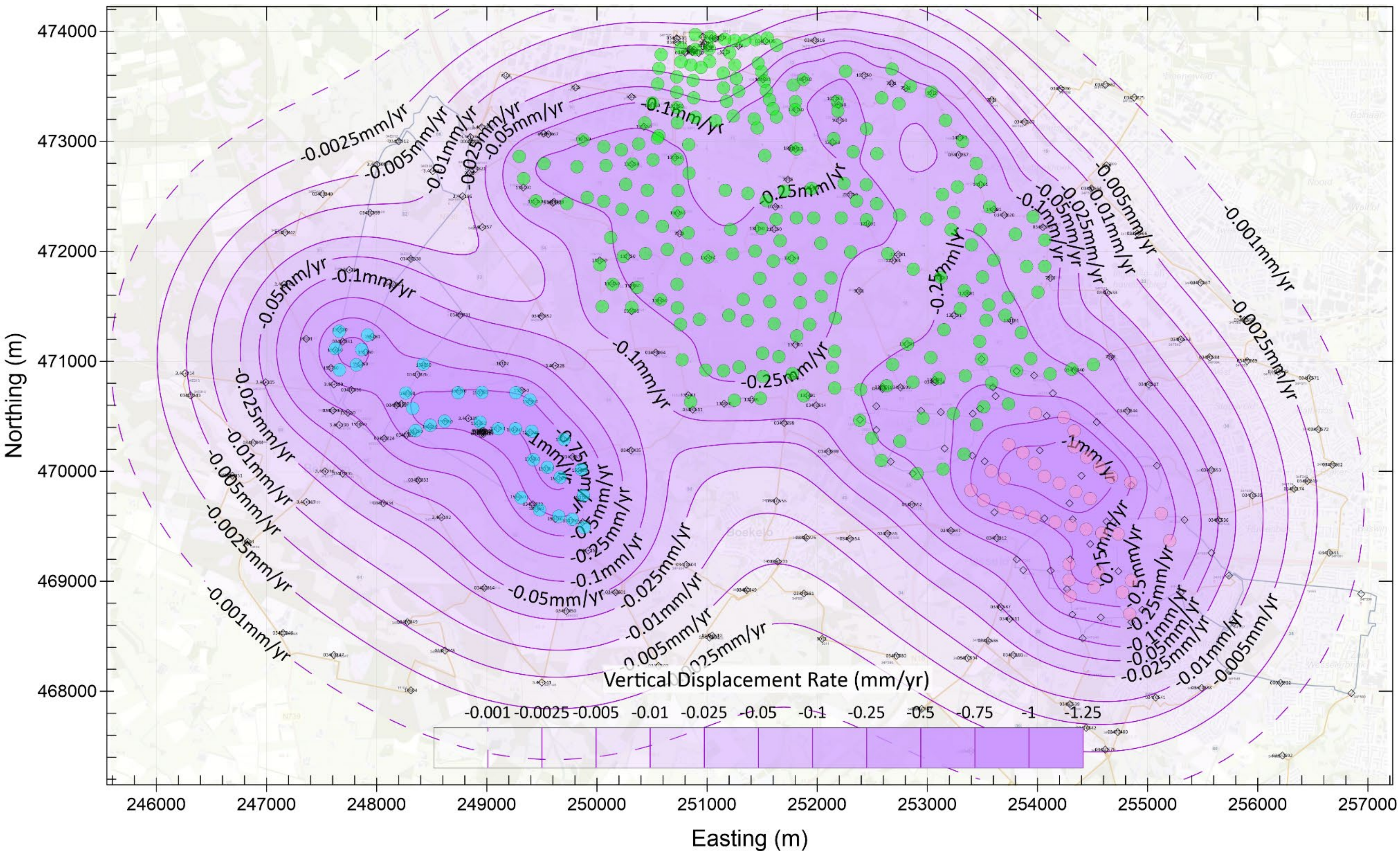

Figure B-16. Vertical Displacement Rate (Millimeters per Year) Predicted Over the Hengelo, Usseler Es, and Ganzebos Brinefields in Year 2100.

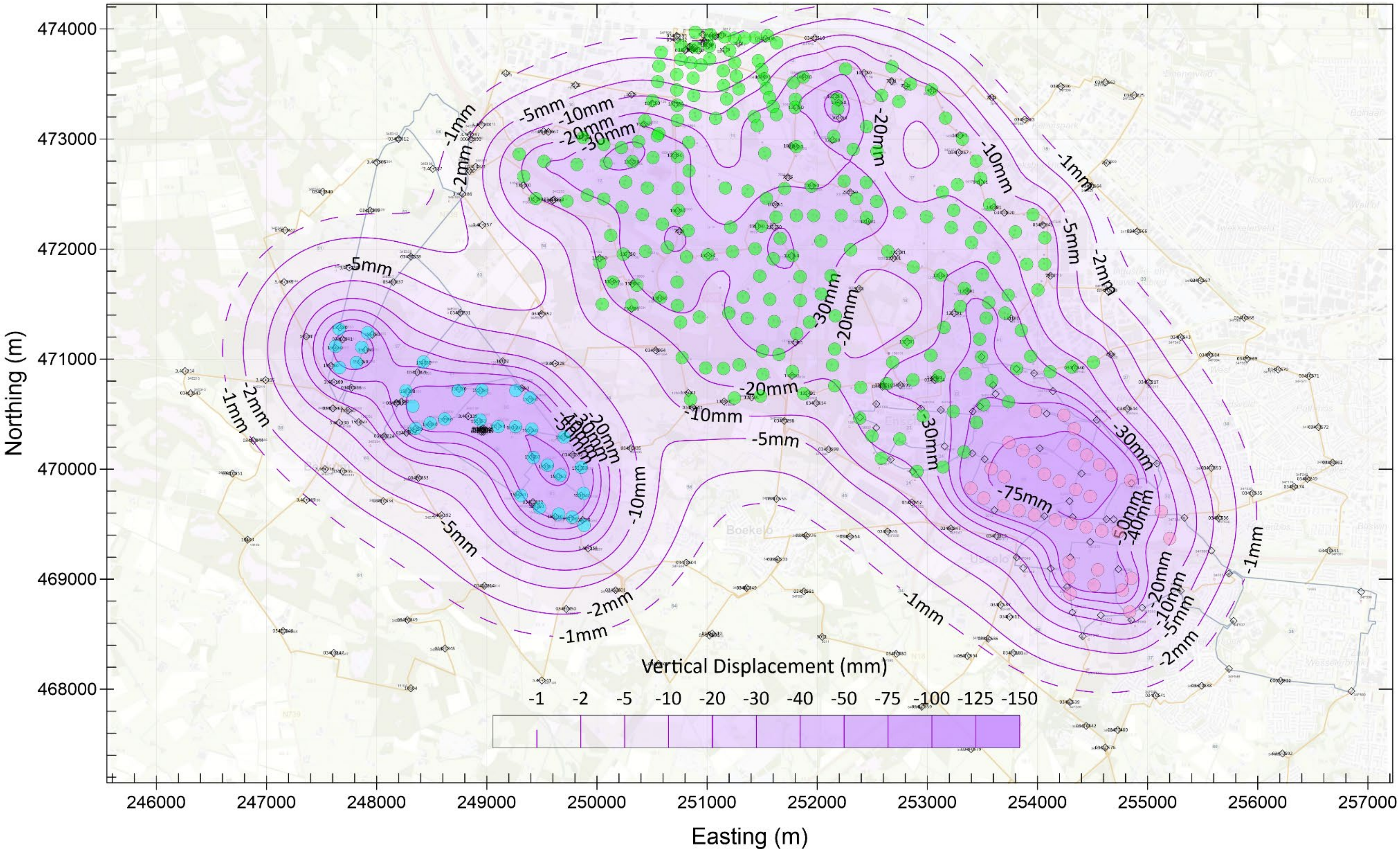

Figure B-17. Vertical Displacement (Millimeters) Predicted Over the Hengelo, Usseler Es, and Ganzebos Brinefields in Year 2100.

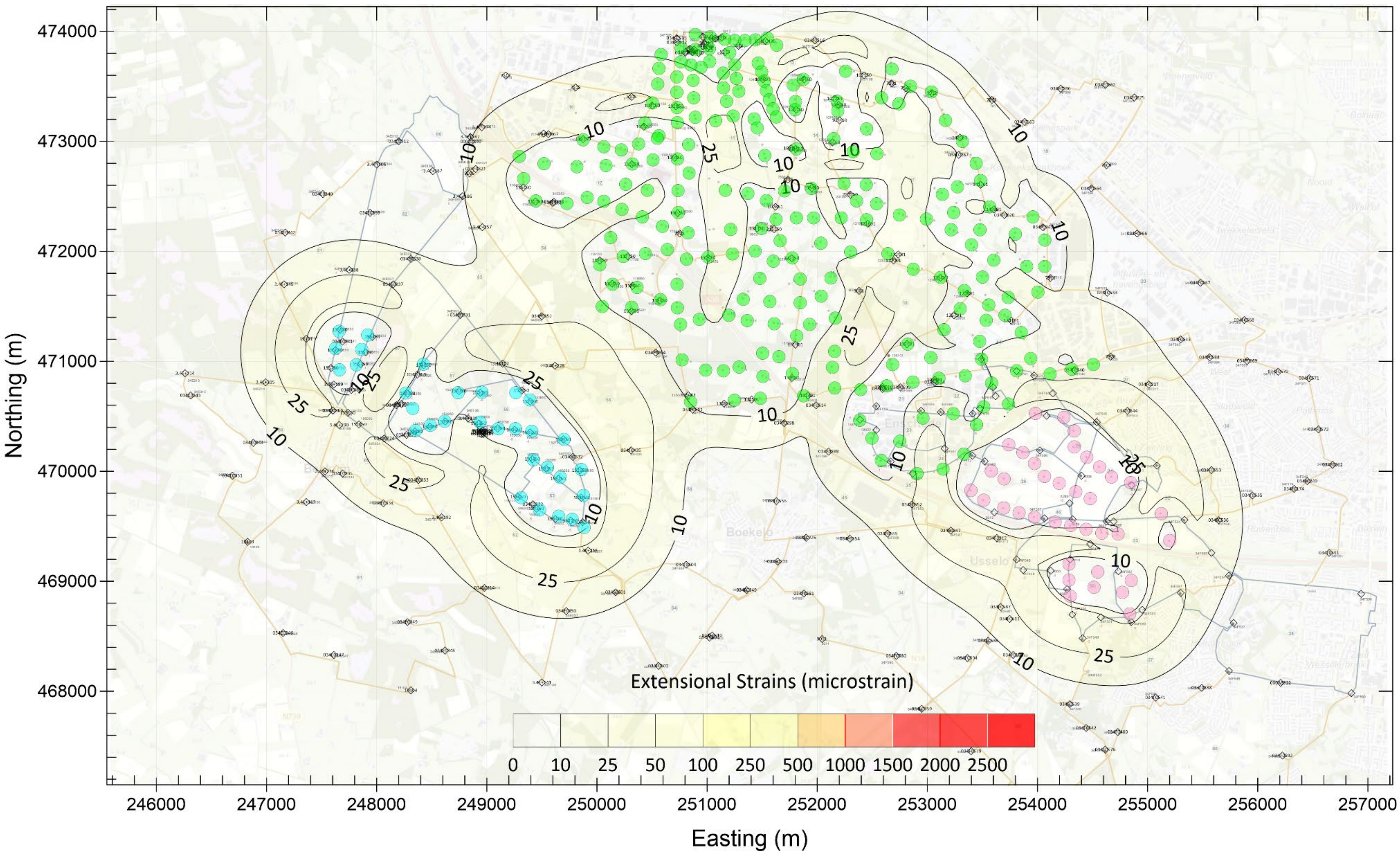

Figure B-18. Horizontal Extensional Strain (Microstrain) Predicted Over the Hengelo, Usseler Es, and Ganzebos Brinefields in Year 2100.

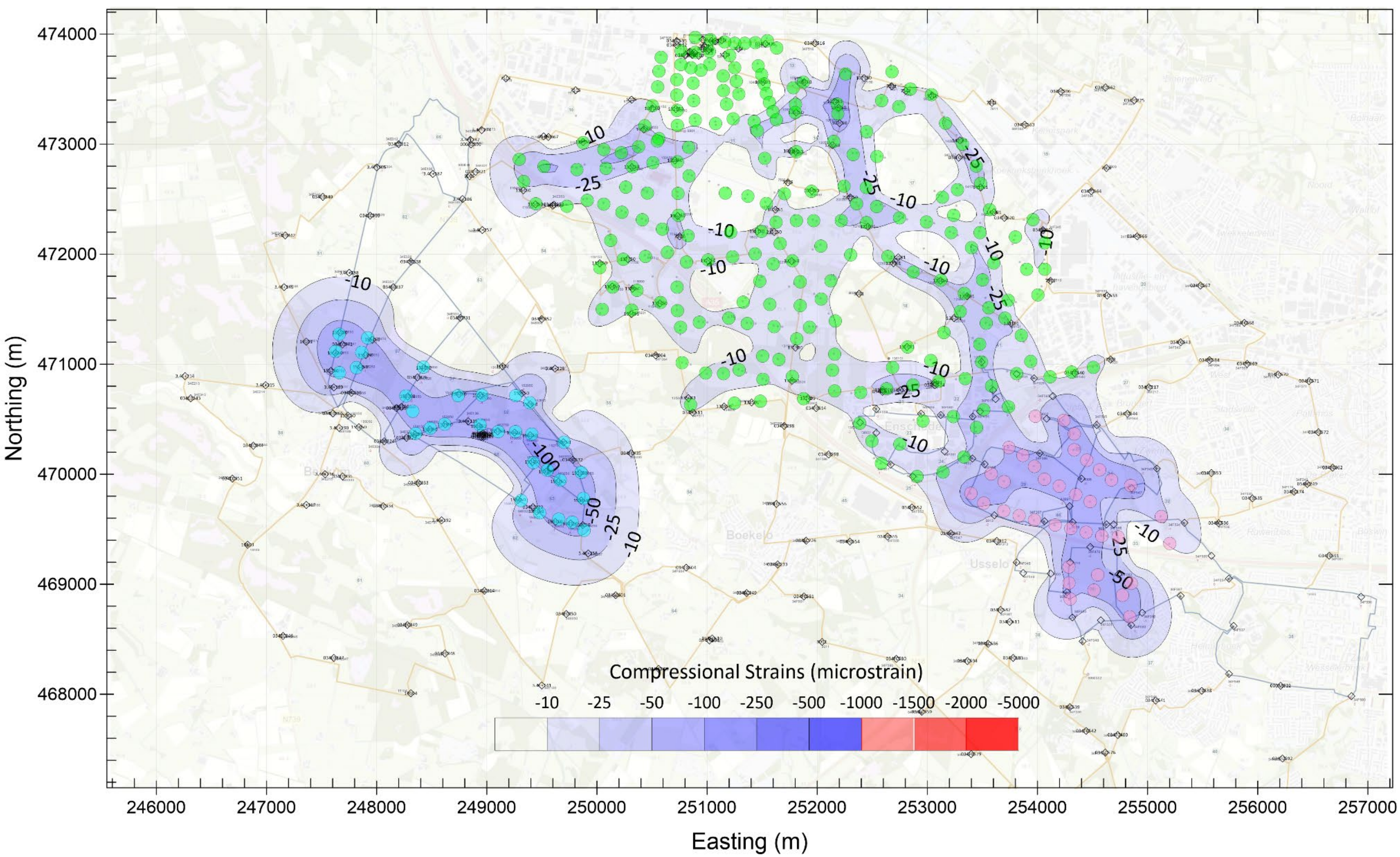

Figure B-19. Horizontal Compressional Strain (Microstrain) Predicted Over the Hengelo, Usseler Es, and Ganzebos Brinefields in Year 2100.

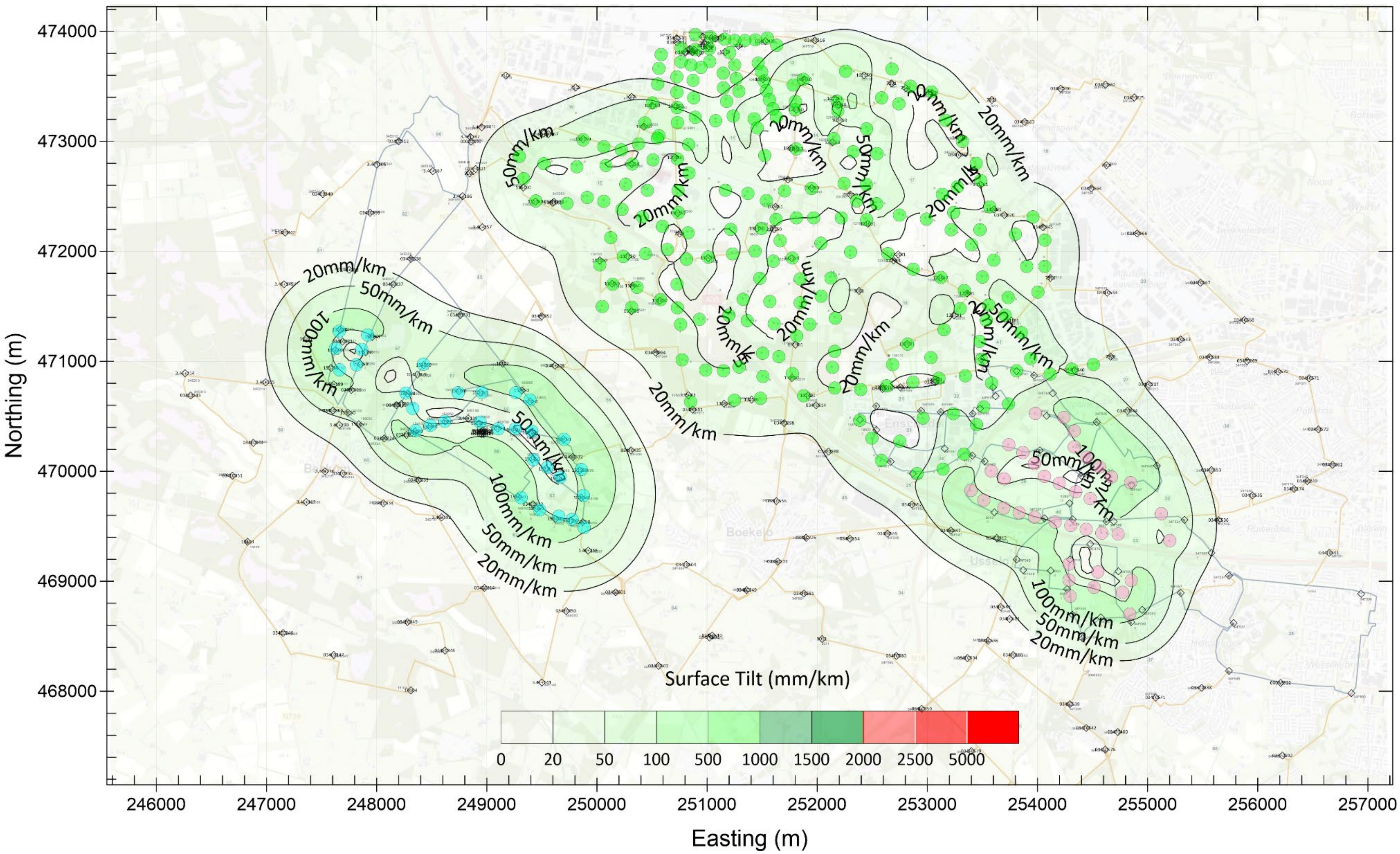

Figure B-20. Ground-Surface Tilt (Millimeters per Kilometer) Predicted Over the Hengelo, Usseler Es, and Ganzebos Brinefields in Year 2100.

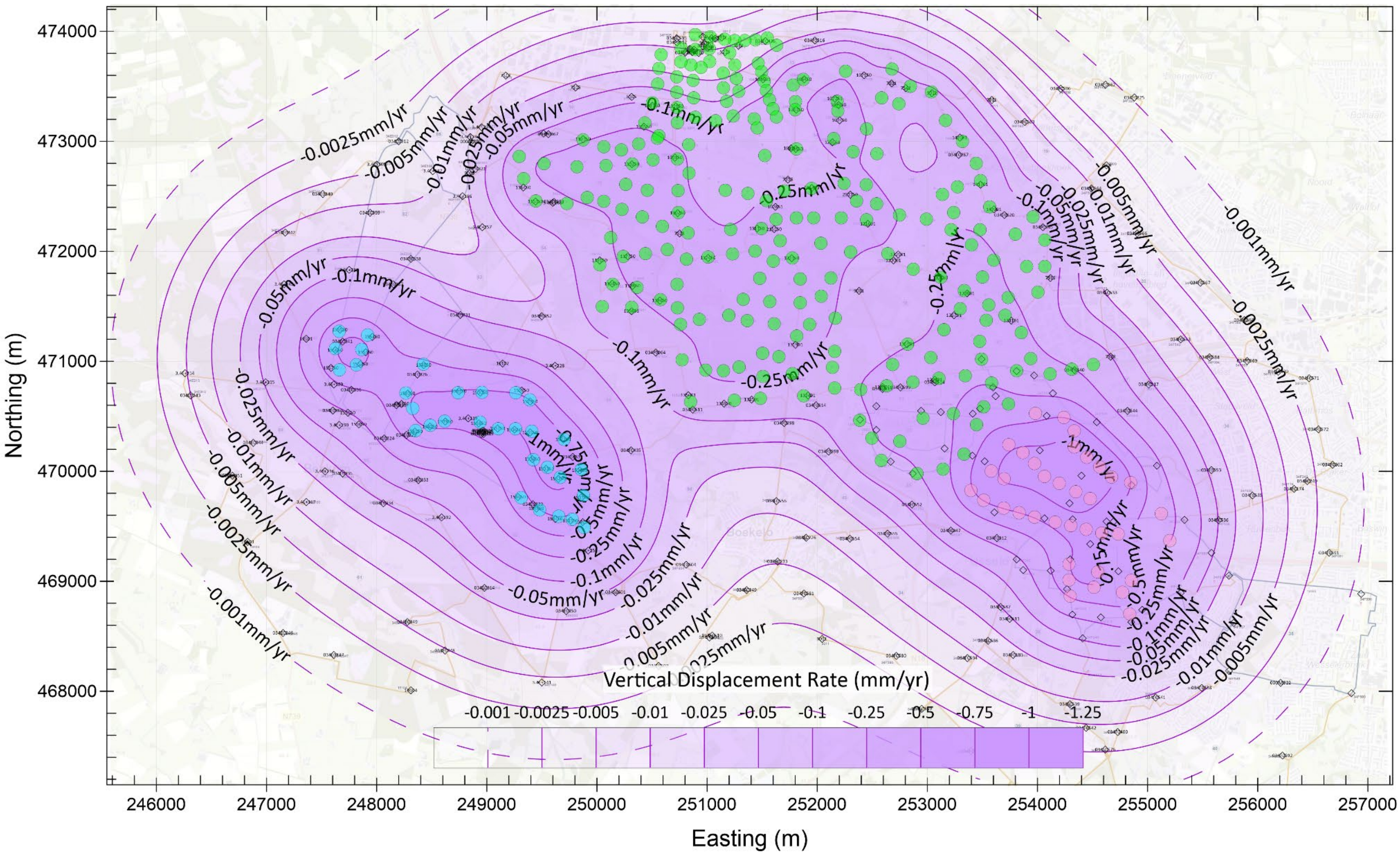

Figure B-21. Vertical Displacement Rate (Millimeters per Year) Predicted Over the Hengelo, Usseler Es, and Ganzebos Brinefields in Year 2125.

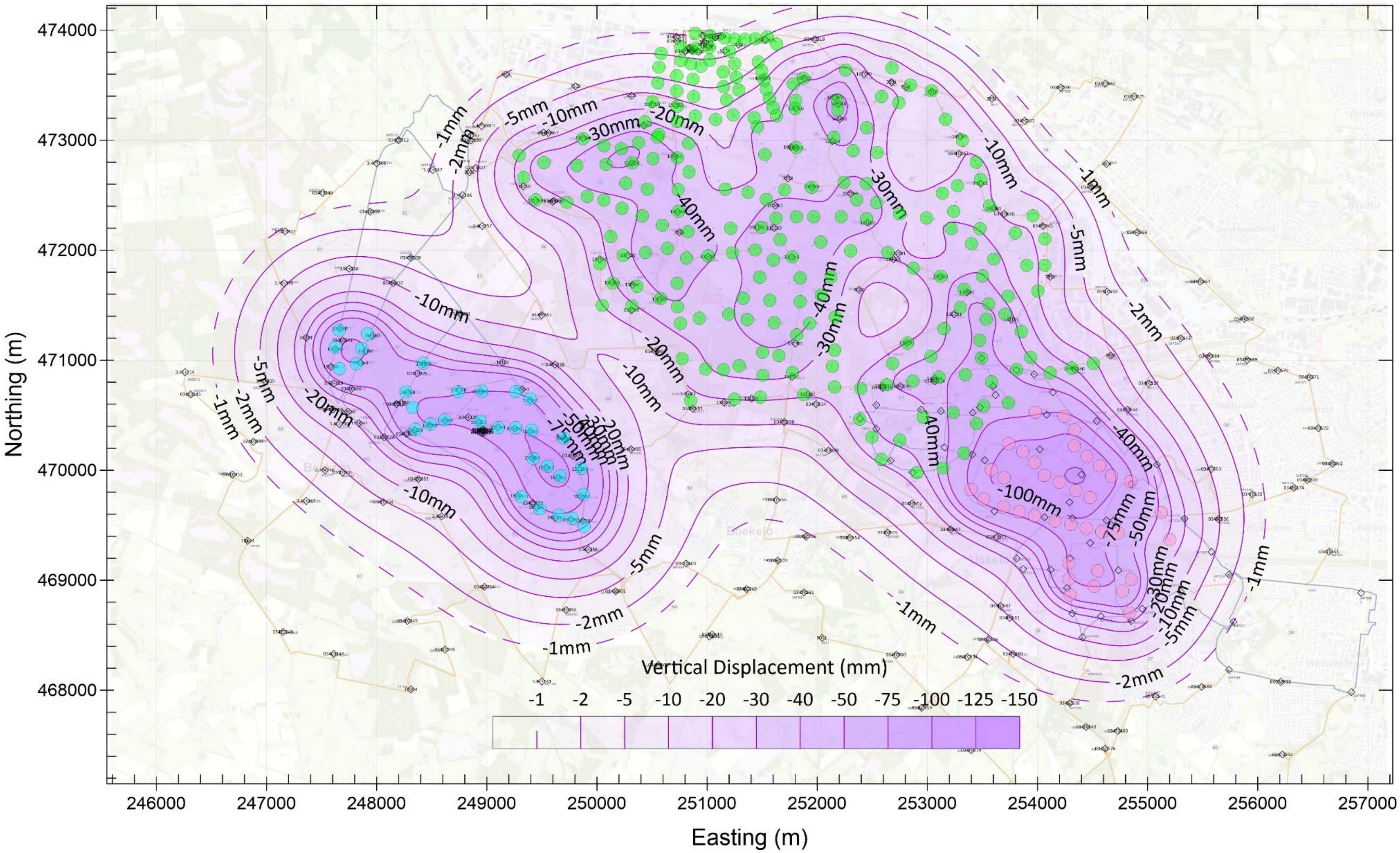

Figure B-22. Vertical Displacement (Millimeters) Predicted Over the Hengelo, Usseler Es, and Ganzebos Brinefields in Year 2125.

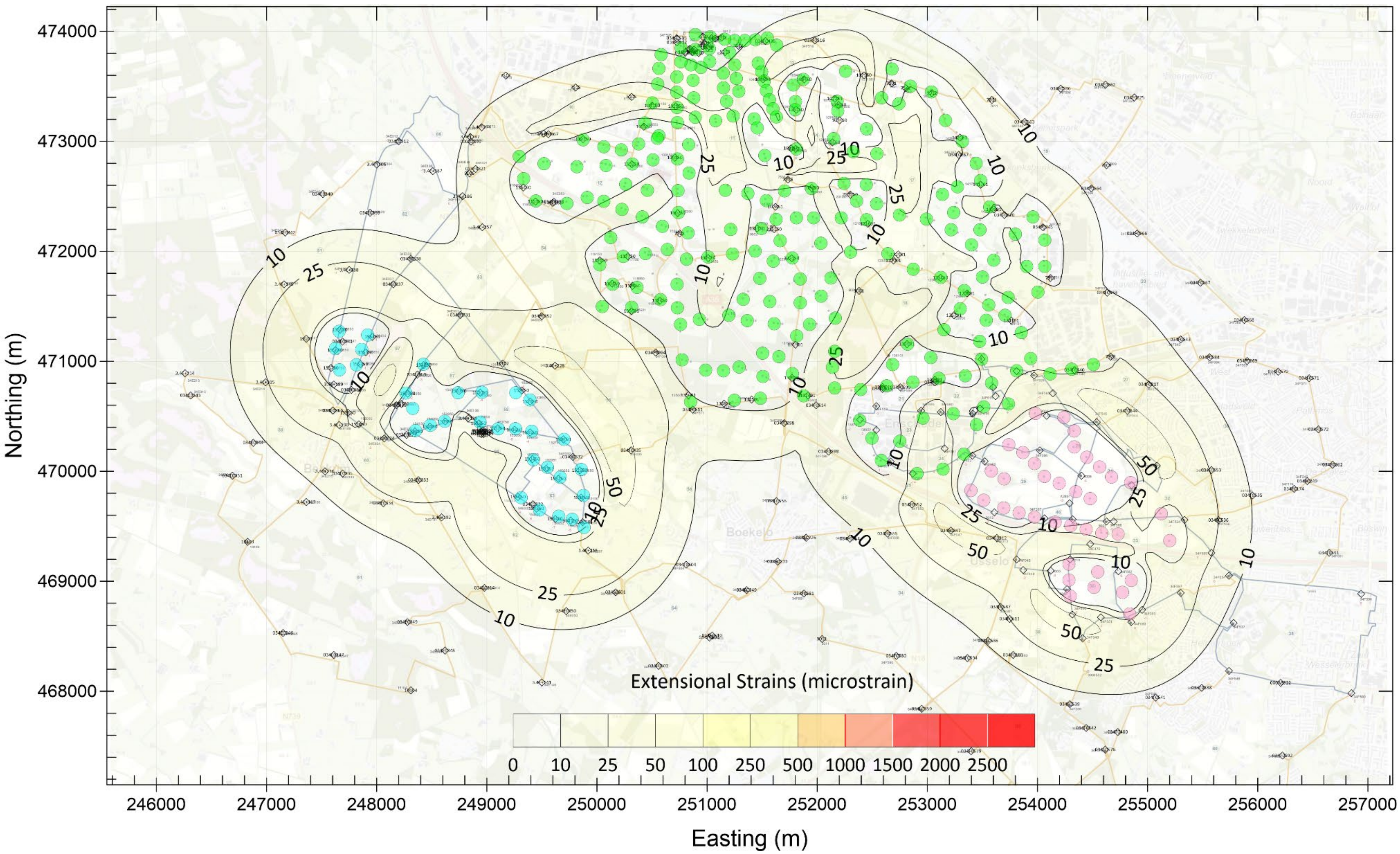

Figure B-23. Horizontal Extensional Strain (Microstrain) Predicted Over the Hengelo, Usseler Es, and Ganzebos Brinefields in Year 2125.

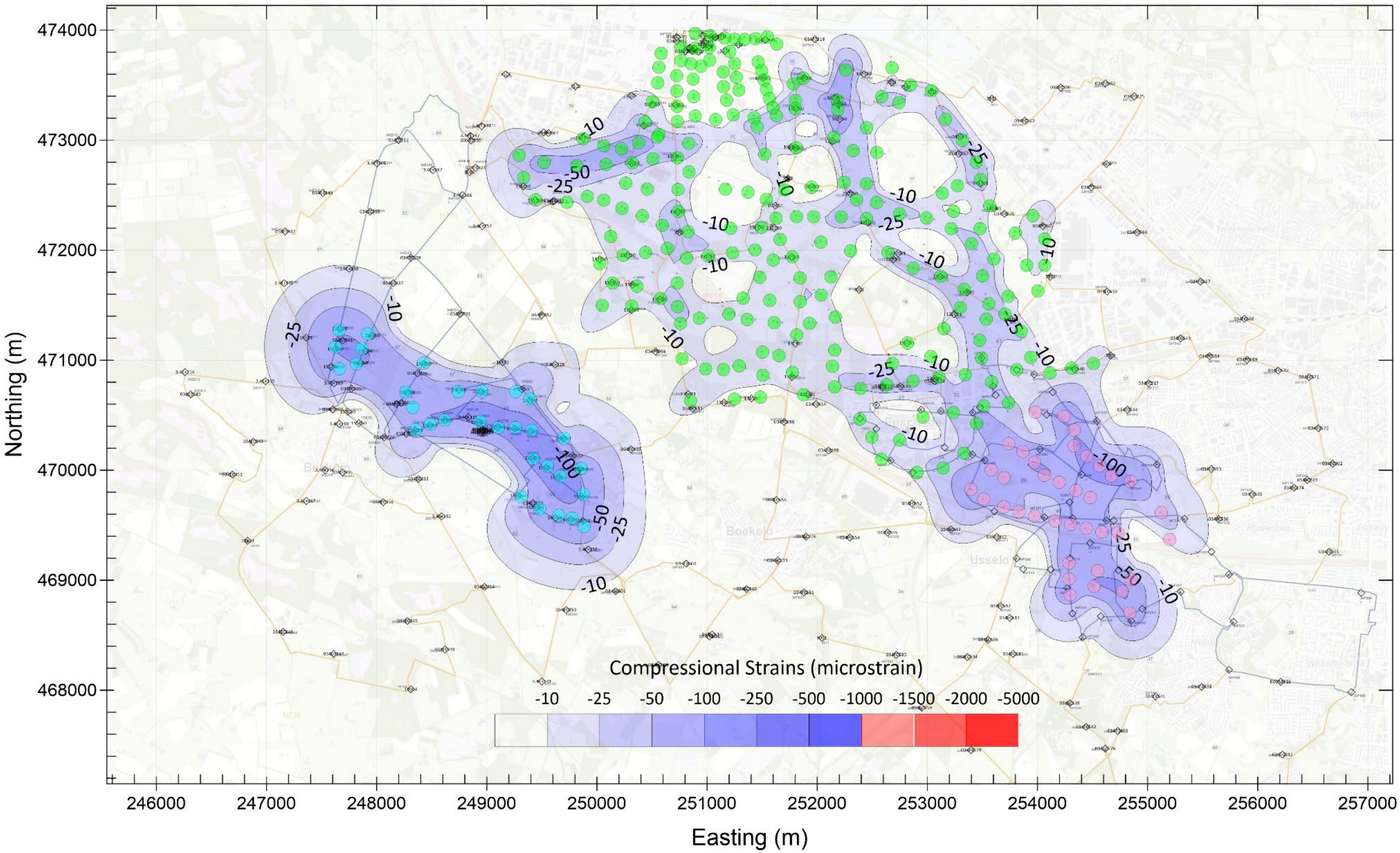

Figure B-24. Horizontal Compressional Strain (Microstrain) Predicted Over the Hengelo, Usseler Es, and Ganzebos Brinefields in Year 2125.

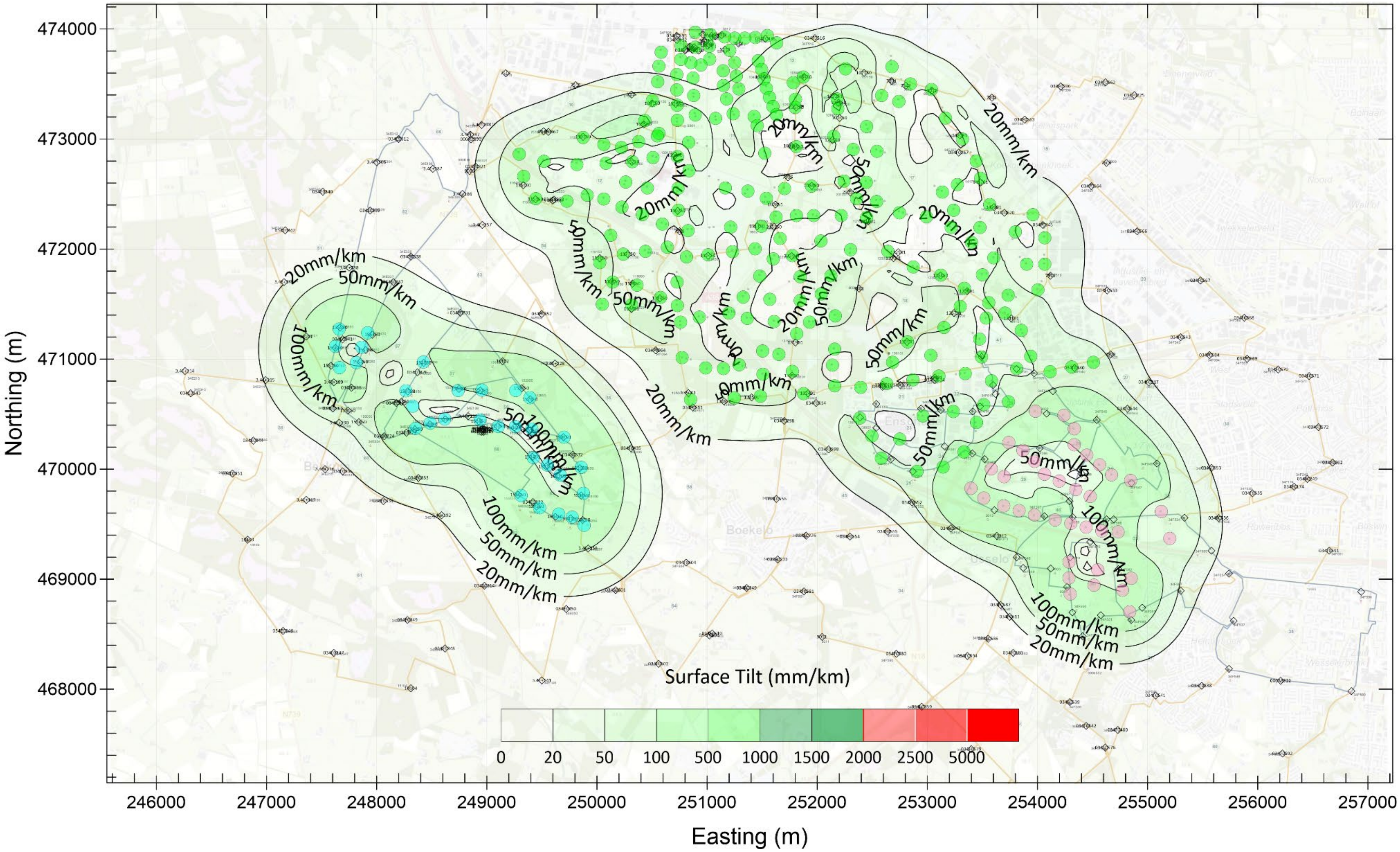

Figure B-25. Ground-Surface Tilt (Millimeters per Kilometer) Predicted Over the Hengelo, Usseler Es, and Ganzebos Brinefields in Year 2125.

APPENDIX C

CONTOURS OF INCREMENTAL SUBSIDENCE AND SUBSIDENCE RATES ATTRIBUTED TO THE USSELER ES AND GANZEBOS BRINEFIELDS IN 2025, 2050, 2075, 2100, AND 2125

RESPEC

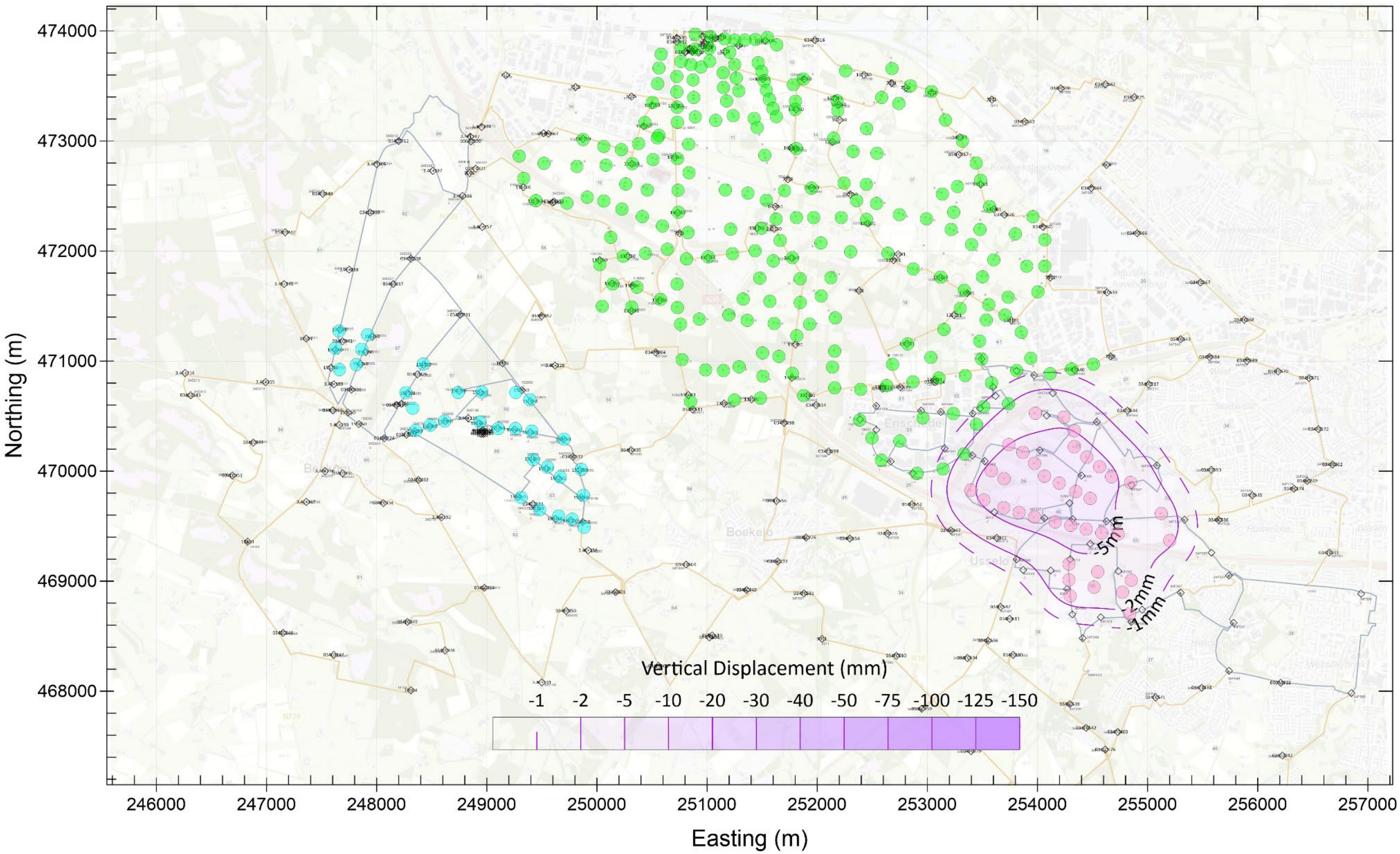

Figure C-1. Incremental Vertical Displacement (Millimeters) Attributed to the Usseler Es Caverns in Year 2025.

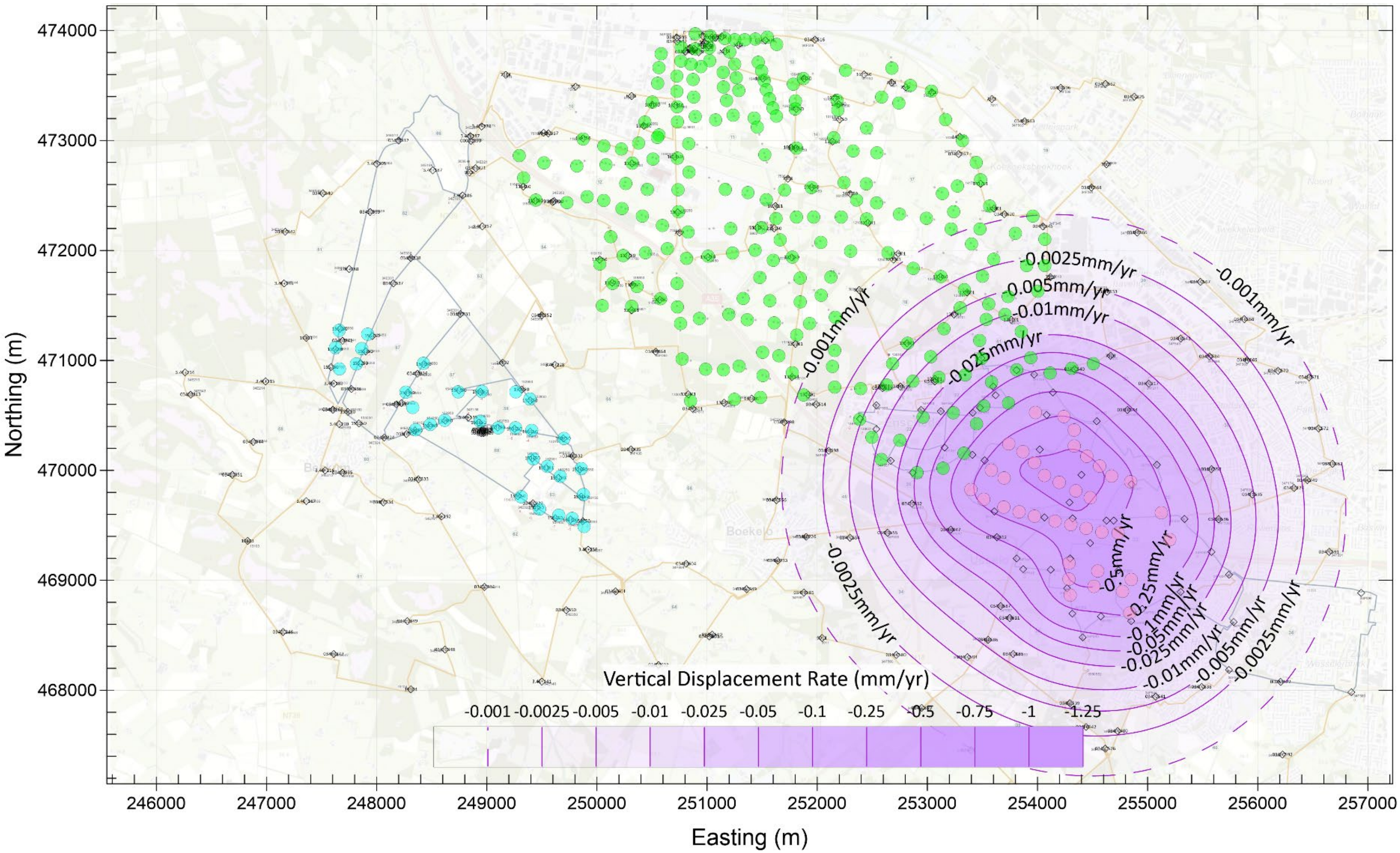

Figure C-2. Incremental Vertical Displacement Rate (Millimeters per Year) Attributed to the Usseler Es Caverns 2025.

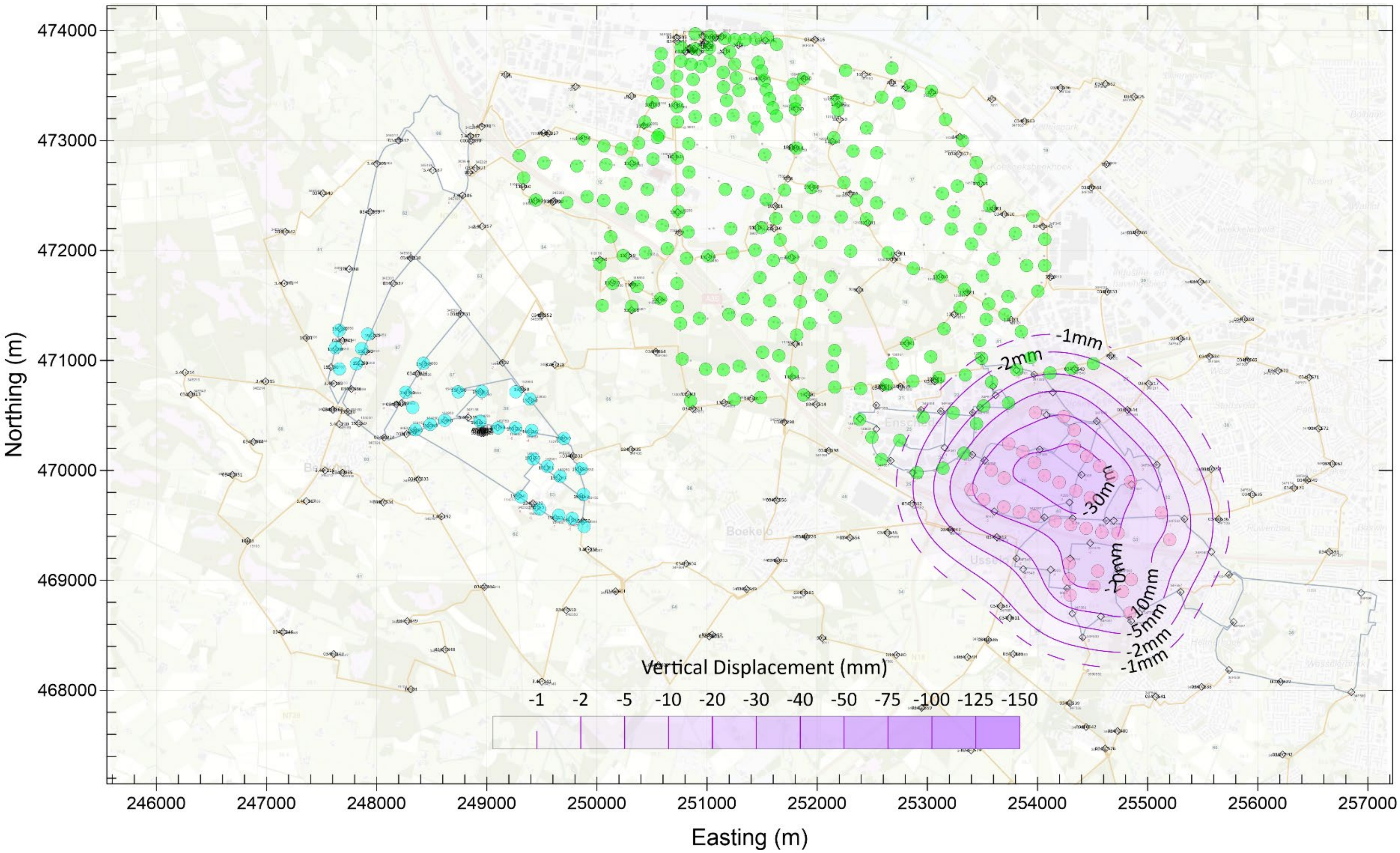

Figure C-3. Incremental Vertical Displacement (Millimeters) Attributed to the Usseler Es Caverns in Year 2050.

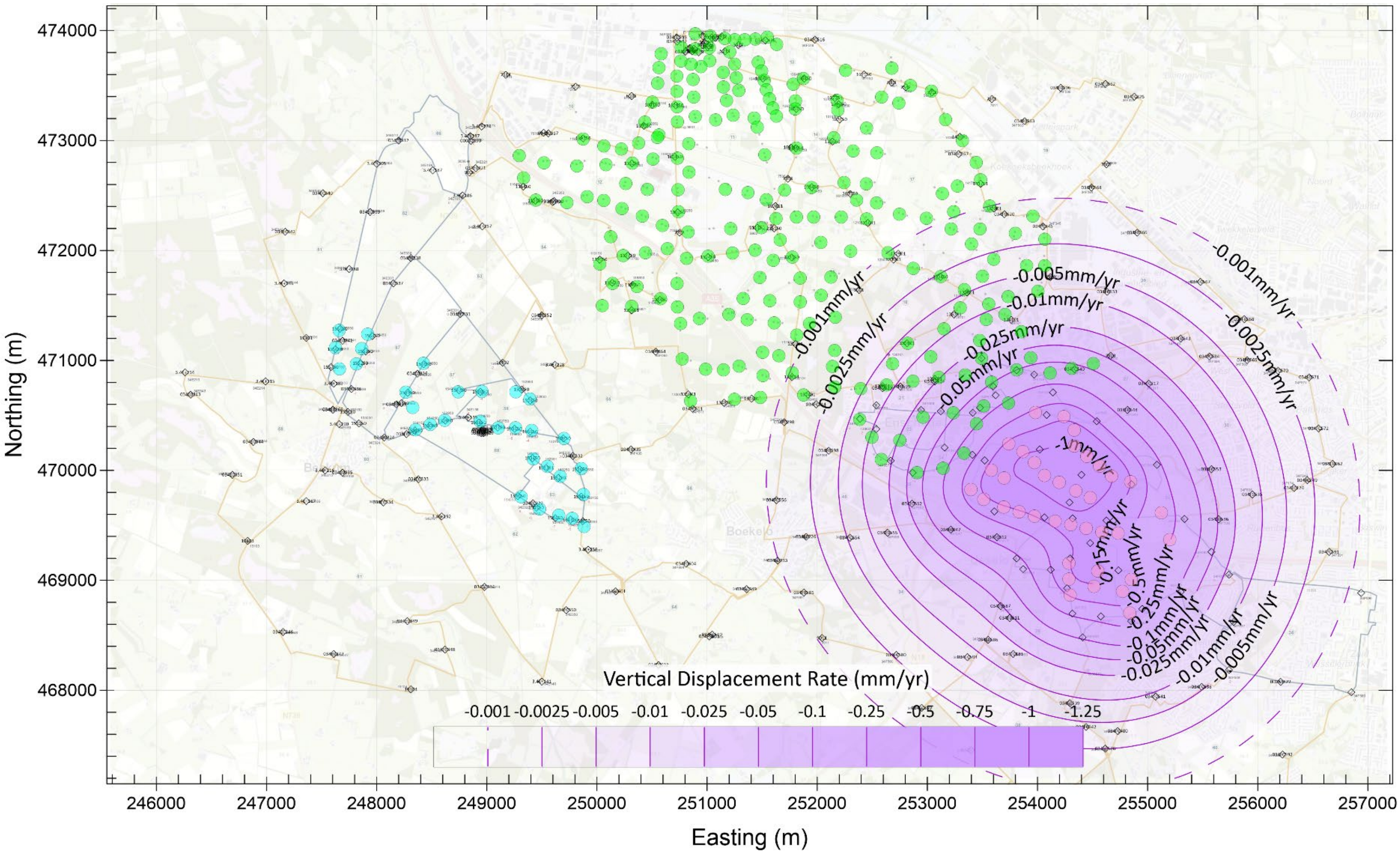

Figure C-4. Incremental Vertical Displacement Rate (Millimeters per Year) Attributed to the Usseler Es Caverns 2050.

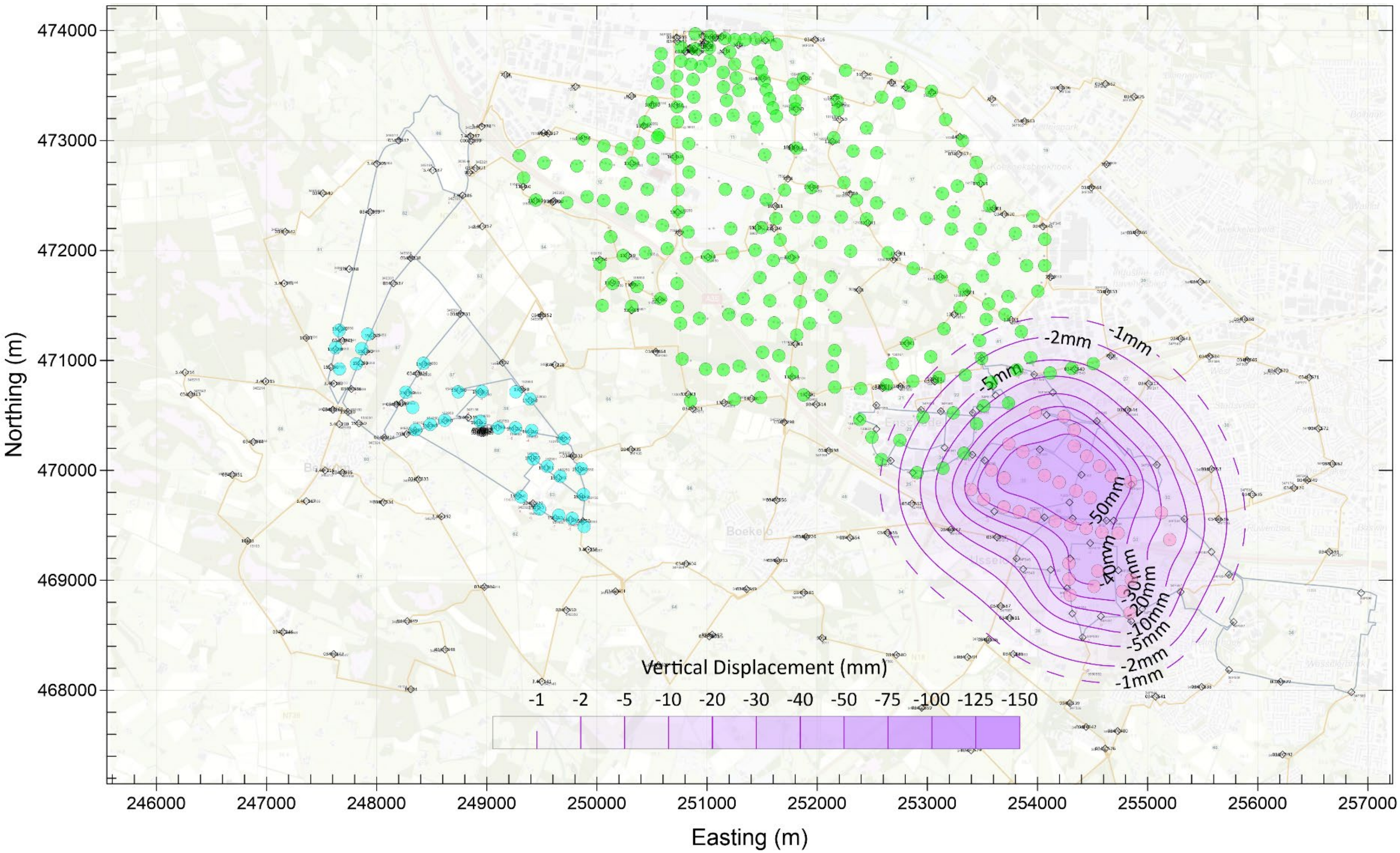

Figure C-5. Incremental Vertical Displacement (Millimeters) Attributed to the Usseler Es Caverns in Year 2075.

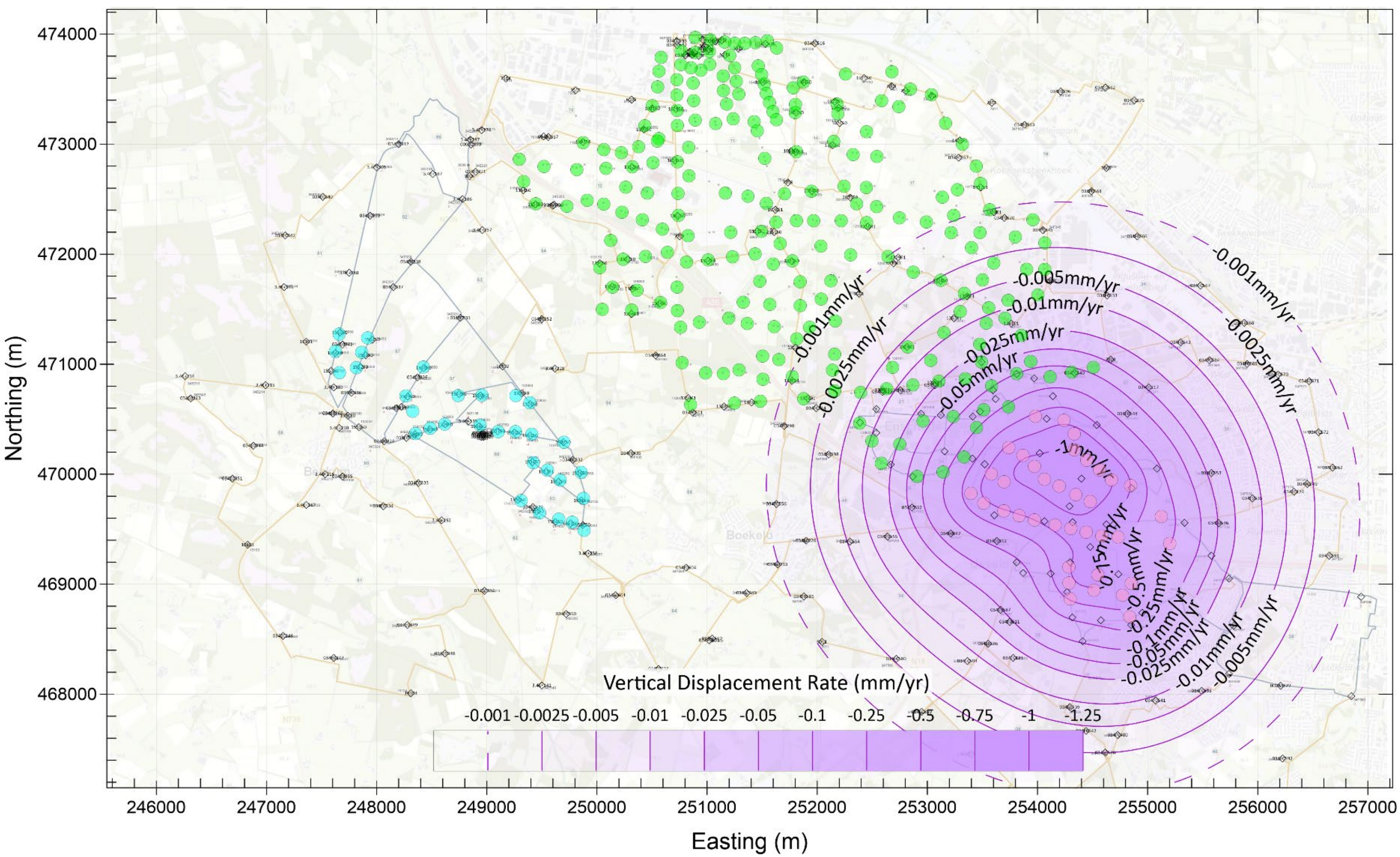

Figure C-6. Incremental Vertical Displacement Rate (Millimeters per Year) Attributed to the Usseler Es Caverns 2075.

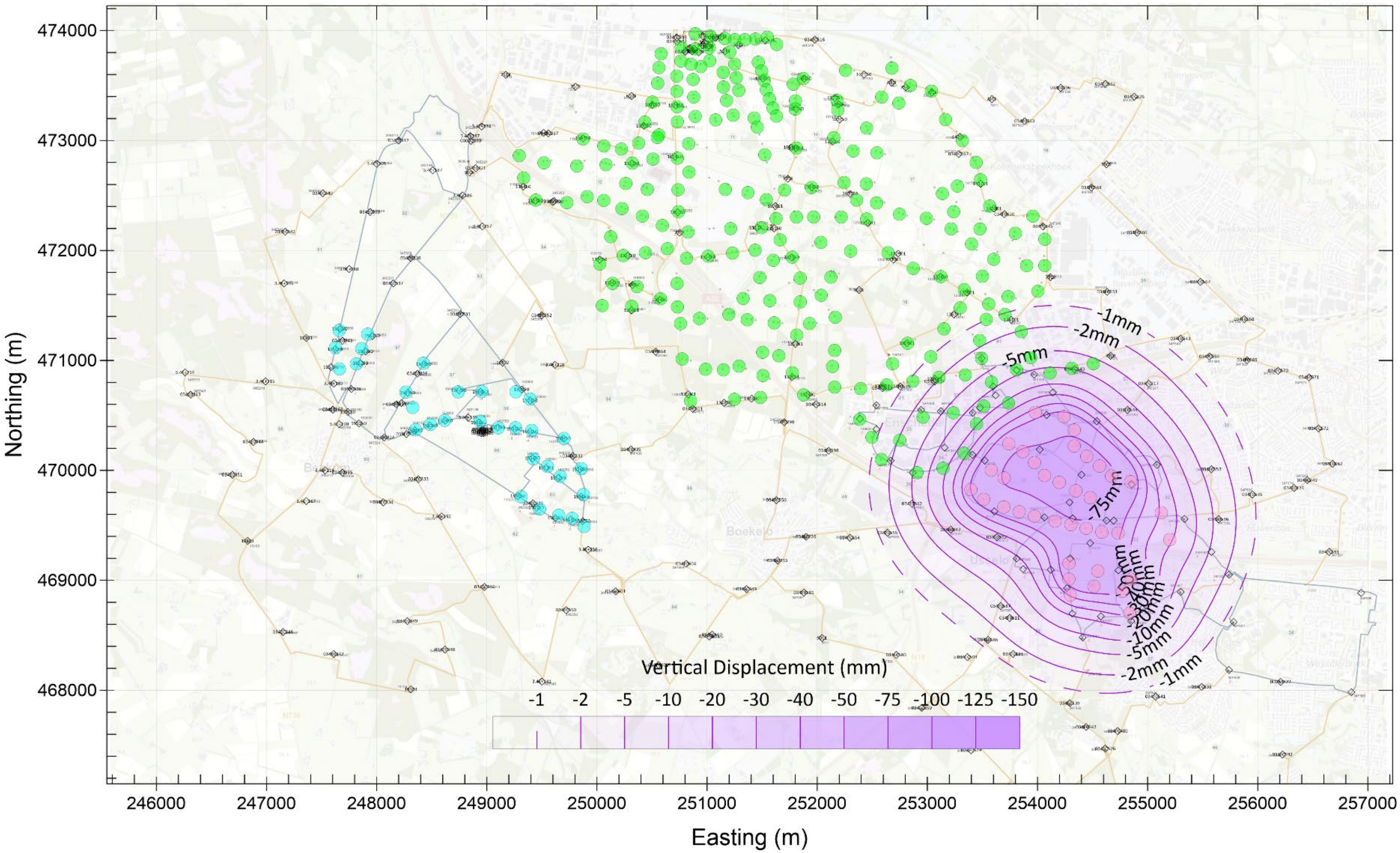

Figure C-7. Incremental Vertical Displacement (Millimeters) Attributed to the Usseler Es Caverns in Year 2100.

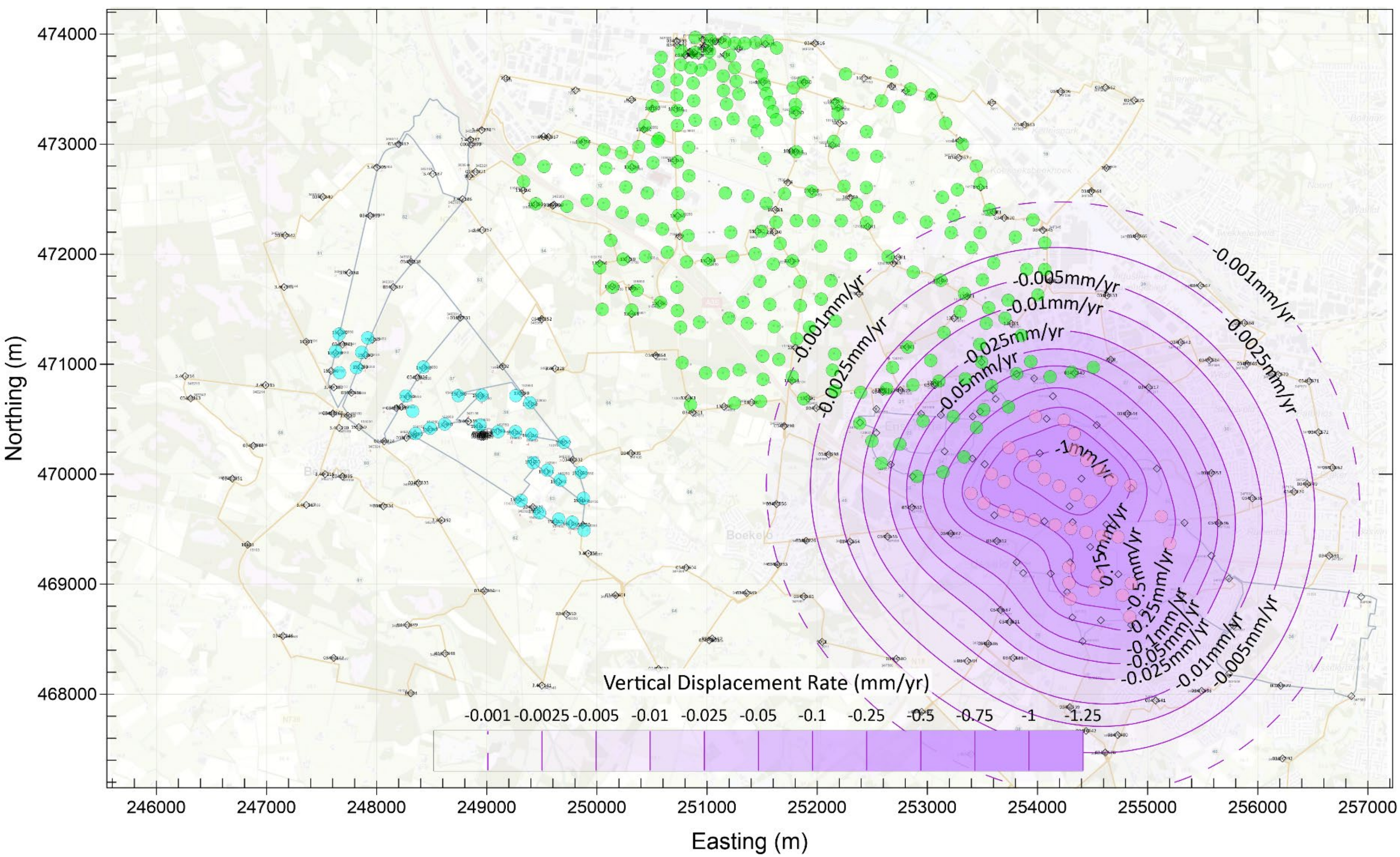

Figure C-8. Incremental Vertical Displacement Rate (Millimeters per Year) Attributed to the Usseler Es Caverns 2100.

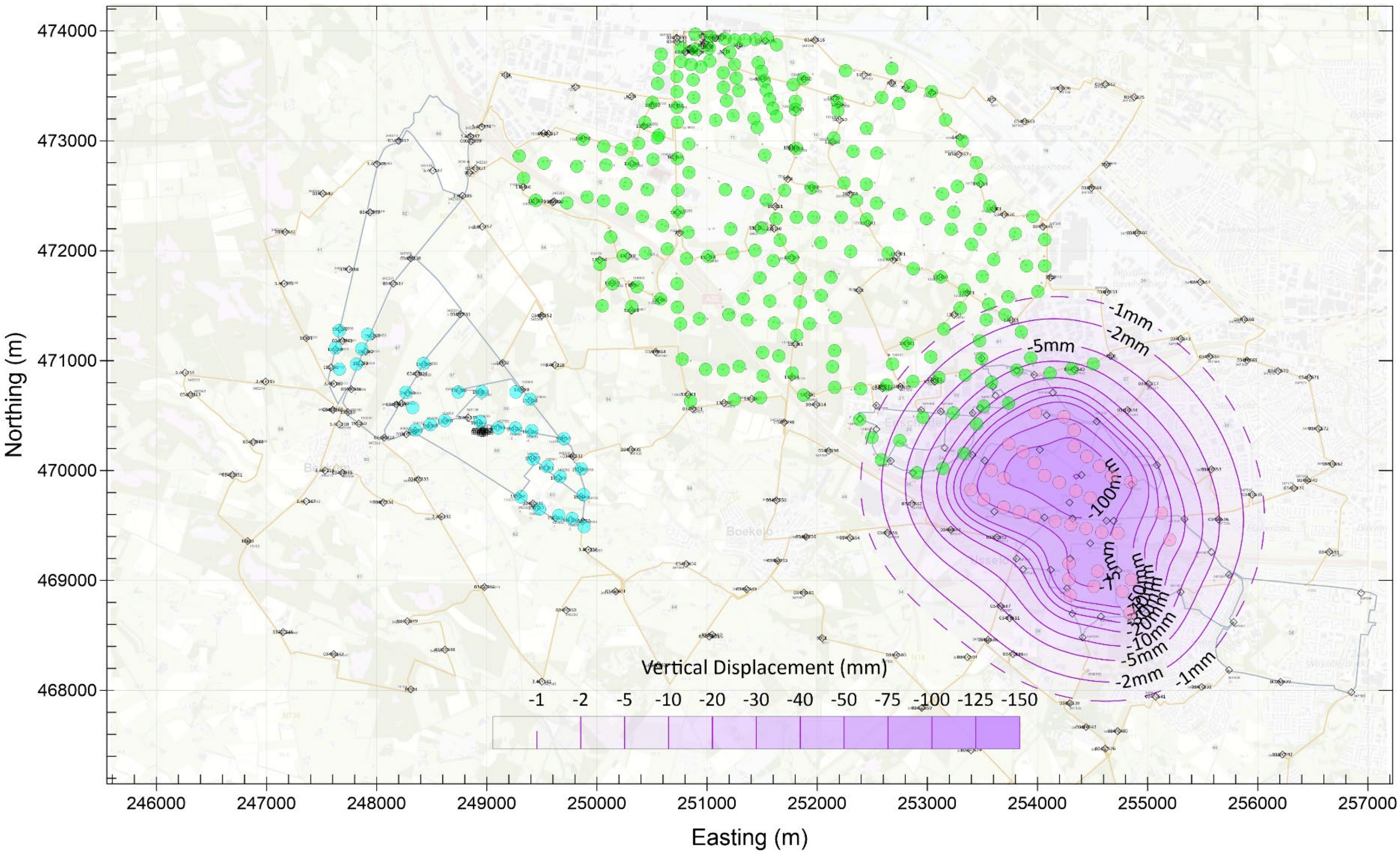

Figure C-9. Incremental Vertical Displacement (Millimeters) Attributed to the Usseler Es Caverns in Year 2125.

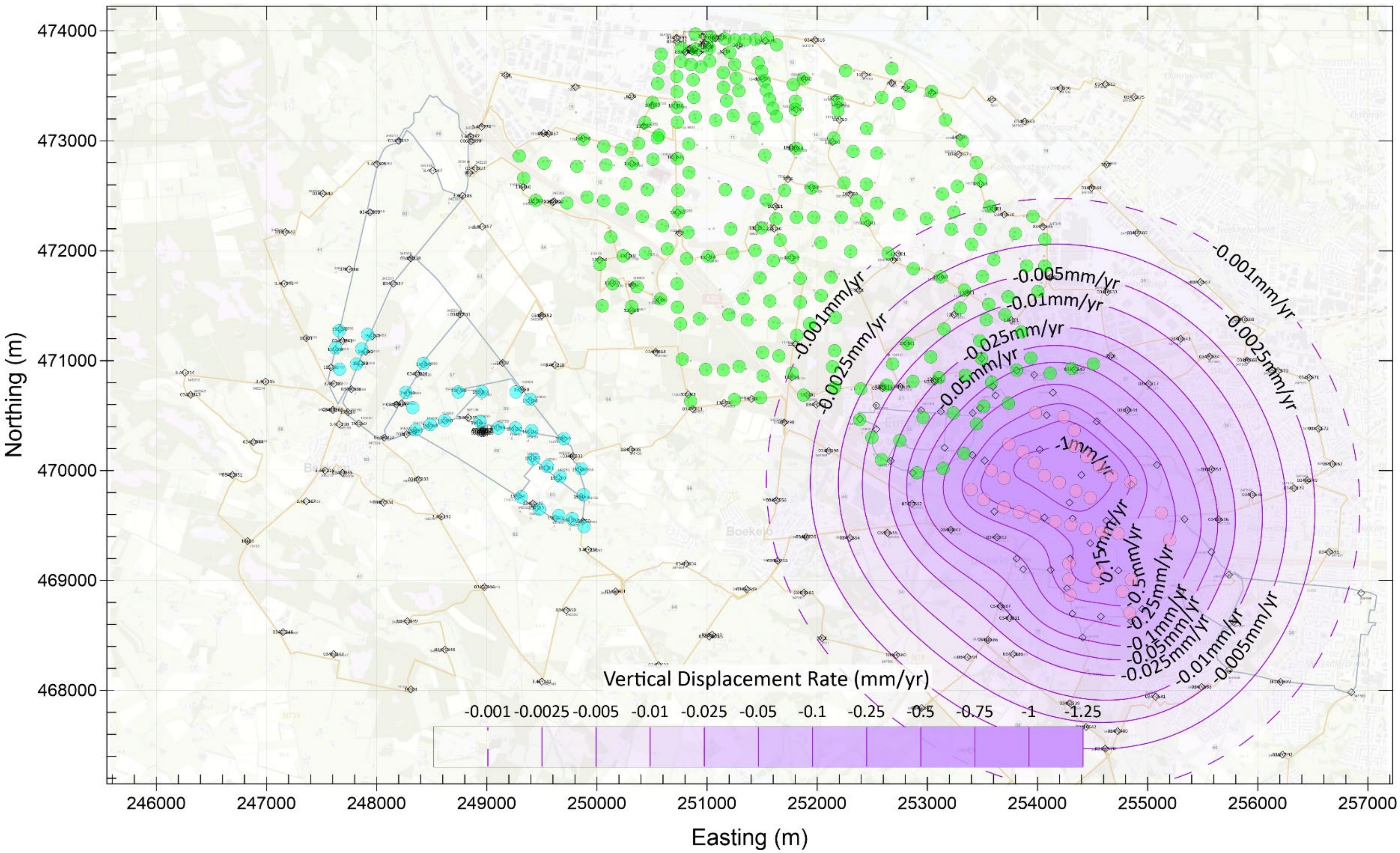

Figure C-10. Incremental Vertical Displacement Rate (Millimeters per Year) Attributed to the Usseler Es Caverns 2125.

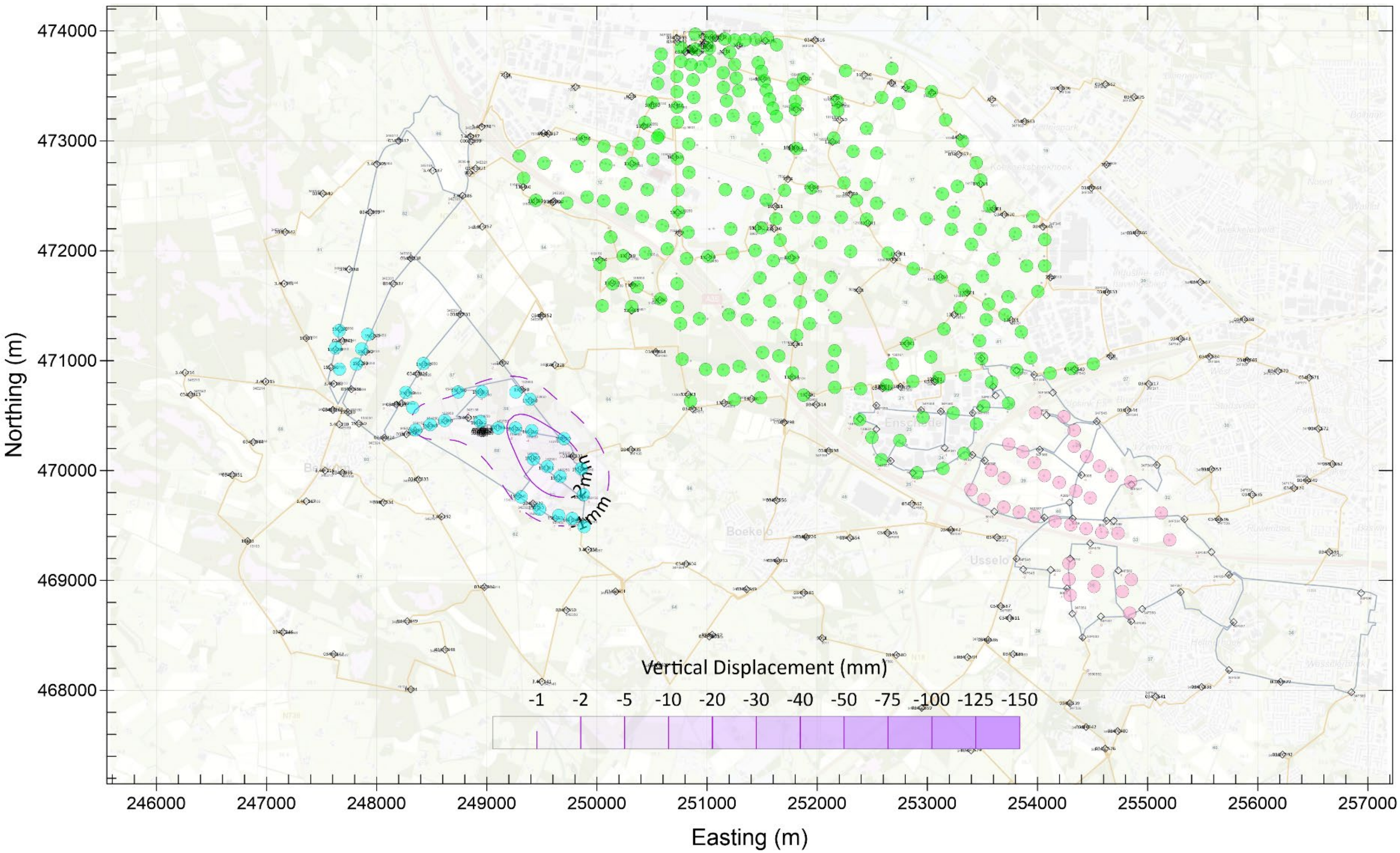

Figure C-11. Incremental Vertical Displacement (Millimeters) Attributed to the Ganzebos Caverns in Year 2025.

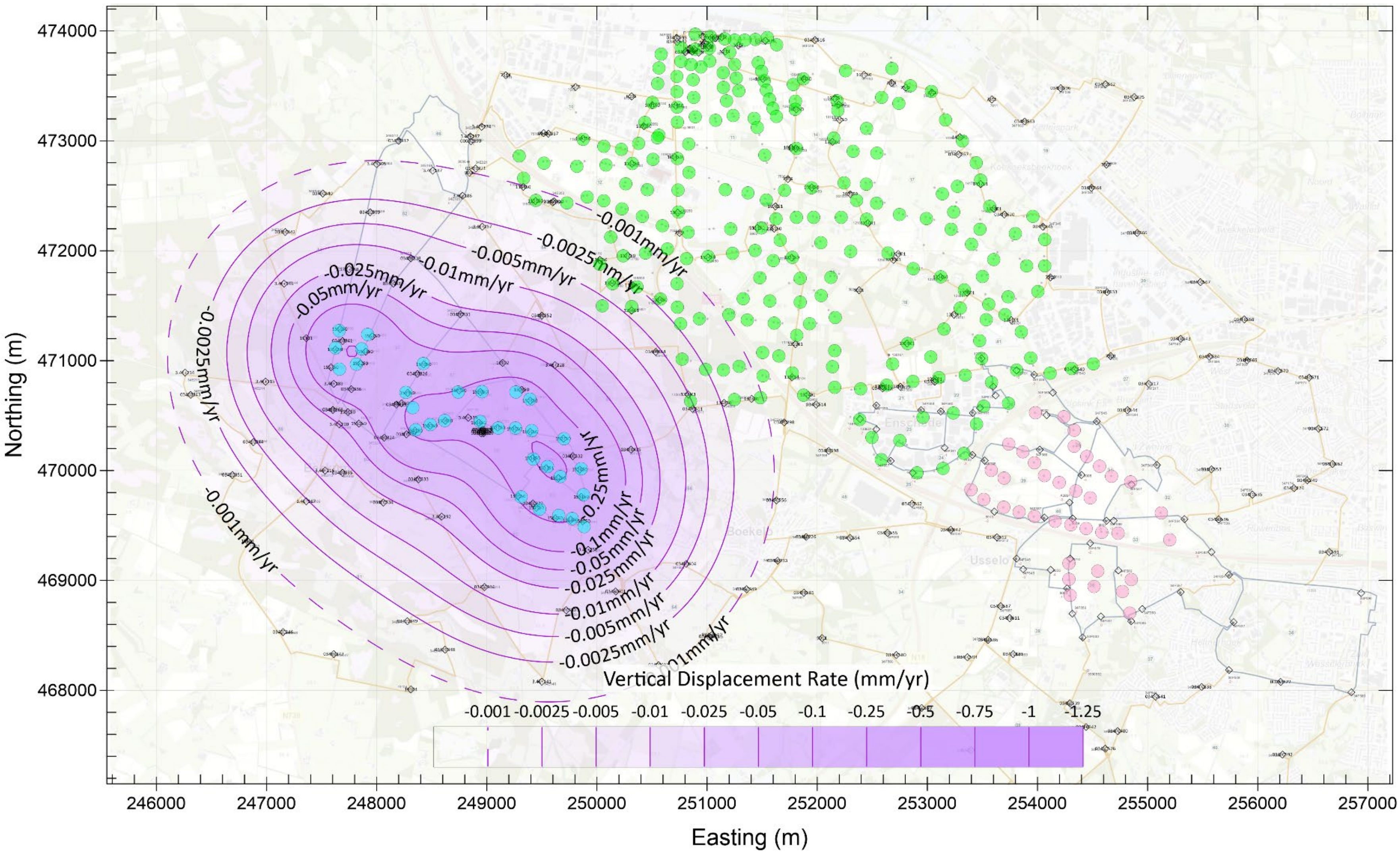

Figure C-12. Incremental Vertical Displacement Rate (Millimeters per Year) Attributed to the Ganzebos Caverns 2025.

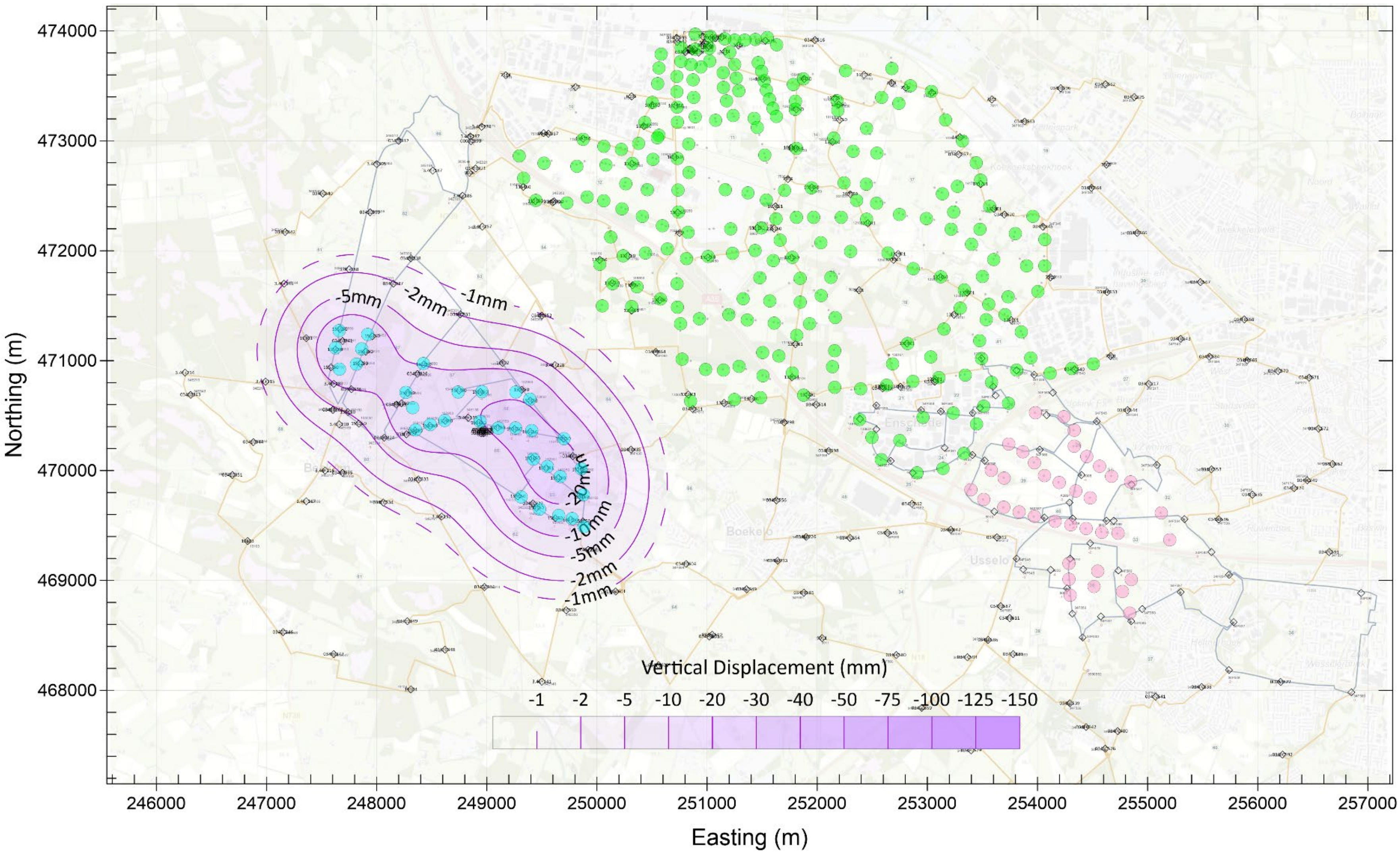

Figure C-13. Incremental Vertical Displacement (Millimeters) Attributed to the Ganzebos Caverns in Year 2050.

RESPEC

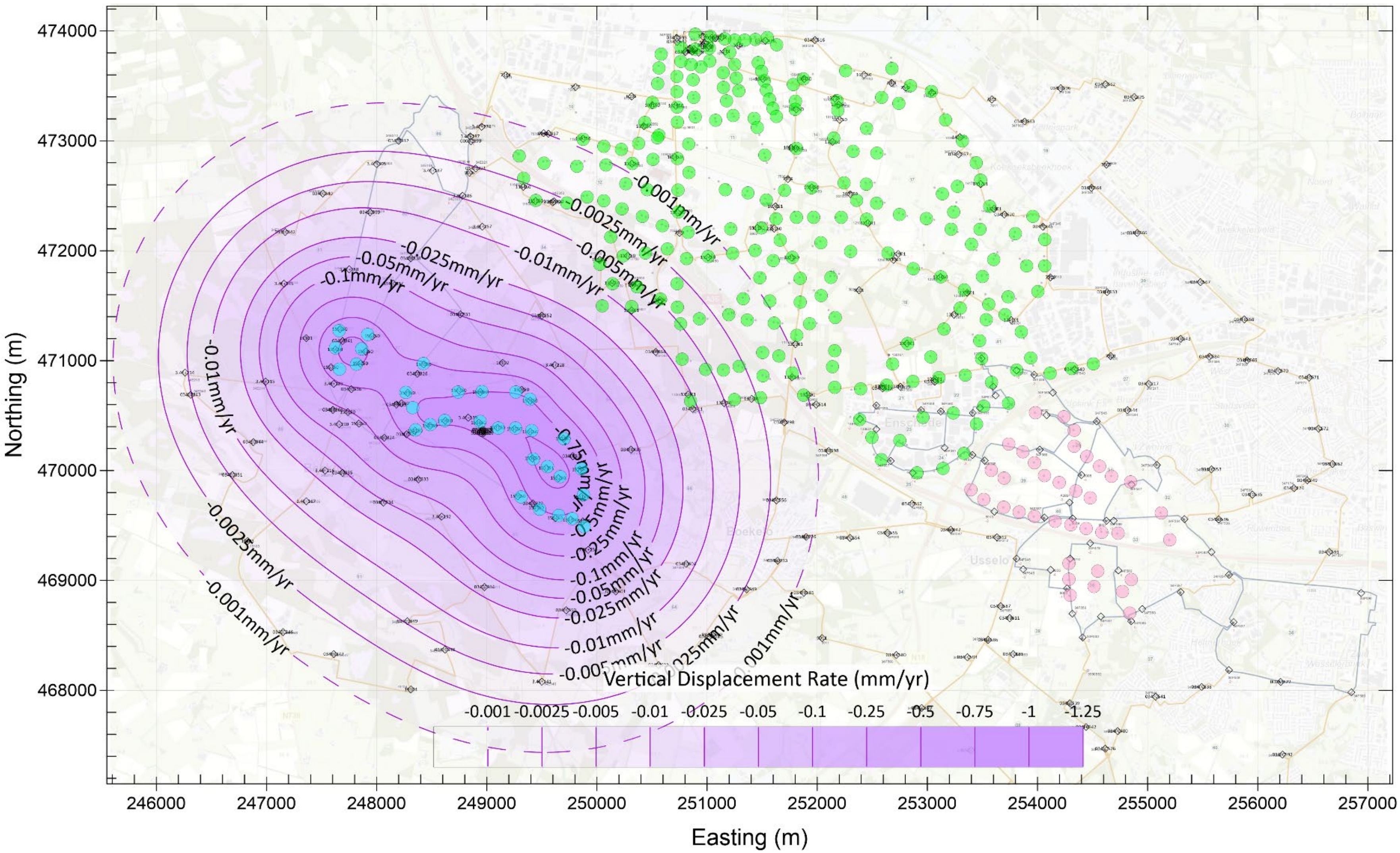

Figure C-14. Incremental Vertical Displacement Rate (Millimeters per Year) Attributed to the Ganzebos Caverns 2050.

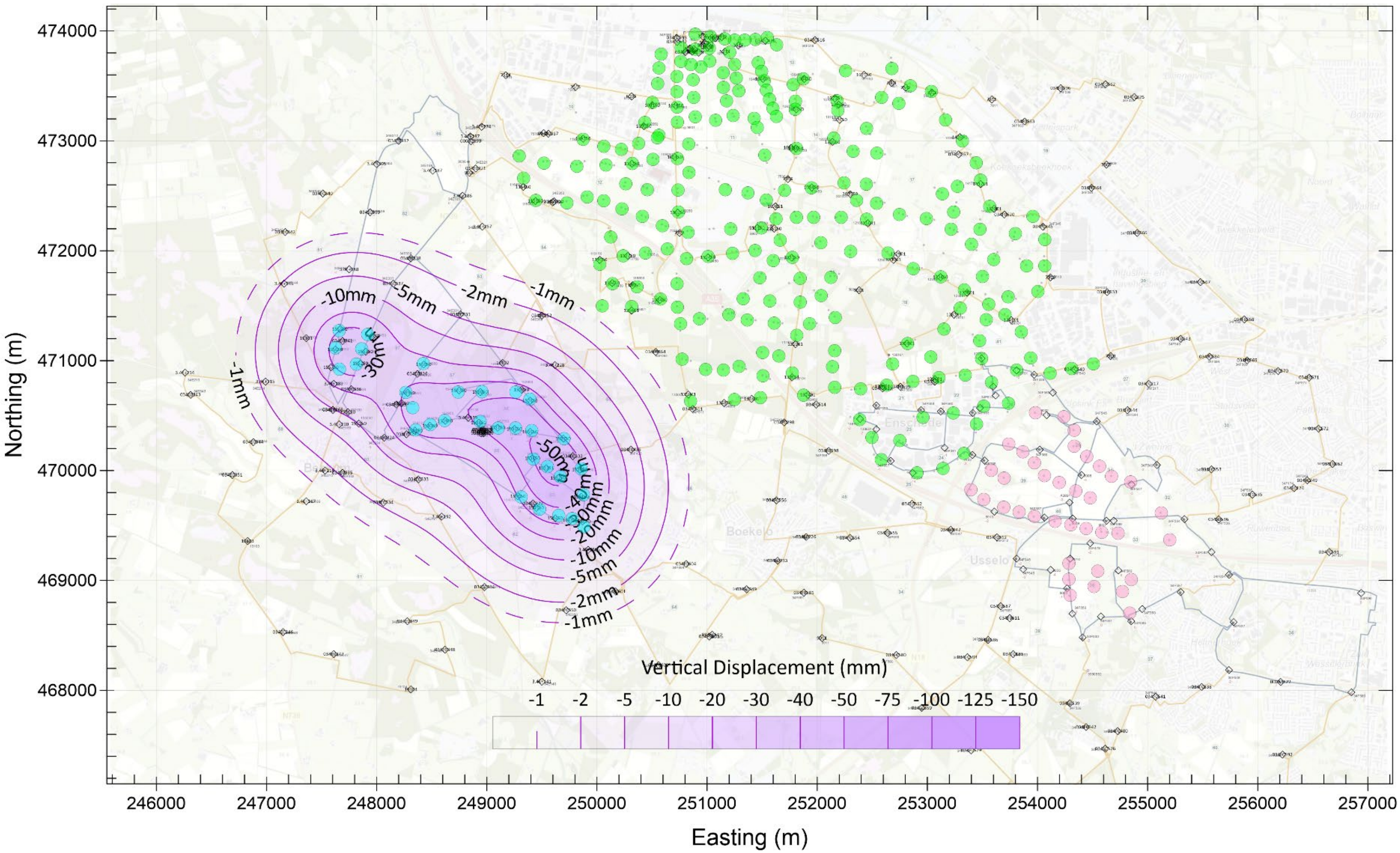

Figure C-15. Incremental Vertical Displacement (Millimeters) Attributed to the Ganzebos Caverns in Year 2075.

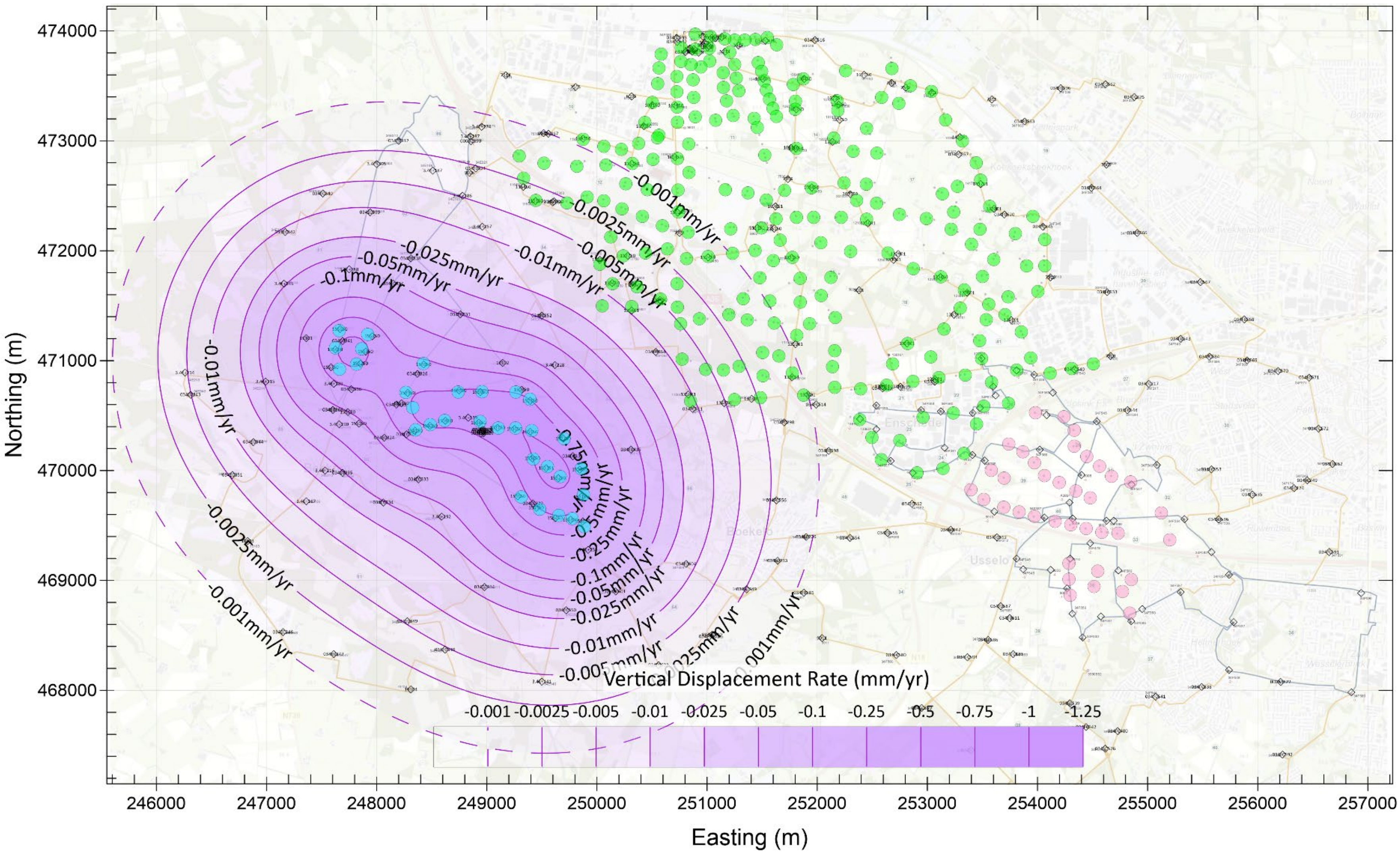

Figure C-16. Incremental Vertical Displacement Rate (Millimeters per Year) Attributed to the Ganzebos Caverns 2075.

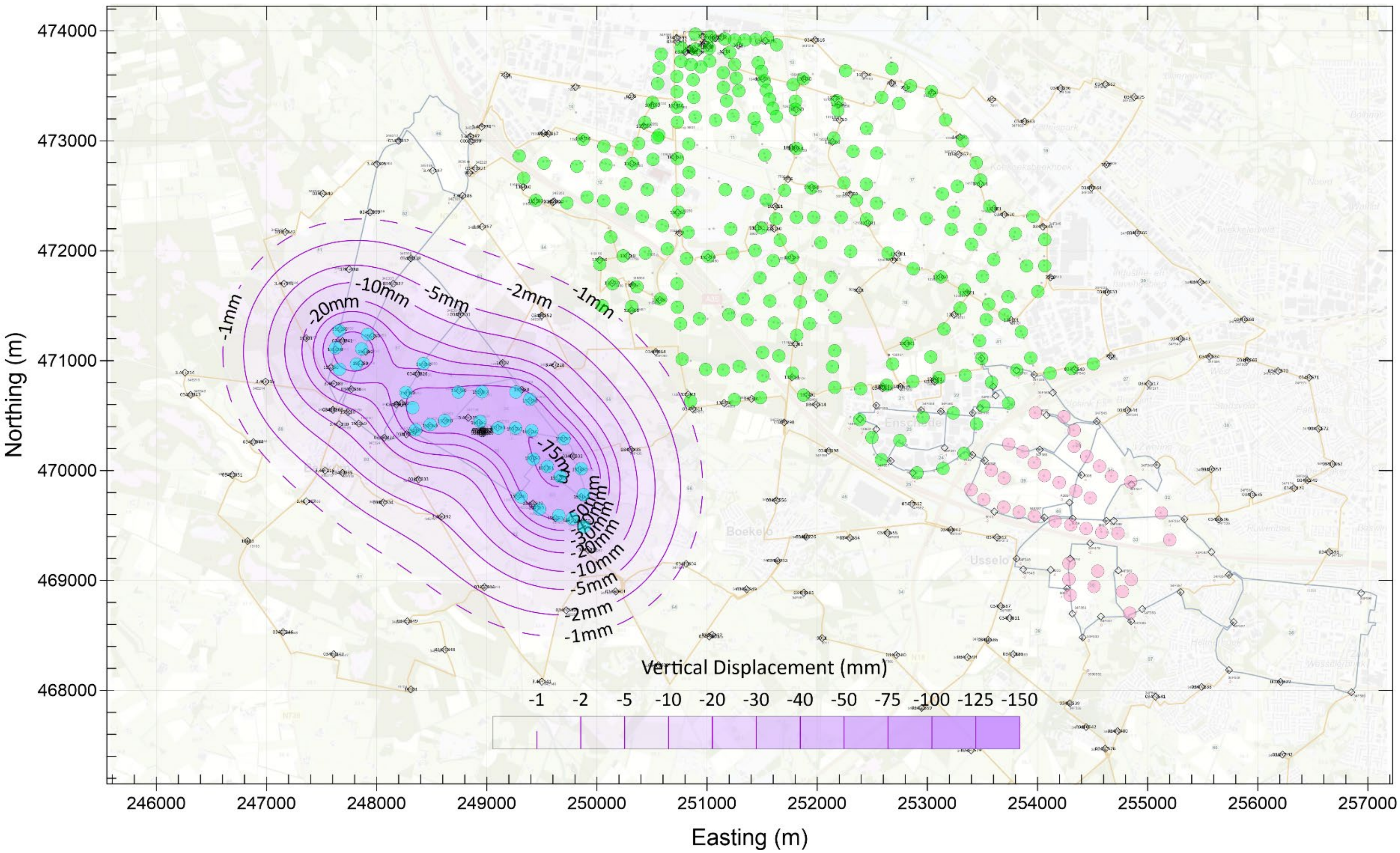

Figure C-17. Incremental Vertical Displacement (Millimeters) Attributed to the Ganzebos Caverns in Year 2100.

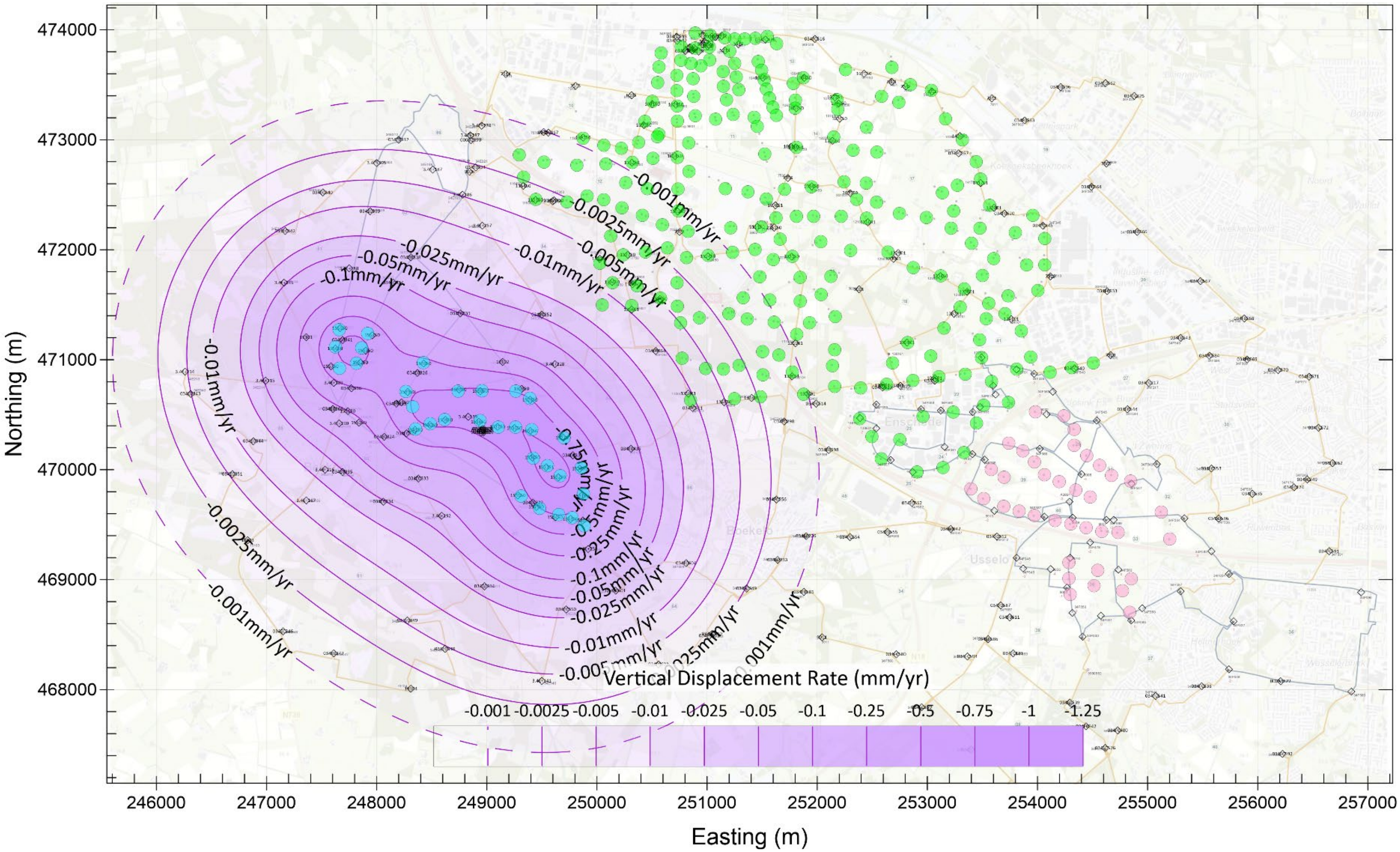

Figure C-18. Incremental Vertical Displacement Rate (Millimeters per Year) Attributed to the Ganzebos Caverns 2100.

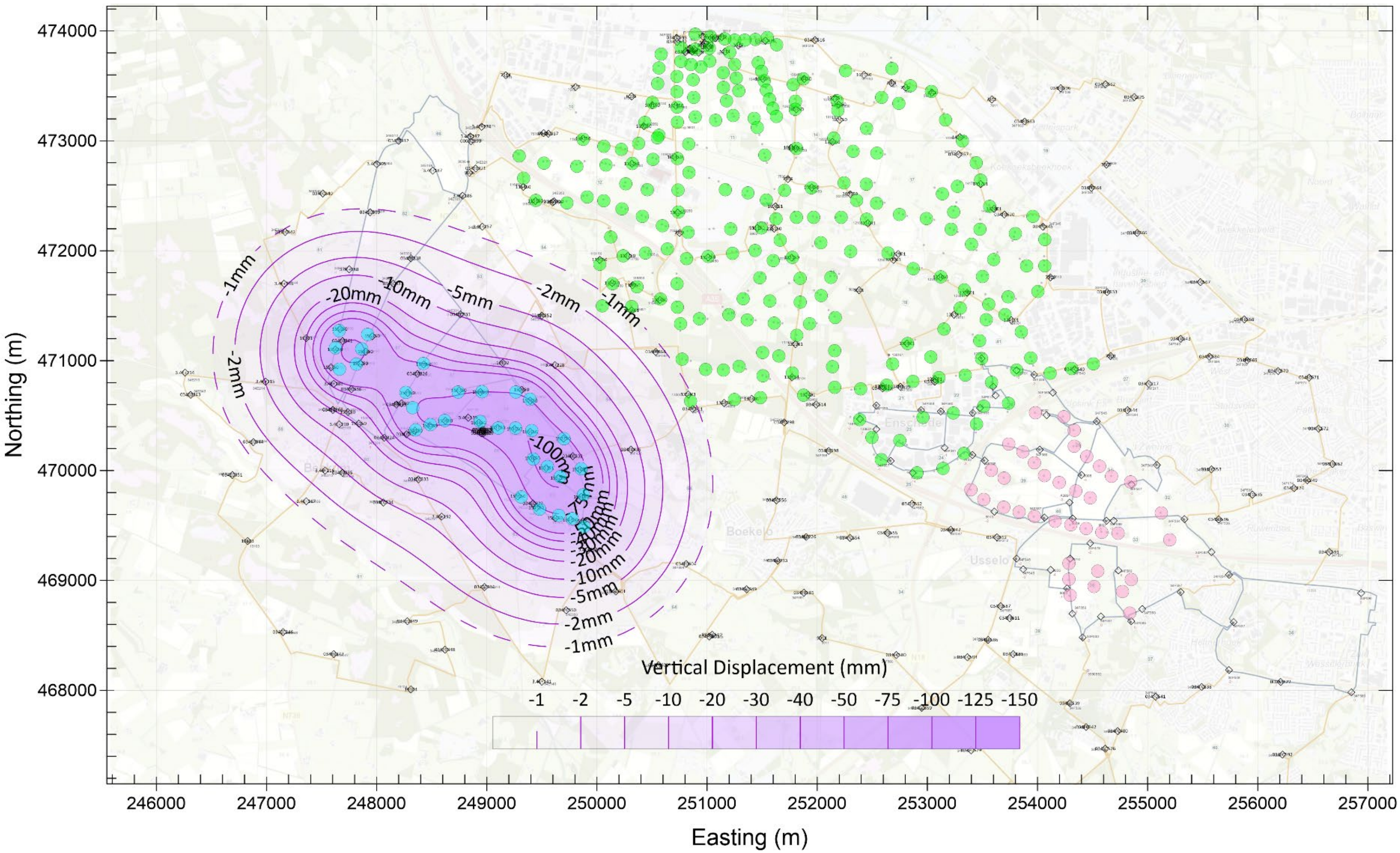

Figure C-19. Incremental Vertical Displacement (Millimeters) Attributed to the Ganzebos Caverns in Year 2125.

RESPEC

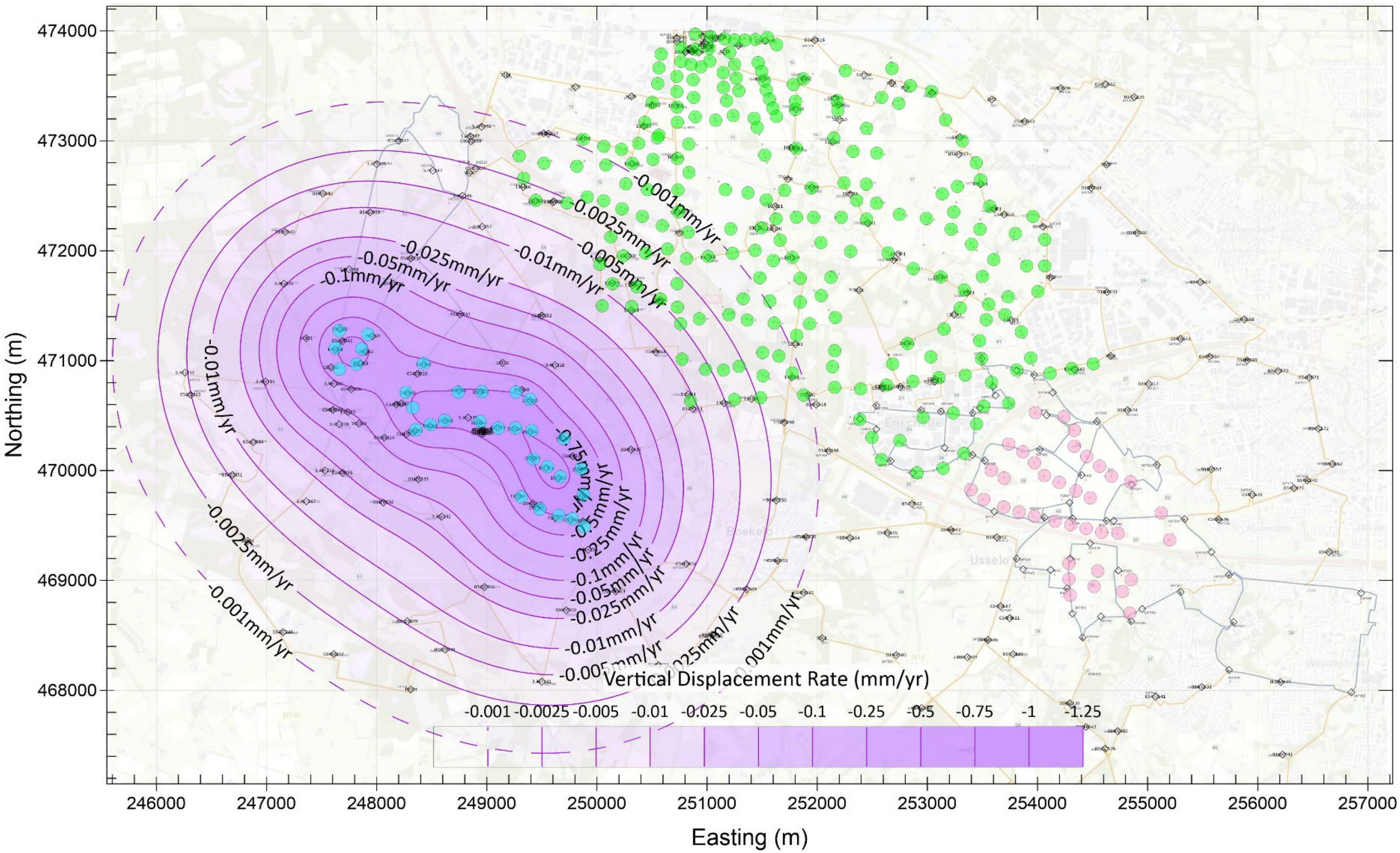

Figure C-20. Incremental Vertical Displacement Rate (Millimeters per Year) Attributed to the Ganzebos Caverns 2125.